TÉCNICO LISBOA

Combined Life Cycle Analysis of Wind Energy and Hydrogen Production

João Maria Pais de Vasconcelos de Herédia

Thesis to obtain the Master of Science Degree in

Mechanical Engineering

Supervisors: Prof. Ricardo Balbino Santos Pereira
Prof. Ana Filipa da Silva Ferreira

Examination Committee

Chairperson: Prof. José Manuel da Silva Chaves Ribeiro Pereira
Supervisor: Prof. Ana Filipa da Silva Ferreira
Member of the Committee: Prof. Carlos Augusto Santos Silva

December 2021

When something is important enough,
you do it even if the odds are not in your favor.
-Elon Musk

Acknowledgments

The work made in this thesis is the combination of the support of several different individuals and the compounded effect of five years of hard work.

I would like to thank my parents for all their support and for everything they have done all these years, specially for all the effort they gave me to get the best education possible.

I would also like to thank Maria Vaz Guedes for all the support, through out the hardest moments and to encourage this thesis to be finished.

Also, I would like to thank my supervisors, Professor Ana Filipa da Silva Ferreira and Professor Ricardo Balbino Santos Pereira for all the help, guidance and wisdom they provided that made this work and thesis a reality. They regularly took valuable time from their schedule to always accompany my progress and provide insightful suggestions and advice.

Last, but certainly not least, to my friends and the rest of my family for always showing an interest in what I was studying, supporting me throughout this journey and believing in me.

Abstract

Green hydrogen is regarded as a promising solution to address the energetic transition, especially in the mobility sector. This work shows a life cycle assessment (LCA) to evaluate the environmental impacts of centralized hydrogen production in Portugal through electricity supply from offshore wind farms (OWF). Two scenarios are considered, with two configurations each. In scenario 1, 5% of small and 16% of heavy vehicles of the Portuguese fleet are considered to be fuel cell electric vehicles (FCEV) by 2050 with a demand of $112.65\,kton\,H_2/year$. Scenario 2 considers 30% of small and heavy vehicles are FCEV with a demand of $435.1\,kton\,H_2/year$ by 2050. Configuration A assumes all generated energy by the OWF serves to produce hydrogen with a plant power ratio (PPR) of 62.5%. In configuration B (PPR=25%), only 38% of the energy is used to produce hydrogen, to take advantage of the curtailment effect. For LCA, the RECIPE method was used and two impact categories were considered: midpoint and endpoint. In the midpoint analysis, OWF has the greatest impact in all categories. In the endpoint analysis, resources are the category with the most impact. Configuration A has 3.65 and 5.21 and configuration B has 6.89 and $9.84\,kg\,CO_2/kg\,H_2$ emissions with and without end-of-life respectively. Compared with steam methane reforming, configuration A and B have a reduction between 55-70% and 15-40% in the CO_2 emissions respectively. Regarding the mobility sector, it was concluded $kg\,CO_2/km$ emissions from the FCEV were 40-80% lower compared to ICE vehicles.

Keywords: Offshore wind energy, Electrolysis, Life cycle assessment, Centralized hydrogen production, Green hydrogen, Fuel cell electric vehicle (FCEV).

Resumo

Hidrogénio verde é considerada uma solução promissora para resolver os desafios da transição energética, especialmente no setor da mobilidade. Nesta dissertação uma análise de ciclo de vida foi feita de modo a avaliar os impactos ambientais do hidrogénio produzido de forma centralizada através da eletricidade proveniente de parques eólicos offshore. São considerados dois cenários, cada um com duas configurações diferentes. No cenário 1, 5% dos veículos ligeiros e 16% dos pesados da frota portuguesa seriam movidos a hidrogénio em 2050 com uma procura de $112.65\,kton\,H_2/ano$. No cenário 2 é considerado uma penetração de 30% nos veiculos leves e pesados, com uma procura de $435.1\,kton\,H_2/ano$ em 2050. A configuração A assume que toda a energia gerada pelo parque eólico serve para produzir hidrogénio com o rácio entre as potências do parque eólico e da central de H_2 de 62.5%. Na configuração B (rácio = 25%), apenas 38% da energia gerada pelo parque eólico vai ser para produzir hidrogénio, para tirar partido do efeito de curtailment. Na análise midpoint, o parque eólico tem maior impacto em todas as categorias. Na análise endpoint, os recursos é a categoria com maior impacto. A configuração A tem 3.65 e 5.21 e a configuração B 6.89 e 9.84 emissões de $kg\,CO_2/kg\,H_2$ com e sem fim de vida respetivamente. Comparando com a reformação do metano, a configuração A e B têm uma redução entre 55-70% e 15-40% nas emissões de CO_2 respetivamente. No sector da mobilidade, conclui-se que as emissões de $kg\,CO_2/km$ dos veículos a hidrogénio são entre 40-80% mais baixas quando comparado com veículos de combustão interna.

Palavras-chave: Energia eólica offshore, Electrólise, Análise de ciclo de vida, Produção centralizada, Hidrogénio verde, Veículo de célula de combustível

Contents

List of Tables

List of Figures

Nomenclature

Acronyms

AEP	Annual Energy Produced.
ALK	Alkaline.
ALO	Agricultural Land Occupation.
AWE	Alkaline Water Electrolyzer.
BEV	Battery Electric Vehicle.
BOP	Balance of Plant.
CC	Climate Change.
CCS	Carbon Capture and Storage.
CH_2	Compressed Hydrogen.
CF	Capacity Factor.
CP	Comboios de Portugal.
DC	Direct Current.
ED	Ecosystem Diversity.
EU	European Union.
EoL	End of Life.
EPT	Energy Payback Time.
FE	Freshwater Eutrophication.
FEco	Freshwater Ecotoxicity.
FCEV	Fuel Cell Electric Vehicle.
FD	Fossil Depletion.
FF	Floating Foundation.
FOWT	Floating Offshore Wind Turbine.
GHG	Greenhouse Gases.
GWA	Global Wind Atlas.
GWP	Global Warming Potential.
H_2	Molecular Hydrogen.
HVAC	High Voltage Alternating Current.
HVDC	High Voltage Direct Current.
HT	Human Toxicity.
H_2O	Water.
HER	Hydrogen Evolution Reaction.
HH	Human Health.
HHV	Higher Heating Value.
HRS	Hydrogen Refuelling station.
IEA	International Energy Agency.

IC	Investment Cost.
ICE	Internal Combustion Engine.
IR	Ionising Radiation.
IRENA	International Renewable Energy Agency.
LCA	Life Cycle Assessment.
LCIA	Life Cycle Impact Assessment.
LCI	Life Cycle Inventory.
LHV	Lower Heating Value.
LOHC	Liquid Organic Hydrogen Carrier.
MD	Metal Depletion.
ME	Marine Eutrophication.
MEco	Marine Ecotoxicity.
MEA	Membrane Electrode Assembly.
Mt	Million Tons.
MVAC	Medium Voltage Alternating Current.
NG	Natural Gas.
NLT	Natural Land Transformation.
OD	Ozone Depletion.
OER	Oxygen Evolution Reaction.
OWF	Offshore Wind Farm.
PE	Polyethylene.
PEM	Proton Exchange Membrane.
PEMWE	Proton Exchange Membrane Water Electrolysis.
PMF	Photochemical Matter Formation.
POF	Photochemical Oxidant Formation.
PP	Polypropylene.
PPM	Parts Per Million.
PPR	Plant Power Ratio.
PV	Photovoltaic.
RA	Resource Availability.
RES	Renewable Energy Sources.
RNC2050	Roteiro para a Neutralidade Carbónica 2050.
SMR	Steam Methane Reforming.
SOE	Solid Oxide Electrolysis.
TA	Terrestrial Acidification.
TDS	Total Dissolved Units.
TE	Terrestrial Ecotoxicity.
TLP	Tension Leg Platform.
TOE	Ton of Oil Equivalent.
ULO	Urban Land Occupation.

UV Ultraviolet.

WD Water Depletion.

WT Wind Turbine.

Greek Symbols

ΔG Gibbs free energy variation.

ΔH Enthalpy variation.

ΔS Entropy variation.

ρ Density.

η_{ele} Electrolyzer stack efficiency.

η_F Faraday efficiency.

η_V Voltage efficiency.

Roman Symbols

A Rotor disk area.

a Axial induction factor.

C_p Power coefficient.

C_E Specific energy consumption.

f_{H_2} Hydrogen production rate.

D Diameter.

F Faraday constant.

L Liter.

l Length.

m Mass.

P Rotor Power.

P_w Kinetic power of the wind.

Q Heat.

u Wind velocity.

u_∞ Free wind velocity.

V_{cell} Cell voltage.

V_{ohm} Ohmic over voltage.

V_{rev} Reversible cell voltage.

V_{tn} Thermo-neutral voltage.

z Elevation.

Chapter 1

Introduction

1.1 Motivation

The Paris Agreement, signed by almost every nation in the world aims to keep the global temperature rise this century well below 2 ° C above pre industrial levels and to pursue efforts to limit the temperature increase even further to 1.5 ° C [1]. To achieve the targets in the Paris agreement, the global energy system must undergo a profound transformation from largely based on fossil fuels to an efficient and renewable low carbon energy system with a reduction of around 3.5% of CO_2 emissions per year from now until 2050 [2] as shown in Figure 1.1.

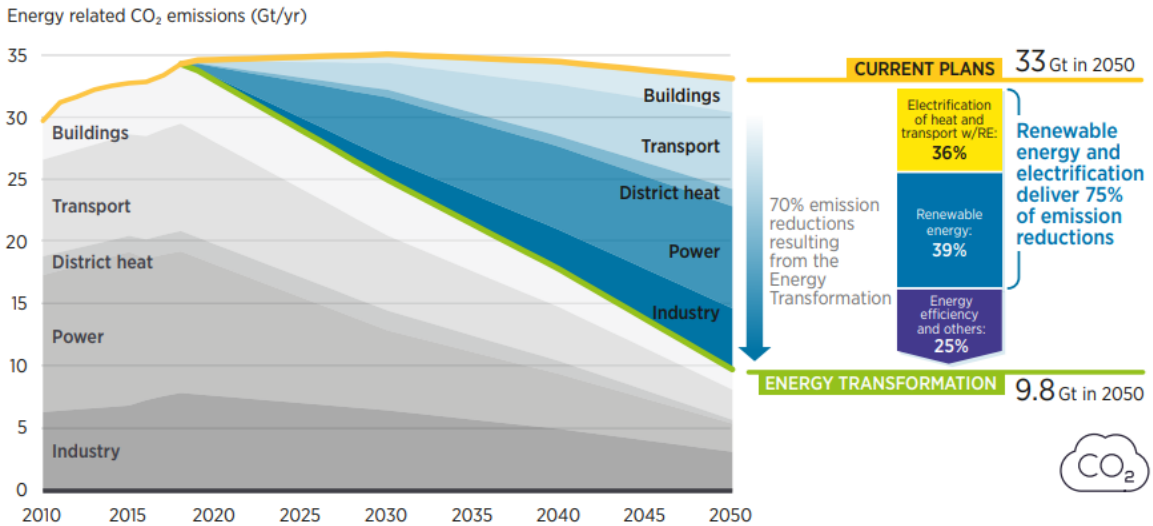

Note: Renewables" implies deployment of renewable technologies in the power sector (wind, solar PV, etc.) and end-use direct applications (solar thermal, geothermal, biomass). "Energy efficiency" contains efficiency measures deployed in end-use applications in the industry, buildings and transport sectors (e.g., improving insulation of buildings or installing more-efficient appliances and equipment). "Electrification" denotes electrification of heat and transport applications, such as deploying heat pumps and electric vehicles.

Figure 1.1: CO_2 emissions reduction from energy transformation compared to the current plans 2010-2050, from [2].

To meet this objective, renewable energy's share of global final energy consumption needs to increase from 18% today to 65% in 2050 and green hydrogen could be the missing link in the energy transition allowing large amounts of renewable energy to be channelled from the power sector into sectors for which electrification is difficult such as transports, buildings and industries [1].

The motivation to study the life cycle of hydrogen production by offshore wind energy in Portugal is threefold:

1. **Portugal pledged to ensure neutrality of its emissions by the end of 2050 as a contribution to the Paris agreement by developing the road map for the carbon neutrality 2050 (RNC2050) [3].**

   Portugal's annual emissions reached the maximum value of approximately $85\,Mt\,CO_2$ in 2005. Since then, the emissions have been decreasing and currently are around $60\,Mt\,CO_2$. But in order to get to the carbon neutrality by 2050, translates on a trajectory of emissions reductions of 45% to 55% by 2030, 65% to 75% by 2040 and 85% to 90% by 2050 compared to 2005 values according to [3] and assuming a carbon sink value in between $9 - 13\,Mt\,CO_2$ as shown in Figure 1.2. By sector, the emissions are distributed by: 25% in energy production, 25% in transport, 23% in industry, 10% in agriculture, 8% in other energy uses and 8% in waste [3].

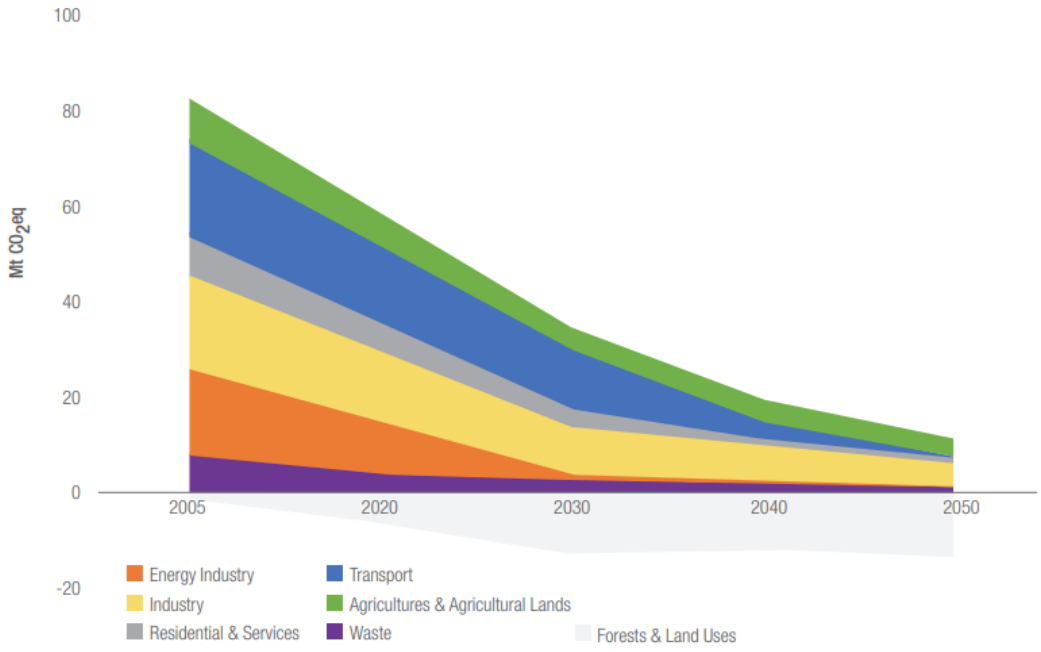

Figure 1.2: Sector contribution of the greenhouse gases (GHG) emissions reduction trajectory by 2050 in Portugal, from [3].

2. **Offshore wind energy production is rapidly growing and technologies are developing.**

   As shown in Figure 1.3, offshore wind power installation has been increasing since 2000 with the first commercial scale offshore wind farm (OWF) commissioned in 2002 in Denmark with an installed capacity of $160\,MW$. By the end of 2019, the world's installed offshore wind capacity

accounted $29\,GW$ [2]. Around 90% of global installed offshore wind capacity is commissioned and operated in the North sea and nearby the Atlantic ocean [2]. According to [4], offshore wind capacity could reach $228\,GW$ by 2030 and by 2050 would increase substantially to $1\,000\,GW$ globally, as innovation continues to develop. Asia would take the lead in the coming decades with more than 60% of global installations by 2050, followed by Europe with 22%, which means $220\,GW$ installed offshore wind power in Europe by 2050. A more ambitious vision, defined by [5] sees an installed capacity of $450\,GW$ only in Europe by 2050, with $9\,GW$ allocated in Portugal. The average offshore wind turbine (OWT) size are constantly increasing. In the beginning of 2000s the average size of an OWT was around $44\,m$ of radius with an output power of $1.6\,MW$. Nowadays, they are on a range of 10 MW with a radius of $164\,m$ and they are expected to grow to an output capacity of $15 - 20\,MW$ by 2030 with a radius of more than $230\,m$.

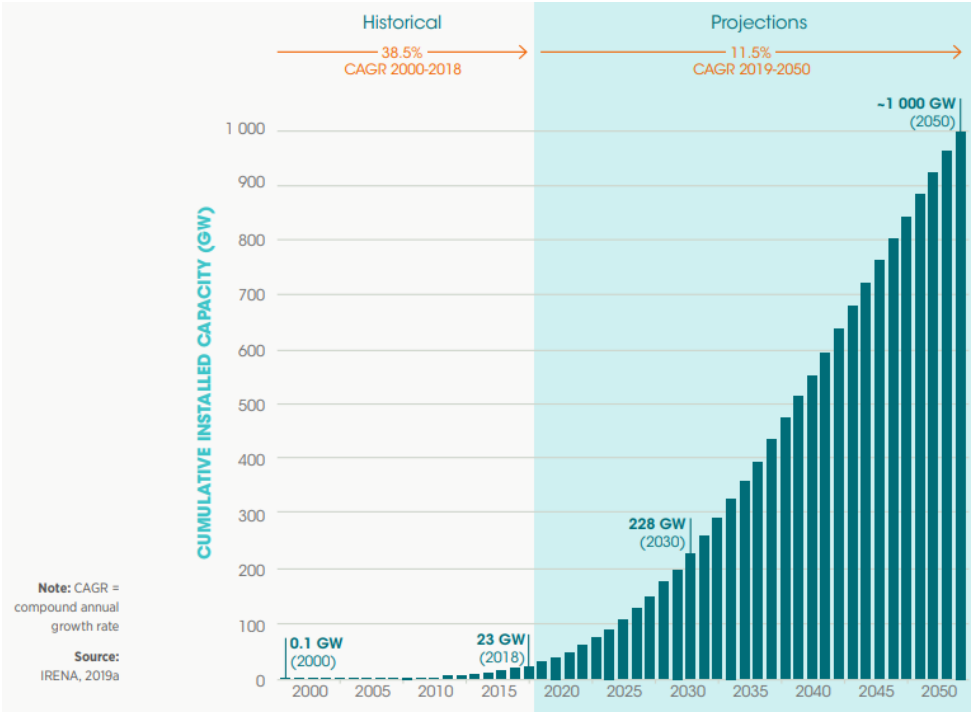

Figure 1.3: OWT cumulative installed capacity 2000-2050, from [6]

3. **Power-to-hydrogen on the global energy transition could be the solution to help decarbonise some of the most fossil fuel dependent sectors.**

   Hydrogen is an energy carrier and not a source of energy, being a complement to the electricity in the energy transition [1]. The hydrogen industry is well established and has decades of experience in industrial sectors. However, currently 96% of hydrogen production is fossil-fuel based, being steam methane reforming (SMR) the most common way of producing hydrogen with methane and coal as source emitting $830\,Mt$ of CO_2 per year and only around 4% of global hydrogen supply is produced via electrolysis [1] as shown in Figure 2.1 a). In figure 2.1 b), the global hydrogen market is presented and is possible to see that its use in the chemical and petrochemical industry is essential with a global share of 54% on the production of ammonia, 35% for the

chemical industry and 6% for a range of applications in the electronics industry [7].

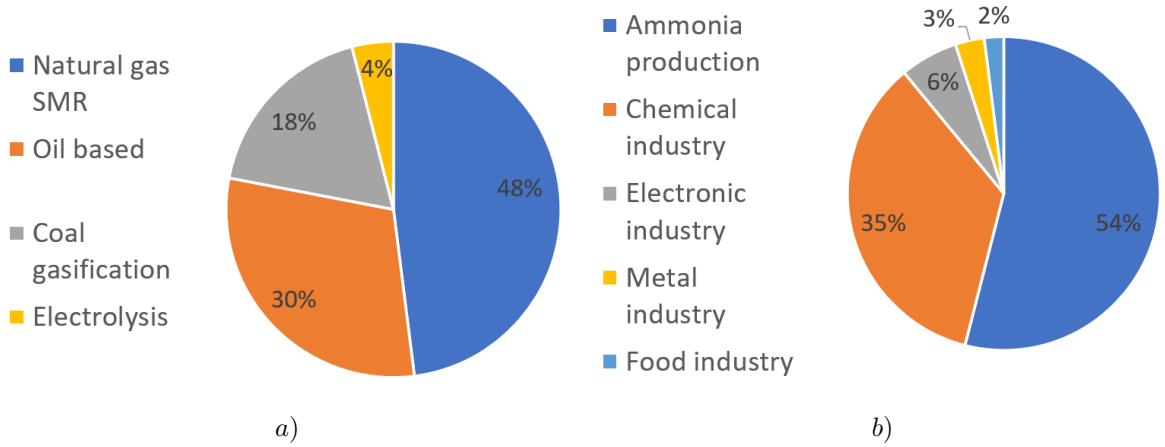

Figure 1.4: a) Shares of production methods for hydrogen worldwide [8], b) Distribution of the global hydrogen market [7].

A colour code nomenclature for hydrogen is used in order to to facilitate this discussion [9]:

- **Grey hydrogen:** is produced with fossil fuels by SMR or coal gasification. This entails substantial CO_2 emissions, which makes these hydrogen technologies unsuitable for a route towards net zero emissions.
- **Blue hydrogen:** is grey hydrogen with carbon capture and storage (CCS). Can be an initial solution while green hydrogen ramps up production and storage capacity to meet the continuous flow requirements. CCS efficiencies are expected to reach between 85-95% at best which means that 5-15% of CO_2 will still be emitted, reducing the CO_2 emissions but doesn't meet the requirements of a net zero future.
- **Turquoise hydrogen [10]:** is an emerging decarbonisation option that is still in pilot stage. Like grey and blue hydrogen, turquoise hydrogen also uses methane as a feed-stock through the process of pyrolysis producing hydrogen and carbon as outputs. However, the carbon is in solid form rather than CO_2. As a result, there is no requirements for CCS and the carbon can even be used in other applications, such as a soil improver or in the manufacturing of certain goods such as tyres.
- **Green hydrogen [11]:** is the hydrogen produced from renewable energy. It is the most suitable for a fully sustainable energy transition with zero emissions. **The most established technology options for producing green hydrogen is water electrolysis fuelled by renewable electricity.** This technology is the focus of this thesis. Green hydrogen production through electrolysis is consistent with the net-zero route and allows the exploitation of synergies from sector coupling, thus decreasing technology costs and providing flexibility to the power systems.

Different energy storage technologies have been proposed in literature [12]:

- **Mechanical energy storage:** flywheel, pumped hydro, gravity and compressed air.
- **Chemical energy storage:** hydrogen, bio fuel and bio diesel.
- **Electrochemical energy storage:** super capacitor and batteries.
- **Superconducting magnetic energy storage.**
- **Cryogenic energy storage:** liquid air energy storage.

The hydrogen from renewable energy has the technical potential to channel large amounts of renewable electricity with the advantage of storing large quantities for long periods of time. When compared to the other technologies mention before, hydrogen storage has better performance as shown in Figure 1.5. So, hydrogen could be the solution to help decarbonise some of the most dependent fossil fuel sectors such as heating, transports and industrial processes such as steel and iron manufacture [1].

With the advancements in power-to-hydrogen technology and the falling of offshore wind costs, along with the changes in policy, this combination could constitute an emerging economically viable business model [11].

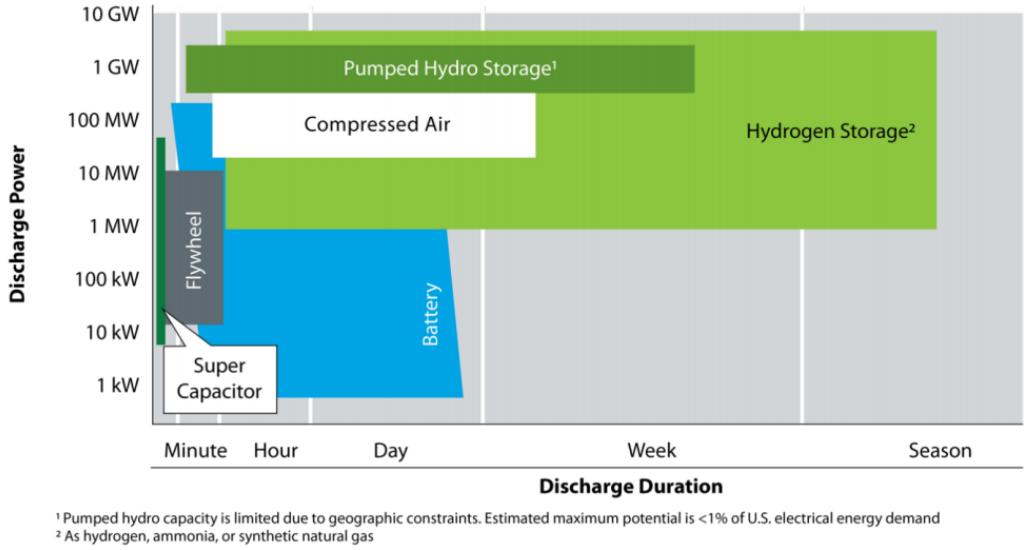

Figure 1.5: Optimal power and discharge-duration characteristics of energy storage technologies, from [13].

Portugal made its policy and intentions very clear, with the publication of the National strategy for hydrogen based on the path and discussion related to the PNEC 2030, RNC2050 and in the draft of the national strategy for hydrogen (EN-H_2) [14], [3] and [15]. This strategy aims to promote the gradual introduction of hydrogen as a sustainable pillar and a more comprehensive strategy of transition to a decarbonized economy. Based on the current national energy system, a set of strategic configurations were determined for the hydrogen value chain [14]:

- **Power-to-power (P2P):** is the stored hydrogen obtained from the excess of renewable electricity which can be reconverted again to electricity through the use of fuel cells.

- **Power-to-mobility (P2M):** is the hydrogen transported or locally produced to provide hydrogen refuelling station (HRS), with particular focus on heavy transportation, railway (on non-electrified lines), taxis, fleets of companies and ships.
- **Power-to-gas (P2G):** is the hydrogen that can be directly injected into the natural gas (NG) grid or converted into synthetic methane via a methanation process.
- **Power-to-industry (P2I):** is the hydrogen that can replace the NG in the industrial sector.
- **Power-to-synfuel (P2Fuel):** is the production of fuels that could be decarbonized, replacing them by synthetic fuels of renewable origin.

1.2 Objectives

The main objective of this thesis is to analyze whether the hydrogen production by offshore wind energy is viable in Portugal from an environmental perspective. This study focus on the mobility sector. The following tasks are proposed:

- Create scenarios to study a realistic case in Portugal of hydrogen production from wind energy to the mobility sector.
- Life cycle assessment (LCA) using the SimaPro software. For the life cycle analysis, the RECIPE method was used and two impact categories were considered: midpoint and endpoint.
- Quantify the CO_2 emissions of the H_2 from offshore wind energy production and compared with other energy sources.
- Regarding mobility sector, compare fuel cell electric vehicles (FCEV) CO_2/km emissions with internal combustion engine (ICE) vehicles.

1.3 Thesis Outline

This thesis is divided in five main chapters:

1. **Chapter 1 - Introduction:** is dedicated to introducing the work, main motivations and objectives to be attained.
2. **Chapter 2 - State of the art:** of the OWF, different types of hydrogen production, different type of compressors and hydrogen storage technology are covered.
3. **Chapter 3 - Methodology:** the methods used in the dissertation in order to achieve the goals proposed are presented in this chapter.
4. **Chapter 4 - Results and discussion:** the results of the life cycle impact assessment (LCIA) of hydrogen production are reported, analysed and commented.
5. **Chapter 5 - Conclusion:** the main conclusions of the thesis, final remarks and the future work to be developed are discussed.

Chapter 2

State of the Art

2.1 Current Situation and Projects of Hydrogen Production

Green hydrogen production is a topic which acquires more and more relevance as the concerns about CO_2 emissions grow. Today, around $120\,Mt$ of hydrogen are produced each year of which $80\,Mt$ is pure hydrogen and the other $40\,Mt$ is mixed with other gases [6]. IRENA's renewable energy road map (REmap) analysis indicates a 6% hydrogen share of total final energy consumption by 2050, while the Hydrogen Council in its road map suggests that a 18% share can be achieved by 2050 [6].

The number of announced projects has increased drastically in the last years, as it did with their size. In 2015 the average announced proton exchange membrane water electrolysis (PEMWE) project was around $1\,MW$, in 2020 its capacity multiplied up to $20\,MW$ and for the next years, projects in the GW range have already been announced [16].

The importance of H_2 for the coupling of renewable energy sources (RES) is of great importance since the energy systems are advancing towards sustainable energy generation in the long term, as already stated in the introduction of this thesis, with the policies of some of the major institutions worldwide with clear objectives to cut its emissions to zero by 2050.

Policy support is starting to grow as policymakers accept this energy vector as a key enabler in order to achieve the climate targets. H_2 is already in the energy road maps of numerous countries worldwide [16]. The foundation of the clean H_2 alliance by the European Union (EU) has the clear goal of bringing investors together with governmental, institutional and industrial partners in order to identify technological needs, investment opportunities and regulatory barriers. This strong momentum green H_2 is experiencing is supported by the great projections regarding its use in many different applications in the medium to long term, being expected to provide a clean and cost competitive alternative for well-established applications such as fuel for transportation or industry and feed stock for the chemical industry and new applications such as seasonal energy storage [16].

Nevertheless, H_2 must overcome several challenges to allow its widespread adoption and cost reduction to achieve cost competitiveness with fossil fuel alternatives. Some of the most significant obstacles H_2 supply chain is facing are the lack of infrastructure for transportation, storage and delivery [16]. Also,

the lack of an established value chain for the production of the necessary equipment to produce, handle and deliver H_2 is causing that equipment prices remain higher than what is needed in order to bring down the H_2 production costs. Eventually, there are issues with the absence of international regulation, which creates uncertainty for all the different stakeholders, specially investors [16].

The biggest project of hydrogen production from offshore wind energy is the AquaVentus which is a $10\,GW$ consortium that is currently made up of 27 leading international companies, organisations and research institutions [17]. The project family surrounding the AquaVentus initiative includes numerous sub-projects along the value chain from hydrogen production in the North Sea to transport to buyers on shore.

HyDeal Ambition expects to build $95\,GW$ worth of solar capacity to power $67\,GW$ capacity of electrolyzers by 2030 delivering $3.6\,Mt/year$ of green hydrogen to users in the energy, industry and mobility sectors via the gas transmission and storage network [18]. The main goal is to deliver green hydrogen across Europe at €1.5/kg before 2030 and to be cheaper than grey hydrogen.

Table 2.1 summarizes some of the projects for green hydrogen production in different countries with the indicative of the strong interest worldwide in green H_2 with many more pilot and early-commercial projects that show a clear trend towards larger electrolyzers and technological improvements:

Table 2.1: International projects for green hydrogen production in different countries. Symbol † refers to a project where the electricity comes exclusively from wind.

Country	Projects
Germany [6]	Energy Park Mainz - $6\,MW$ PEM electrolyzer (2017) †
	Projects approved by the government in 2019:
	Element eins - $100\,MW$ electrolyzer †
	EnergieparkBL - $35\,MW$ electrolyzer †
	GreenHydroBL - $35\,MW$ electrolyzer
	HydroHub Fenee - $17.5\,MW$ electrolyzer
Netherlands [19]	NortH2, $3-4\,GW$ of wind to produce 800 $kt\,H_2/year$ †
France [6]	Les Hauts de France - Five $100\,MW$ electrolyzers (2021) †
UK [20]	Gigastack - $100\,MW$ PEM electrolyzer from offshore wind †.
Canada [6]	Air Liquide - $20\,MW$ PEM electrolyzer powered by renewables.
Australia [6]	Asian Renewable Energy Hub - 15 GW electrolyzers (2027/28)
	HyEnergy Zero Carbon Hydrogen - $8\,GW$ electrolyzers
	H2-Hub Gladstone - $3\,GW$ electrolyzers
China [6]	Beijing Jingneng Inner Mongolia - $5\,GW$ hybrid solar and wind to produce $500\,kton\,H_2$.
	Yellow Sea - $2\,GW$
Japan [6]	FH2R - $10\,MW$ electrolyzer from a $20\,MW$ solar PV project.

2.1.1 Portugal Hydrogen Projects

Portugal is still far behind in the hydrogen implementation. But, there is a strong interest from the Portuguese government in the implementation of hydrogen in the value chain of the country. The biggest

projects in Portugal are [21]:

- **H2Sines** which aims to replace the coal power plant in Sines by an hybrid wind and PV park with centralized green hydrogen production to be transported in gaseous state by ship to northern Europe and sold in Netherlands and Germany, but looks like it's not going forward because according to the more recent news, EDP is stepping up of the project.

- **H2Enable - The Hydrogen Way for Our Chemical Future** is a Bondalti's €2.5 billion plan in Estarreja with development and implementation until 2040. The project is based on four phases and assumes the materialization of various financial conditions, technological evolution, involvement of partners and development of the national and European hydrogen market. The project aims to produce green hydrogen for direct sale on the market and for the manufacture of green ammonia.

- **Comboios de Portugal (CP) with hydrogen trains** which aims the conversion of CP diesel trains to hydrogen units, avoiding the need to electrify several lines. The project has a value of €250 million [21].

- **Trustenergy** which owns the Tapada do Outeiro NG power plant in Gondomar, intends to produce hydrogen and may even promote the decarbonization of its own combustion process thought the mixture of green hydrogen in the NG.

Currently, the majority of hydrogen produced in Portugal comes from NG and it is used almost fully in the industrial sector. About $65\,kt$ $(187\,ktoe)$ were produced in 2018 in Portugal. This value fell 7.7% compared to 2017 values, as a result of a reduction in refining activity, also seen in the consumption of hydrogen as seen in Figure 2.1 a). This decrease was also registered in the use of NG for the production of hydrogen, with a drop of 10.6% [15] which is possible to verify in the Figure 2.1 b).

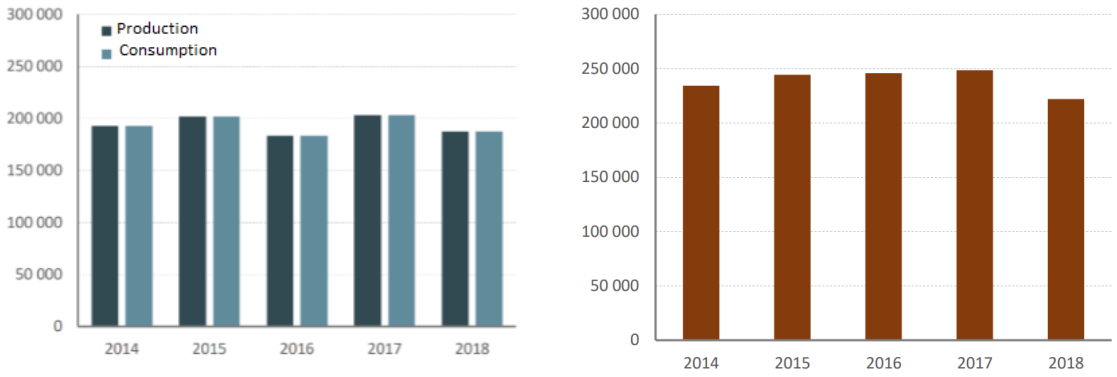

$a)$ $b)$

Figure 2.1: a) Evolution of hydrogen production and consumption (toe), b) Evolution of NG consumption for the production of hydrogen (toe), from [15].

2.2 Offshore Wind Energy

In this thesis, the source of electricity to produce hydrogen is the offshore wind energy. First of all when the production is high and demand is low, **is possible to take advantage of the curtailment effect which is a loss of potentially useful energy.** The wind turbines aren't working and instead of the energy being dissipated because there is no capacity to store that energy, this wind energy can be used to produce hydrogen as a form of storing energy to be used later. Secondly, is considered an OWF because compared with a PV farm there is no need for huge areas of land with a lot of deforestation and compared with onshore there is better conditions to extract energy from the wind in offshore with less turbulence and greater average velocity. It's used a OWF instead of a PV farm because Finally the wind energy is a renewable source of energy.

An **OWF** is composed by **wind turbines**, **inter array cables**, **offshore substation**, **transmission system** and an **onshore substation** as shown in Figure 2.2 [11].

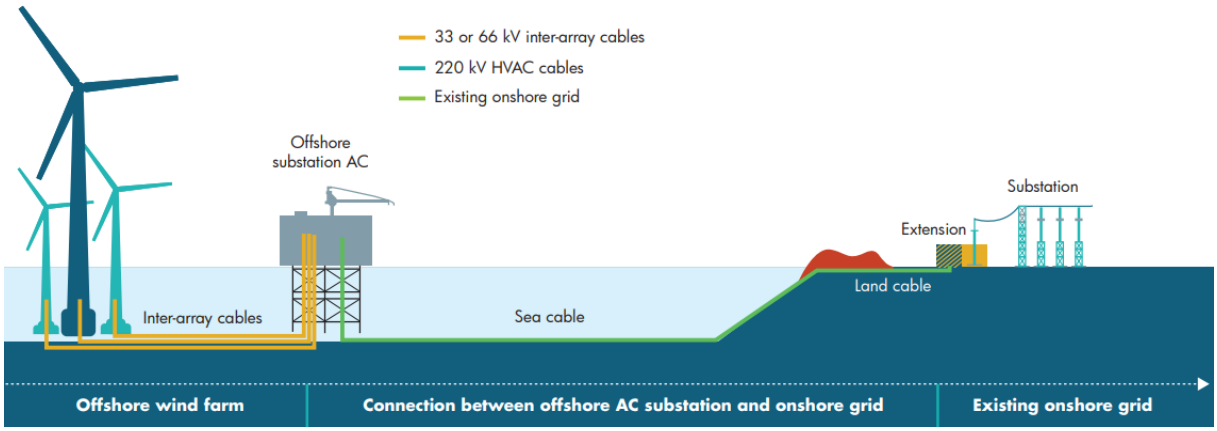

Figure 2.2: Components of an OWF [11].

2.2.1 Wind Turbine (WT)

A WT consists of a **mechanical device specifically designed to extract kinetic energy from the wind and convert part of it into useful mechanical energy**. The most commonly produced and used WT is the horizontal axis wind turbine (HAWT). The main components of a HAWT is **the rotor, nacelle, tower and foundation**. HAWT working principle is the following: as the wind flows across the blades, the air pressure on one side of the blade decreases and a lift force is produced, which creates a torque that drives the main shaft. The electro-mechanic conversion happens due to the fact that the main shaft is connected to the generator through a drive train [22]. A WT is characterized by its power curve, which expresses the output power in function of the wind speed.

2.2.1.1 Wind turbine operating regions

The performance of a given WT can be related to three key points on the velocity scale [23]:

- **Cut-in speed**: is the minimum wind speed at which the machine will deliver useful power.
- **Rated wind speed**: is the wind speed at which the rated power (generally the maximum power output of the electrical generator) is reached.
- **Cut-out speed**: is the maximum wind speed at which the turbine is allowed to deliver power (usually limited by engineering design and safety constraints)

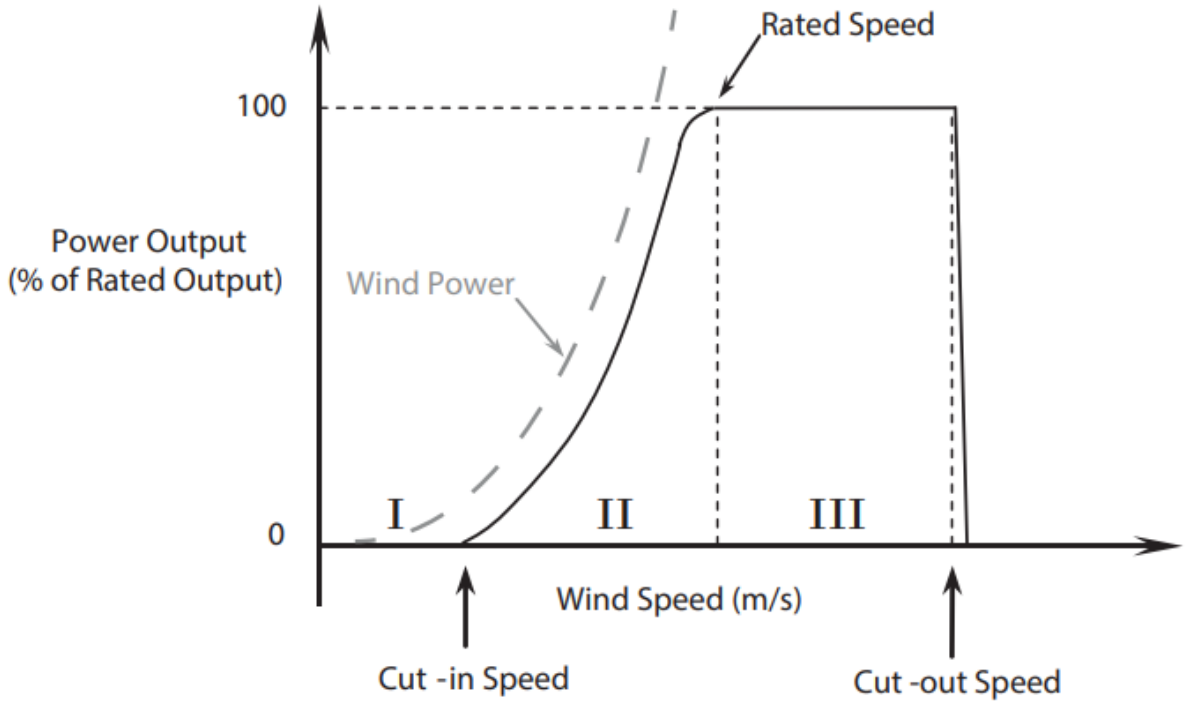

Figure 2.3: Typical WT power curve, from [23].

The available power in the wind due to its kinetic energy can be derived by evaluating the mass of wind flowing through an imaginary rotor disk of area A, which is swept by the rotor blades and it's given by the well-known expression 2.1 [22]:

$$P_w = \frac{1}{2}\rho A u^3 \tag{2.1}$$

where P_w (W) is the instantaneous kinetic power of the wind available at surface of area $A(m^2)$, $\rho(kg/m^3)$ is the air density which is assumed to be constant with a standard sea-level density of $1.225\,kg/m^3$ and $u(m/s)$ is the wind velocity.

To evaluate the rotor performance in extracting energy from wind, the power coefficient C_P, which is defined as the dimensionless ratio of the power extracted by the rotor to the kinetic available power in the wind is used in equation 2.2:

$$C_P = \frac{Rotor\ Power}{Power\ of\ the\ wind} = \frac{P}{\frac{1}{2}\rho A u^3} \tag{2.2}$$

The Power and Cp curves (in this thesis for the Vestas V164 $8MW$ turbine) were obtained using excel as shown in Figure 2.4 in order to obtain the annual energy produced (AEP) of each WT and for the OWF together with the weibull probability distribution function as shown later in equation 2.13.

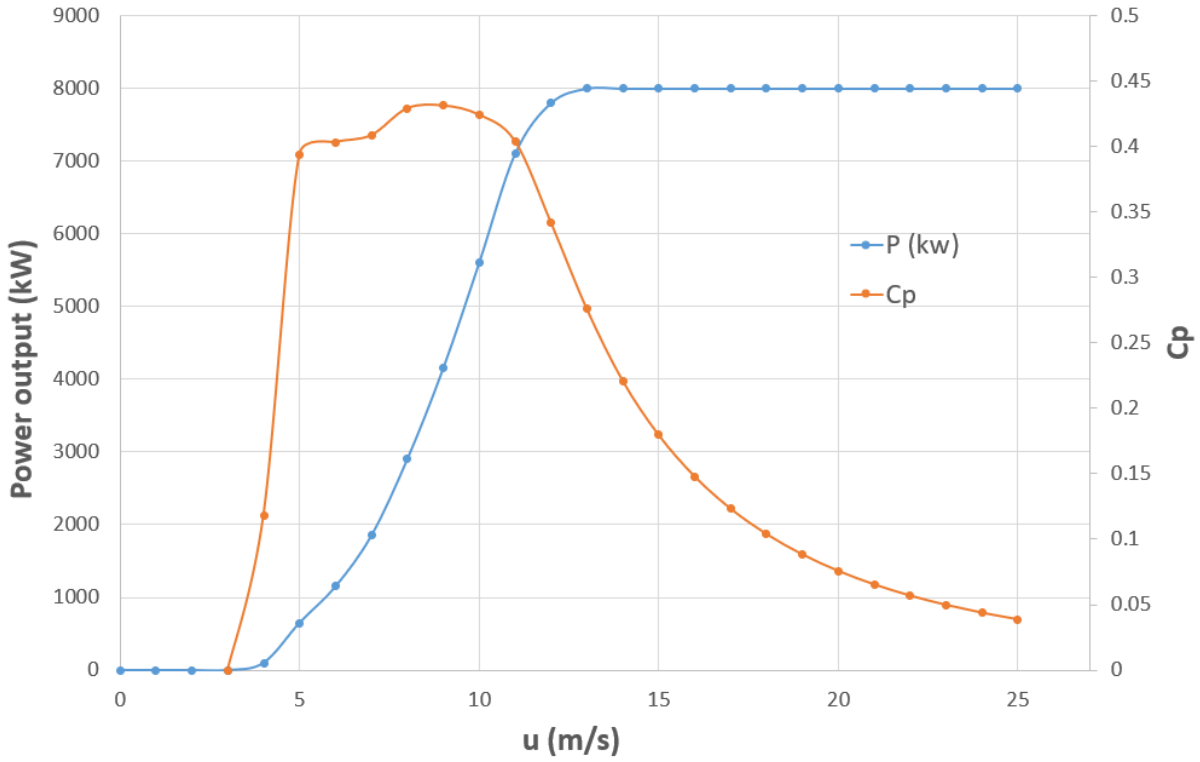

Figure 2.4: Power and Cp curve of Vestas 164 $8\,MW$.

The overall turbine efficiency is a function of both the rotor power coefficient C_P and the mechanical efficiency η_{mech} (including drive train, generator and all the electrics) of the WT [22]. The η_{mech} is considered to be 95% according to [22]:

$$\eta_{overall} = \eta_{mech}.C_P = 0.95C_P \tag{2.3}$$

Thus:

$$P_{elec} = \frac{1}{2}\rho A u^3(\eta_{mech}.C_P) = \frac{1}{2}\rho A u^3(0.95C_P) \tag{2.4}$$

2.2.1.2 Offshore Wind Substructure Technology

There are two main technologies of substructures for turbines: bottom-fixed and floating platforms as shown in figure 2.5.

The type of used substructure is directly related with the water depth where they are located. There are three main levels of water depths:

- **Shallow waters:** $< 30\,m$ depth, where **monopile** and **gravity base** bottom-fixed foundations are used. **Gravity base foundations** are typically situated in water depths less than $10\,m$, they are

made of concrete and are appropriate for the clay and sandy soil conditions. **Monopile structure** consists of a one single steel tube pile and they are considered the most economic for water depths until $30\,m$ [24].

- **Transitional waters:** $30 - 50\,m$ depth where **tripod** and **jacket** bottom-fixed foundations are the best economical option [25].

- **Deep water:** $50 - 200\,m$ depth use floating platforms such as **spar**, **semi-submersible platform** and **tension leg platform (TLP)**.The advantages and disadvantages of each of the floating technologies are presented in table 2.2.

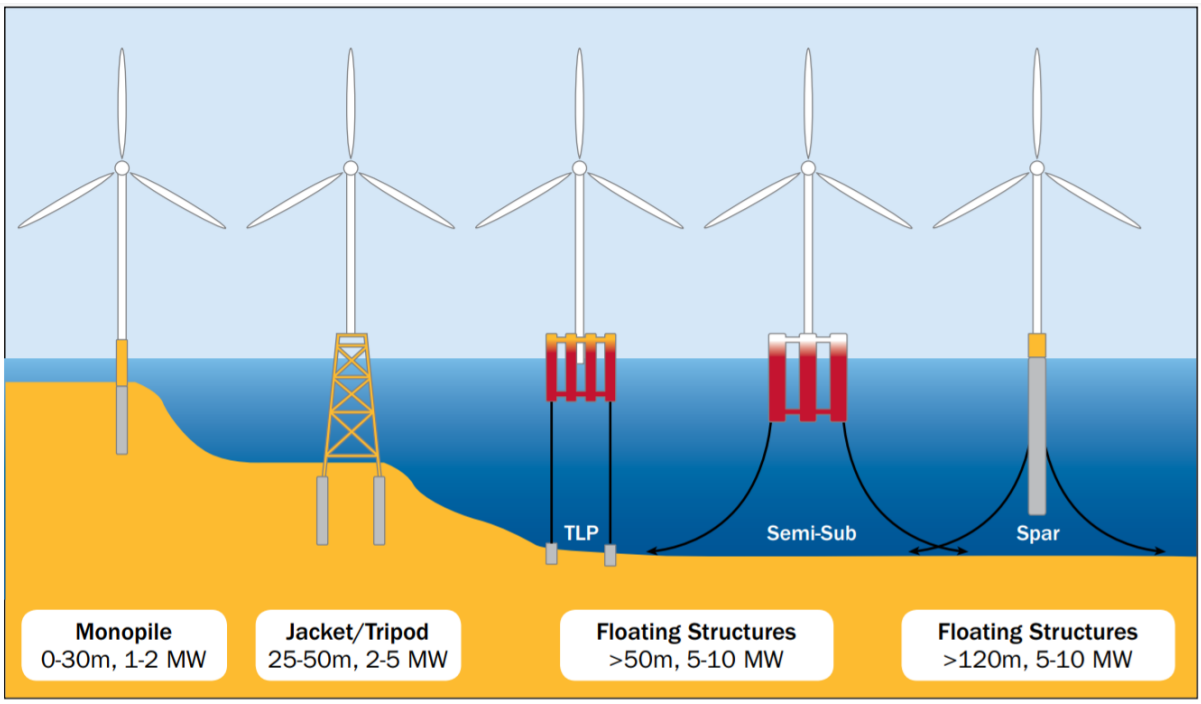

Figure 2.5: Offshore wind foundations, from [26].

As the Portuguese coast has a shore profile with a very accentuate slope, the floating technologies are the more appropriate. The WindFloat platform is a floating semi-submersible and triangular foundation, but as there is no freely available data of the WindFloat Atlantic semi-submersible platform, the chosen model was the UMaine VolturnUS-S reference platform (semi-submersible type) [27] as shown in Figure 2.6. It's possible to install the WT of any manufacture without having to make changes to the turbine or the platform, is extremely stable resulting from water ballast that doubles the mass of the structure (static stability) and stabilization plates at the base of the columns that significantly limit and attenuate the movements of the structure (dynamic stability) and the construction is done entirely on land including the assembly of the turbines which leads to a simplified installation process, avoiding difficult and expensive work on the sea [28].

Table 2.2: Advantages and disadvantages of floating foundation technologies [29].

Technology	Advantages	Disadvantages
Spar buoy	Tendency for lower critical wave-induced motions. Simple design. Lower install mooring cost.	Offshore operations require heavy-lift vessels and currently can be done only in relatively sheltered deep water. Needs deeper water than other concepts.
Semi-submersible	Constructed onshore or in a dry dock. Transport to site using conventional tugs. Lower installed mooring cost.	Tendency for higher critical wave-induced motions Tends to use more material and larger structures. Complex fabrication compared with other concepts.
Tension leg platform	Tendency for lower critical wave induced motions. Low mass. Can be assembled onshore.	Harder to keep stable during transport and installation. Higher installed mooring system. Impact of possible high frequency's dynamic effects on turbine.

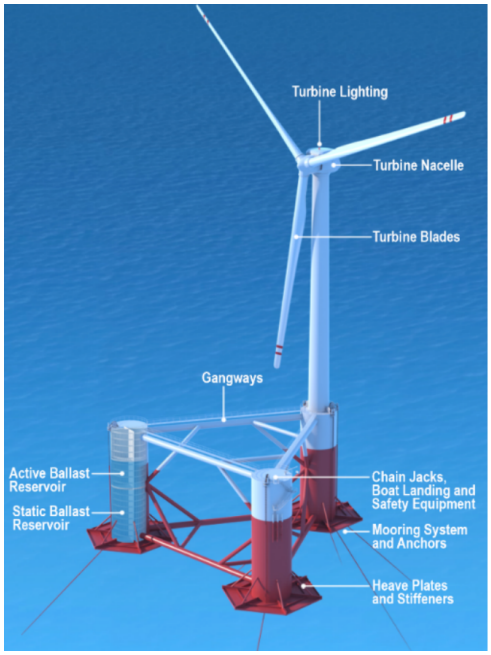

Figure 2.6: OWT and floating foundation, from [28].

2.2.2 Inter Array Cables

The inter array cables connect the WTs within the array to each other and to an offshore substation if present. The turbine generator has a low voltage (usually, less than $1\,kV$) which is not high enough for direct interconnection to other turbines, so a turbine transformer steps up the voltage to a range from $10 - 66\,kV$ for cable connection [30]. The cables are buried $1 - 2\,m$ underground and connect to the transformer of the next turbine in the string. The power carried by cables increases as more turbines are connected and the cable voltage may increase to handle the increased load. **The amount of cabling required depends on the layout of the farm, the distance between turbines and the number of turbines [30].** In Figure 2.7 is possible to see the relationship between the inter array cable length in km as a function of the capacity in MW of the OWF.

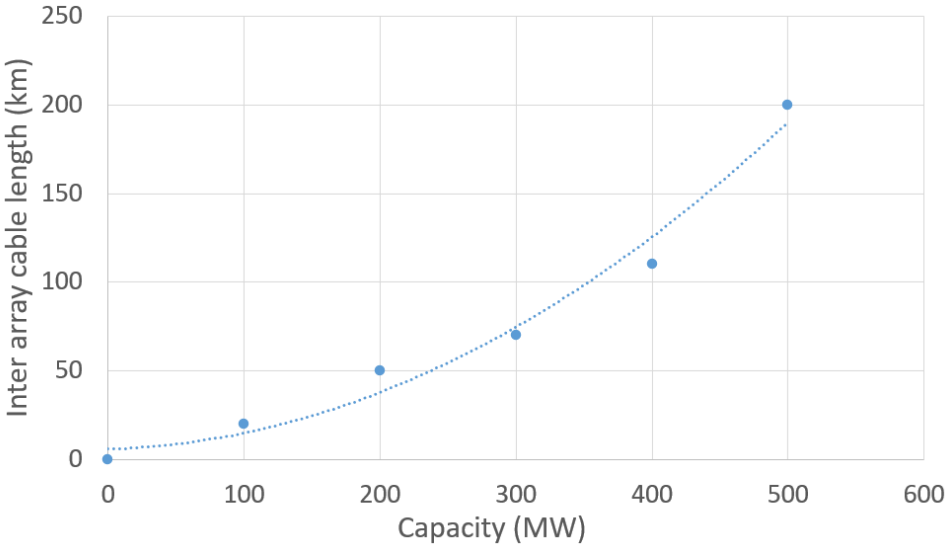

Figure 2.7: Relationship between inter-array cable length and OWF capacity, adapted from [30].

Inter array cables weight density is around $20 - 40\,kg/m$ according to [30]. The mass density of the inter array cable is going to be considered as $30\,kg/m$ or $30\,ton/km$. The mass of cables in tons can be expressed by equation 2.5:

$$m_{cables} = 30 \times (0.0007P^2 + 0.02P + 6.07) \tag{2.5}$$

where P is the power of the OWF in MW and 30 is the weight density in ton/km.

2.2.3 Offshore Substation

The purpose of an offshore substation is to minimize transmission losses by transforming the voltage of the electricity generated at the WTs to a higher voltage suitable for transmission to shore, usually from $33 - 66\,kV$ to $155\,kV$. The substation is sized with the appropriate power rating (MVA) for the project capacity and steps up the line voltage from the collection system voltage to a higher voltage level usually that of the point of interconnection (POI) [30]. Power that flows on higher voltage lines will minimize line loss and increase the overall efficiency of the system.

All OWFs require substations but not all substations are located offshore. In Figure 2.8, an offshore substation is presented. The need for offshore substations depends on the power generated and the distance to shore which determines the trade offs between capital expenditures and transmission losses. Substations are positioned within the wind farm at a location that minimizes export and inter array cable distance [30].

The mass in tons of the topside of the offshore platform is expressed as a linear function of the rated capacity of the wind farm (P) in MW as obtained from a curve fit to data from Kaiser and Snyder166 given by equation 2.6 [31]. Kaiser and Snyder also give an empirical expression for the mass of the jacket foundation in tons as a function of water depth (h) and OWF rated power (P) presented in equation 2.7 from [30].

$$m_{topside} = \frac{P}{0.133} \tag{2.6}$$

$$m_{jacket} = 16.042.h^{0.19}.(m_{topside})^{0.48} \tag{2.7}$$

where P is the power of the OWF in MW and h is the depth at the location of the offshore substation in meters.

Figure 2.8: Offshore Substation, from [32].

2.2.4 Transmission System

The transmission system or export cable is responsible for exporting the energy produced by the WTs and gathered by the collection system to the onshore substation. There are several types of technology that can be used and the factors that influence their selection are the amount of power to be transmitted, the distance of transmission and economic reasons [33]:

- **Medium voltage alternating current (MVAC) system** merges the collection into the transmission as the cables that gather energy are the same ones that export it to shore. For a $33\,kV$ collection voltage with powers levels up to $200\,MW$ to be transmitted up to $20\,km$, this option is the most inexpensive one.

- **High voltage alternating current (HVAC) system** is the most common option for transmission distances above $20\,km$ and the most economical one for transmitted distances up to $70-80\,km$ where the voltage level must be raised typically in an offshore substation, in order to avoid the massive energy losses that result from the cable's capacitive current.

- **High voltage direct current (HVDC) system** is the best option when there is the necessity to transmit an enormous amount of power through very long distances (typically beyond $80-100\,km$).

Export cables generally weight between $50-100\,kg/m$ according to [30]. Figure 2.9 shows the relation between the cost of the systems as a function of the distance to shore. In this thesis, the best option is an HVAC system because the OWFs location are not going to be greater than $50\,km$ and as shown in Figure 2.9 is possible to see that for distances up to $50-80\,km$ HVAC is the more cost effective technology.

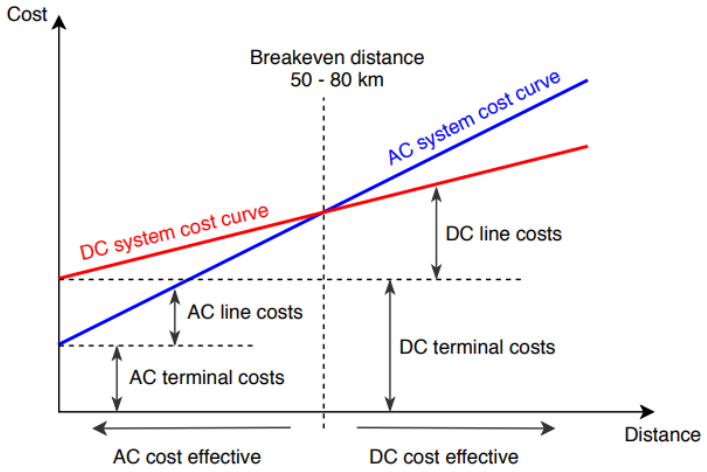

Figure 2.9: HVDC vs HVAC, from [34].

2.2.5 Wind Resource

For the analysis of the energy production behavior, it's necessary to take into account the external wind conditions of the site of production.

2.2.5.1 Wind at farm's location

Portugal has a good offshore wind resource that can be explored, mainly in the north of the country. In order to help policymakers, planners and investors identify high-wind areas for wind power generation, the global wind atlas (GWA) which is a web-based application developed by the Technical University of Denmark (DTU Wind Energy) and the World Bank Group [35] is a tool that can be used.

The OWF location for this thesis is considered to be the same as the Winfloat Atlantic located $20\,km$ off the coast of Viana do Castelo. According to the GWA, the sites average wind speed ($\overline{u}$) at $100\,m$ height is $8.37\,m/s$ [35]. A more detailed average wind speed data (hourly vs. monthly) and a frequency rose of the wind speed direction in the site are given in Figure 2.10. Seasonally, the highest $\overline{u}$ is achieved on Summer afternoons but Winter months present the tendency for higher $\overline{u}$ throughout the day. Autumn is the season with lower $\overline{u}$ values. Daily, there is a tendency for higher $\overline{u}$ in the afternoon and for lower $\overline{u}$ in the morning as shown in Figure 2.10 a). From the wind rose map in Figure 2.10 b), a more frequent wind direction from the North can be noted [35].

At a given point in space, wind velocity vector can be decomposed into:

$$u(t) = \overline{u} + u'(t) \tag{2.8}$$

where $\overline{u}$ is the average wind speed and u' is the component that describes the variation of velocity.

When the data of the average wind speed is not given for rotor's height, it's necessary to adjust the value to the right level. So the power law is used which is defined by equation 2.9:

$$\overline{u}(z) = \overline{u}(z_{ref})(\frac{z}{z_{ref}})^{\alpha} \tag{2.9}$$

where z is the rotor's level, z_{ref} is the measure data's level and α the exponent coefficient that depends on the surface roughness.

The turbulence intensity (I) is related with the average wind speed $\overline{u}$ and the variation of velocity u' by the expression 2.10:

$$I = \frac{\sigma}{\overline{u}} = \frac{u'(t)_{rms}}{\overline{u}} \tag{2.10}$$

where σ is the root square meter (RMS) of the variation of velocity $u'(t)$. So, when the $u'(t)$ increases, indicates a higher level of turbulence. The roughness of the ground and the distance to the ground also have impact on the turbulence. To define the turbulence in offshore conditions, unless site-specific full-scale models are available, one of the main models is the Kaimal spectral model, according to IEC 61400-1 and IEC 61400-3 standards. Although frequently used for offshore conditions, Kaimal spectral model was developed in a flat and homogeneous onshore site, representing the atmospheric turbulence [36].

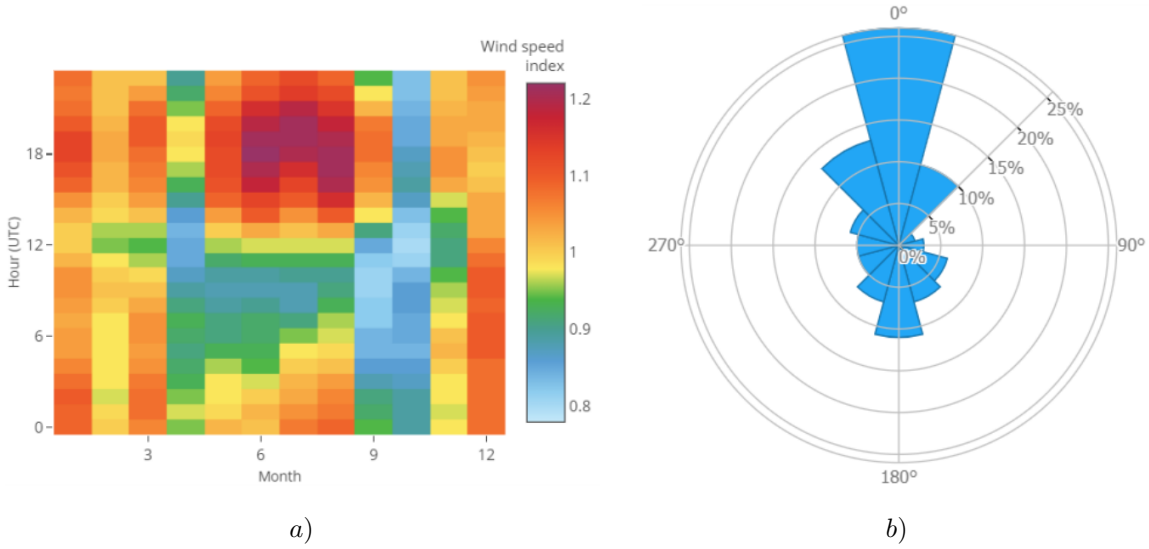

$a)$ $b)$

Figure 2.10: a) Average wind speed map at Viana do Castelo [35], b) Average frequency wind direction in Viana do Castelo [35].

2.2.5.2 Energy production estimation

Wind profiling

In order to proper develop a wind energy project, it's essential to have a good understanding of how the wind behaves on the location reserved for the installation of the wind farm. Several approaches can be taken, from the utilization of a wind atlas or establishment of a meteorological mast at the site. In a pre-project phase, it's useful to have a mathematical tool as a wind data that can describe the quasi-stationary wind. The two commonly used probability distributions in wind data analysis are the Rayleigh and Weibull distribution which describes the likelihood that certain values of wind speed will occur. **In this thesis, the Weibull distribution is considered.** The probability distributions are generally characterized by probability density function (f(u)) and a cumulative density function (F(u)) [33].

The probability density function f(u) and cumulative density function F(u) of Weibull distribution is given by the equations 2.11 and 2.12 [33].

$$f(u) = \frac{ku^{k-1}}{c^k} exp[-(\frac{u}{c})^k] \tag{2.11}$$

$$F(u) = 1 - exp[-(\frac{u}{c})^k] \tag{2.12}$$

where $u\,(m/s)$ is the wind speed, $c\,(m/s)$ the scale factor and k the shape factor. The values of c and k were taken from [37] using the Windgrapher software and are $9.138\,m/s$ and 2.233 respectively. For the calculations of the the wind profiling in this thesis, it was used the Weibull probability density distribution function as shown in Figure 2.11:

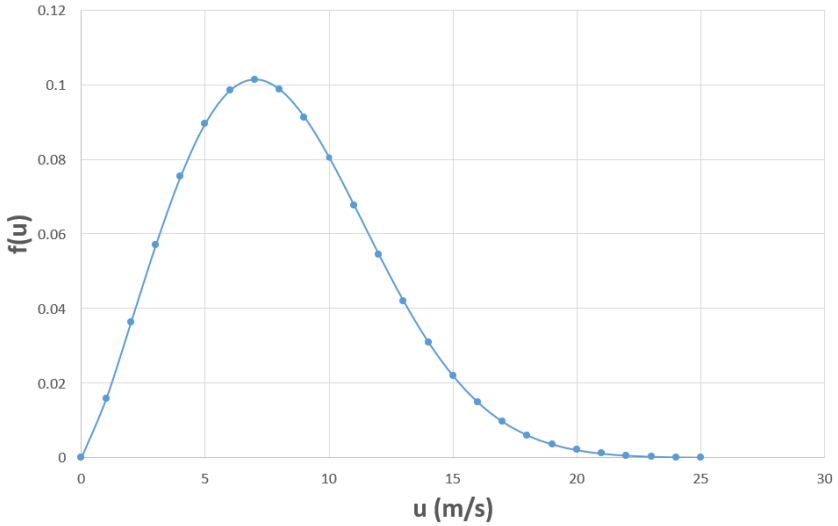

Figure 2.11: Weibull probability density function in Viana do Castelo coast at 120 m height.

The AEP of one WT is obtained by the expression 2.13:

$$AEP_{WT} = availability \times \eta_{mech} \int_{u_{CI}}^{u_{CO}} P(u).f(u)du = 0.9215 \times \int_{u_{CI}}^{u_{CO}} P(u).f(u)du \tag{2.13}$$

where u_{CI} and u_{CO} stands for cut-in velocity and cut-out velocity respectively, P is the rotor power and f is the weibull probability density function. The availability was considered to be 97% according to [38] and η_{mech} is 95% as seen before, which is 92.15% as shown in equation 2.13.

The AEP for all the OWF is shown in equation 2.14:

$$AEP_{OWF} = \eta_{OWF}.N_{WT}.AEP_{WT} = 0.86N_{WT}.AEP_{WT} \tag{2.14}$$

where N_{WT} is the number of WTs in the OWF and η_{OWF} is the efficiency of the OWF including the wake effects and the cable losses. In the calculation model 4% transmission losses and 10% wake losses [39] were considered, so the η_{OWF} used in this thesis is 86%.

The capacity factor (CF) of a WT at a given site is defined as the ratio of the energy actually

produced by the turbine to the energy that could have been produced if the machine ran at its rated power over a given time period as shown in equation 2.15 :

$$CF = \frac{AEP_{WT}}{P_{max}.8760} \tag{2.15}$$

where P_{max} and AEP_{WT} are the rated power and the AEP of one WT respectively and 8760 refers to the number of hours per year.

In table 2.3 is presented the calculations of the AEP_{WT} and AEP_{OWF}.

Table 2.3: AEP calculation for the Vestas $8\,MW$ WT.

$u(m/s)$	$f(u)$	$F(u)$	$Hours/year$	P **(**kw**)**	Cp	**Energy (**MWh**)**
0	0	0	0	0	0	0
1	0.0159	0.0071	138.996	0	0	0
2	0.0363	0.0331	318.184	0	0	0
3	0.057	0.0798	499.219	0	0	0
4	0.0753	0.146	660.397	100	0.118	66.039
5	0.090	0.229	785.162	650	0.394	510.355
6	0.098	0.324	862.617	1150	0.403	992.009
7	0.101	0.424	888.412	1850	0.409	1643.562
8	0.0987	0.524	864.801	2900	0.429	2507.922
9	0.091	0.62	799.66	4150	0.431	3318.588
10	0.08	0.706	704.654	5600	0.424	3946.064
11	0.068	0.78	592.985	7100	0.404	4210.192
12	0.0544	0.84	477.218	7800	0.342	3722.302
13	0.042	0.888	367.623	8000	0.276	2940.981
14	0.031	0.925	271.247	8000	0.221	2169.978
15	0.0219	0.951	191.767	8000	0.18	1534.137
16	0.0148	0.970	129.935	8000	0.148	1039.481
17	0.0096	0.981	84.386	8000	0.123	675.084
18	0.006	0.989	52.53	8000	0.1039	420.238
19	0.0036	0.994	31.341	8000	0.088	250.732
20	0.002	0.997	17.921	8000	0.076	143.369
21	0.001	0.998	9.819	8000	0.065	78.555
22	0.0006	0.999	5.155	8000	0.0569	41.238
23	0.0003	0.9996	2.592	8000	0.0498	20.737
24	0.0001	0.9998	1.248	8000	0.0438	9.986
25	6.6E-05	0.9999	0.576	8000	0.039	4.605
26	0	1	0.254	0	0	0
AEP WT (TWh)						28.73
N						70
AEP OWF (TWh)						1677.88
CF						0.41

2.3 Hydrogen Production

In this section, a background about the hydrogen production is made.

The principle of water electrolysis is to split water into hydrogen and oxygen through the application of direct current (DC) electrical energy [40] as presented in equation 2.16. The electrical energy in this thesis is produced from the wind energy which is a renewable source of electricity.

$$H_2O(l) + Energy \longrightarrow H_2(g) + \frac{1}{2}O_2(g) \tag{2.16}$$

The theoretical energy needed in order to produce $1\,kg$ of H_2 is $39.36\,kWh$ or $142\,MJ$ (HHV) and $33.3\,kWh$ or $120\,MJ$ (LHV) [16]. From stoichiometric results, $9\,kg$ of water are needed to produce $1\,kg$ of H_2, producing $8\,kg$ of O_2 as a by-product [41] and according to the mass balance of equation 2.16.

Hydrogen is the simplest atom and its molecule (H_2) is the most abundant in the universe. However, to generate pure hydrogen, energy must be used. The most relevant physical properties of hydrogen are presented in Table 2.4:

Table 2.4: Physical proprieties of hydrogen [16].

Property of H_2	**Value**
Density (gas) at (0° C, $1\,bar$), $\rho(kg/m^3)$	0.089
Density (liquid) at (-253° C, $1\,bar$), $\rho(kg/m^3)$	70.79
Boiling Point at 1 bar (K)	20.25
LHV (kWh/kg)	33.3
HHV (kWh/kg)	39.4
Auto ignition temperature (K)	844.15
Ignition energy (MJ)	0.02
Ignition range (%)	477

The main three technologies for water electrolysis can be classified based on their electrolyte, operating conditions and ionic agents [42]:

- Alkaline water electrolysis (AWE)
- Solid oxide electrolysis (SOE)
- Proton exchange membrane water electrolysis (PEMWE)

There are more types of water electrolysis processes, but these three are the most used. A brief introduction to the alkaline (ALK) and solid oxide electrolysis is made and for the PEMWE technology a more detailed one because is the the technology used in this thesis.

2.3.1 Alkaline and Solid Oxide Water Electrolysis

2.3.1.1 Alkaline Water Electrolysis (AWE)

AWE was discovered by Troostwijk and Diemann in 1789 and is a mature technology up to the MW range [43]. The AWE cell consists of two electrodes anode and cathode made of nickel materials immersed in an alkaline solution of KOH and/or NaOH electrolyte with a concentration of 20% to 30% to maximize its ionic conductivity, separated by a gas-tight diaphragm (with a thickness in the range of $3\,mm$) which has the function of keeping the product gases apart from one another for better efficiency and safety. The diaphragm must also be permeable to the hydroxide ions and water molecules, should be resistant to the corrosive electrolyte and should not give rise to any significant ohmic resistance within the cell [43], [44]. The membrane in the AWE cells has historically been made from asbestos [44]. But, since asbestos is considered an health hazard which can lead to cancer, newer AWE use other materials that have shown good properties include composite materials such as polyphenylene sulfide (Ryton) and polysulfone bonded zirconium oxide (Zirfon) [44].

AWE uses zero gap configuration, which means that the electrodes are pressed into the diaphragm, in order to reduce the distance between cathode and anode because the transport of electric charges in an electrolyte follows Ohm's law and larger distances between the two electrodes mean larger losses, bringing down the cell efficiency according to [43].

If a DC current is applied, the two water molecules at the cathode (negative pole) suffers reduction with the production of H_2 and hydroxide ions OH^- in the hydrogen evolution reaction (HER). The H_2 is then removed from the electrolyzer, while the OH^- flows through the electrolyte and diaphragm due to the influence of the potential difference induced by the connected circuit to the anode (positive pole) where occurs oxidation with O_2 and H_2O being produced in the oxygen evolution reaction (OER) [45], as shown in equations 2.17, 2.18 and 2.19 and in Figure 2.12.

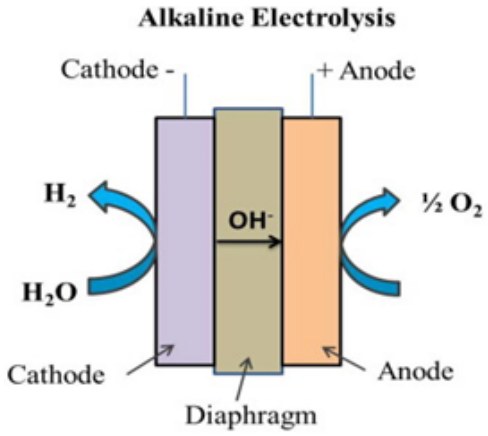

Figure 2.12: Conventional AWE, from [42].

$$Cathode: 2H_2O + 2e^- \longrightarrow H_2 + 2OH^- \tag{2.17}$$

$$Anode : 2OH^- \longrightarrow H_2O + \frac{1}{2}O_2 + 2e^- \tag{2.18}$$

$$Overall\,Cell : H_2O \longrightarrow H_2 + \frac{1}{2}O_2 \tag{2.19}$$

The product gas quality after drying is typically in the range of 99.5-99.9% for H_2 and 99-99.8% for O_2 [46].

2.3.1.2 Solid Oxide Electrolysis (SOE)

The SOE was first introduce by Donitz and Erdle in the 1980s. Is the least developed electrolysis technology being under research stage, with no commercial or pilot projects running yet [16]. The key elements of a SOE cells are a dense ionic conducting electrolyte typically a solid ceramic electrolyte and a gas-tight thin film of yttria (Y_2O_3) - stabilized zirconia (ZrO_2) (YSZ), with good ionic conductivity at the prevailing high operating temperatures and two porous electrodes (anode and cathode) with the cathode being made of cermet, usually consisting of nickel and YSZ and the anode is commonly a composite of YSZ and perovskites such as lanthanum manganites ($LaMnO_3$), ferrites ($LaFeO_3$) or cobaltites ($LaCoO_3$) partially substituted with strontium in order to promote structural and electronic defects that increase the electrocatalytic activity [47].

SOE operates at high pressure and high temperatures around 500 °C to 900 °C [42], thus this technology is attractive when a high-temperature heat source is available such as nuclear energy sector or geothermal energy and utilizes the water in the form of steam [47]. High temperature operation results in higher efficiencies than AWE and PEM but implies a remarkable challenge for material stability [46].

When the required electric potential is applied to the SOE cells, water molecules diffuse at the cathode side and are dissociated to form H_2 gas and O_2. The H_2 gas produced diffuses to the cathode surface and it's driven out of the cell, while oxygen ions (O^{2-}) flow across the electrolyte to the anode where the oxygen ions are oxidized to O_2 gas and transported through the pores of the anode to the anode surface, leaving the cell [48] as shown in equations 2.20 , 2.21 and 2.22.

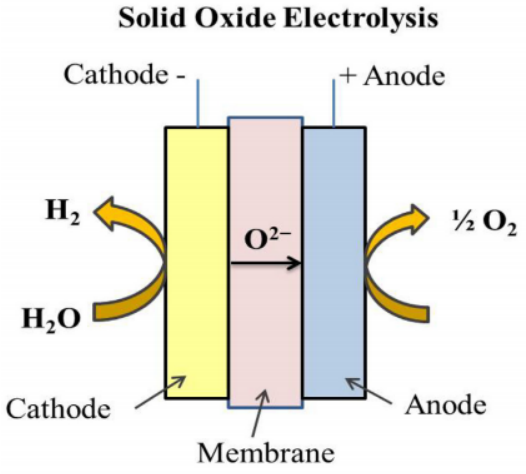

Figure 2.13: Conventional SOE, from [42].

$$Cathode : H_2O + 2e^- \longrightarrow H_2 + O^{2-} \tag{2.20}$$

$$Anode : O^{2-} \longrightarrow \frac{1}{2}O_2 + 2e^- \tag{2.21}$$

$$Overall\,Cell : H_2O \longrightarrow H_2 + \frac{1}{2}O_2 \tag{2.22}$$

2.3.2 PEM Water Electrolysis (PEMWE)

The first PEMWE was idealized by Grubb in the early fifties and developed in 1966 by General Electric Co. to overcome the drawbacks of the AWE [43]. This technology is expected to connect with the biggest share of new installations due to its good performance under variable input of RES [49]. The direct CO_2 emissions of a PEMWE system is zero. However from a life cycle analysis point of view, the use of this technology for hydrogen production is associated with CO_2 emissions [41]. In this thesis, a life cycle analysis is going to be made in order to quantify the CO_2 emissions per kg of hydrogen produced and compared with other technologies.

In PEM water electrolysis, water is pumped to the anode where it's split into O_2, H^+ and electrons as shown in equation 2.24. These protons (H^+) travel via the proton conducting membrane to the cathode side and the electrons exit from the anode through the external power circuit, which provides the driving force (cell voltage) for the reaction. At the cathode side the protons and electrons re-combine to produce the hydrogen as shown in equations 2.23 [42]. The overall equation is shown in 2.25 and in Figure 2.14.

$$Cathode : 2H^+ + 2e^- \longrightarrow H_2 \tag{2.23}$$

$$Anode : H_2O \longrightarrow \frac{1}{2}O_2 + 2H^+ + 2e^- \tag{2.24}$$

$$Overall : H_2O \longrightarrow H_2 + \frac{1}{2}O_2 \tag{2.25}$$

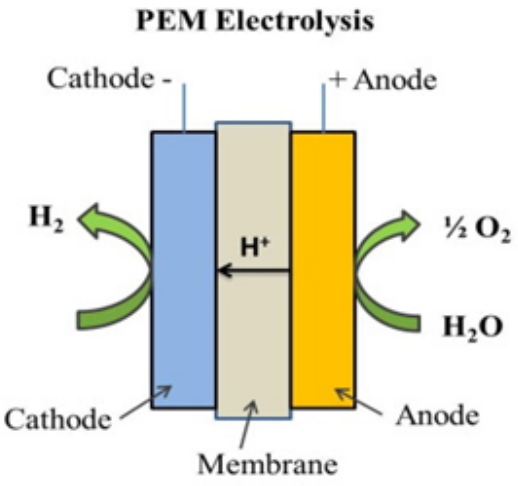

Figure 2.14: Conventional PEMWE, from [42].

2.3.2.1 Efficiency of PEM

The electrolyzer converts electric and thermal energy into chemical energy, since it's an electrochemical device. According to the fundamentals of thermodynamics, for a given temperature and pressure, the required energy for the reaction is determined by the enthalpy variation (ΔH). Part of the energy is electric, and it corresponds to the Gibbs free energy change (ΔG). Other part is thermal energy (Q) that is a product between the process temperature (T) and the entropy change (ΔS) [47]. The electrolysis process has a positive change of enthalpy and Gibbs free energy, being an endothermic and non spontaneous chemical reaction, respectively [47]. Equation 2.26 presents the relation between these proprieties:

$$\Delta G = \Delta H - Q = \Delta H - T.\Delta S \tag{2.26}$$

The lowest required voltage for the electrolysis is called the reversible cell voltage (V_{rev}). However, in the most commercial electrolyzers also the thermal energy ($T.\Delta S$) is provided by means of electricity, where the required voltage is higher than V_{rev} [47]. In this case, the minimum energy voltage is known as the thermo-neutral voltage (V_{tn}). In an ideal process, V_{rev} should be equal to the enthalpy voltage ($V.\Delta H$) since all the energy required is equal the enthalpy variation. Due to the thermodynamic irreversibilities, mainly related with water vapor contained in the hydrogen and oxygen flows, the lower temperature and pressure compared with the set-point conditions of the water supplied, and the thermal losses due to convection and radiation, the energy consumption of the process increases and the V_{tn} is higher than $V.\Delta H$ in a real process [47].

The efficiency of the PEM electrolyzer cell is calculated by the **Faraday efficiency and voltage efficiency.**

Voltage Efficiency

For an ideal process, the value for the reversible and thermo-neutral voltages at these conditions are, respectively, $1.23\,V$ and $1.48\,V$ as shown in eq. 2.27 and eq. 2.28 [42].

$$V_{rev} = \frac{\Delta G}{nF} = 1.23V \tag{2.27}$$

$$V_{TN} = \frac{\Delta H}{nF} = 1.48V \tag{2.28}$$

where $\Delta G = 237.22\,kJ/mol$ is the Gibbs free energy at standard conditions for water, $\Delta H = 285.84\,kJ/mol$ is the change of enthalpy, $n = 2$ is the number of electrons involved and $F = 96500\,C/mol$ is the Faradays constant, at standard temperature and pressure (298.15 K and 1 atm).

The cell's voltage in a PEM electrolyzer cell can be expressed as the sum of the reversible potential and its over-potentials [50]:

$$V_{cell} = V_{rev} + \eta_{ohm} + \eta_{act} + \eta_{con} \tag{2.29}$$

where V_{rev} is the reversible potential, η_{act}, η_{ohm}, and η_{con} are the activation, ohmic and concentration over-potentials.

The ohmic overpotential, η_{ohm} is the resistance caused against the flow of electrons and electronic resistance of the PEM and contributes with significant losses [51]. Depends on the type of PEM and electrode material and the best selection of material has a potential to enhance the overall performance. The ohmic overpotential is linearly proportional to the current. The opposition to the ions flow of the electrolyte also promotes the ohmic losses [47].

The activation over voltage, η_{act}, is due to the electrode kinetics. To transfer electric charge between the chemical species and the electrodes an energy barrier needs to be overcome. This energy barrier depends on the catalytic proprieties of the electrode and causes an over voltage that behaves with a logarithmic tendency in respect to the electric current [47].

The concentration over-potential, η_{con} is caused by mass transport processes and it's usually much lower than η_{ohm} and η_{act} [47].

The cell's LHV and HHV voltage efficiency can be calculated from the cell voltage V_{cell}, reversible voltage V_{rev} for LHV and thermo-neutral voltage V_{TN} for HHV as shown in equations 2.30 and 2.31.

$$\eta_{v,cell}(LHV) = \frac{V_{rev}}{V_{cell}} = \frac{1.23}{V_{cell}} \tag{2.30}$$

$$\eta_{v,cell}(HHV) = \frac{V_{TN}}{E_{cell}} = \frac{1.48}{V_{cell}} \tag{2.31}$$

The efficiency of low temperature electrolyzer is often given based on the HHV as it corresponds to the enthalpy of reaction at standard conditions from liquid water to gaseous hydrogen. However, for the evaluation of an overall process chain, the partial efficiencies of the process steps and fuel prices are usually referred to the LHV [46], so in this thesis is considered LHV values as reference.

Under typical operating conditions the cell voltages are between $1.5\,V$ and $2\,V$, with cell voltage efficiencies of 60-80% based on LHV [46].

Faraday efficiency

Faraday efficiency (η_F) can be defined as the ratio between the ideal electric charge and the real electric charge that is consumed by the electrolysis to produce a given amount of hydrogen. Lower Faraday efficiencies are mainly caused by electrical current losses and cross permeation of product gases. Electrical current losses, also called parasitic currents [46], appear in the system and do not contribute for the hydrogen production. Usually this efficiency takes higher values (98-99.9%) when the electrolyzer operates at rated production conditions. Lower current densities and higher temperatures cause lower electric resistance and, consequently, an increase of parasitic currents. Moreover, higher temperatures and pressures facilitate the cross permeation, especially when the current densities are low [46].

At nominal current density, Faraday efficiency of a PEM electrolyzer is nearly 100% at pressures up to 20 bar decreasing to 90% at a pressure of $130\,bar$ according to the literature [46].

Cell efficiency

The efficiency of the PEMWE cell is calculated by the equation 2.32 according to [50].

$$\eta_{cell} = \eta_v . \eta_f \tag{2.32}$$

where (η_f) is the Faraday efficiency and (η_v) is the voltage efficiency.

Electrolyzer stack efficiency

The stack efficiency is obtained by the ratio between the energy contained in the hydrogen produced and the electricity consumption. So, the electrolyzer stack efficiency can be obtained by equation 2.33 [46]:

$$\eta_{ele} = \frac{LHV_{H_2}}{C_E} \cdot 100 \tag{2.33}$$

where the LHV_{H_2} is $3.00\,kWh/Nm^3$ and C_E is the specific energy consumption. The specific energy consumption is obtained by the equation 2.34:

$$C_E = \frac{\int_0^{\Delta T} N_{cell} \cdot I_{cell} \cdot V_{cell} dt}{\int_0^{\Delta T} f_{H_2} dt} \tag{2.34}$$

where N_{cell} the number of cells in the electrolyzer, I_{cell} is the cell current, V_{cell} the cell voltage and f_{H_2} is the hydrogen production rate. The hydrogen production rate in an ideal electrolysis cell is proportional to the current, I_{cell}. Equation 2.35 shows how the hydrogen production rate f_{H_2} can be expressed in Nm^3/h, assuming the same current for all cells [47]:

$$f_{H_2} = \eta_F \frac{N_{cell} \cdot I_{cell} \cdot 22.41 \cdot 3600}{n \cdot F \cdot 1000} \tag{2.35}$$

PEM system Efficiency

The PEMWE system efficiencies with all utilities (electronics, pumps, safety equipment, infrastructure) to deliver H_2 at industry grade 5.0 (99.999%) and 30 bar pressure are typically in the range of 50% to 70% (LHV) with typical values of 60% [52] and around 10% to 20% lower than the cell efficiencies, as shown in the Figure 2.15 for the plant Energiepark Mainz already in production with an electrolyzer Siemens silyzer 200.

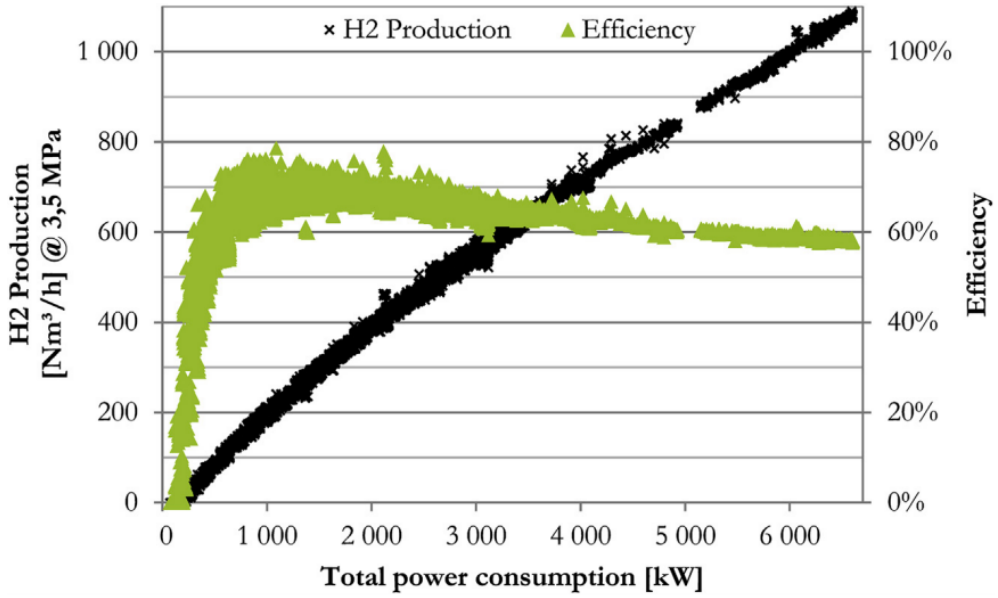

Figure 2.15: Hydrogen production and efficiency as a function of the total power consumption of a PEMWE production plant, from [52].

2.3.2.2 PEM Cell Components

PEM cells are divided in two areas, anode and cathode composed by the bipolar plates, current collectors and electrocatalytic layers which are separated by the proton exchange membrane (PEM) as shown in Figure 2.16.

Membrane Electrode Assembly (MEA)

The MEA is the main element of the cell and is composed by the **membrane**, **electrocatalysts** [42] and **current collectors.**

- **Membrane**

  The most commonly used membranes are perfluorosulfonic acid polymer membranes such as nafion, fumapem, flemion and aciplex, being the most used Nafion membranes because operates at higher current densities, have high durability, high proton conductivity and good mechanical stability [43]. Currently, membranes have a thickness of $200\,\mu m$ but it seems possible to reduce the thickness up to $50\,\mu m$ in the coming years [41]. Experimental tests with thinner membranes showed good results allowing to intensify the current density as the ohmic resistance of the cell is significantly reduced, but at the same time it has to be ensured that the permeation losses and degradation processes are not increasing too much with the thinner membranes [41].

- **Electrocatalysts**

  The Electrocatalysts used are different depending on the reaction to be activated. In the cathode side typically platinum (Pt) based materials are used for a standard catalyst for the HER [41] with material loading's of $0.2\,mg\,Pt/cm^2$, being possible to reduce to $0.025\,mg\,Pt/cm^2$ without significantly influencing cell performance according to [41], allowing to reduce the price of the cell.

Other material option that allows to reduce the price of the cell and have exhibited almost similar performance than conventional platinum is palladium (Pd), which is earth abundant and cheaper compared to platinum, so can be a substitute for Platinum cathodic catalyst layer [42].

In the anode side, Iridium and/or Ruthenium oxides (IrO_2, RuO_2 and $Ir_xRu_{1-x}O_2$) are used for the anodic catalystic layer for the OER [42]. This reaction is much slower than HER, so more catalyst surface area is necessary. The state-of-the art material mass for the anode is $2\,mg\,Ir/cm^2$, but by using improved catalysts with higher surface area, a reduction of the Iridium content to $0.2\,mg\,Ir/cm^2$ at increased current densities of $3\,A/cm^2$ is assumed to be possible in the near future [41].

- **Current collectors or porous transport layers (PTL)** carry the electric power towards the electrodes, provide a distributed supply of reactant water and facilitate the evacuation of the recently formed gases (O_2 and H_2). The materials used for current collectors can be titanium, niobium, stainless steel, but overall titanium is the best performing material [42].

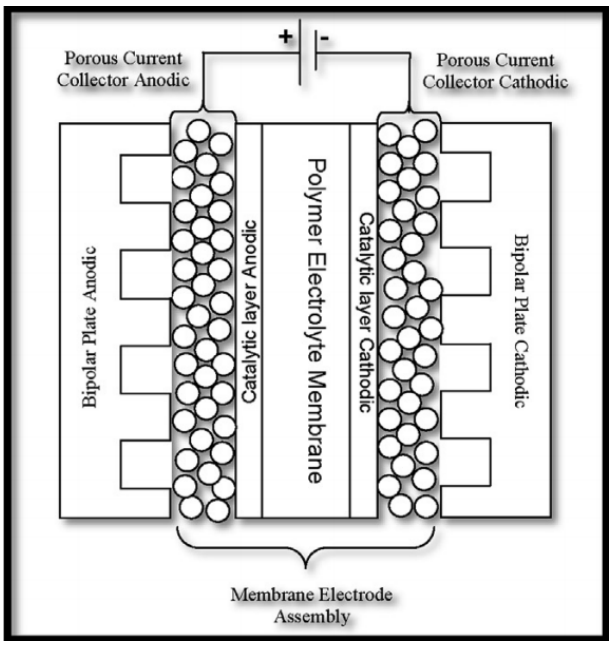

Figure 2.16: PEM Cell Components, from [51].

Bipolar Plates

Bipolar plates are the structure that encase the two half cells (anode and cathode) and also provides the contact point with the external power source. Is responsible for 48% of the overall cell cost and are made of titanium, stainless steel and graphite typically [42]. These plates work under high pressure and corrosive environments, so its composition plays a significant role in order to avoid failure and titanium materials give outstanding strength, high thermal conductivity, low permeability and low resistivity [43]. The titanium bipolar plate thickness in current state-of-the-art is about $3\,mm$, but can be reduced to $0.3\,mm$ in the near future by forging of thin sheet metal instead of destructive milling or etching of thicker base material, allowing to reduce the material usage and the price of the cell [41].

2.3.2.3 PEM System Components

The PEMWE system is shown in the Figure 2.17.

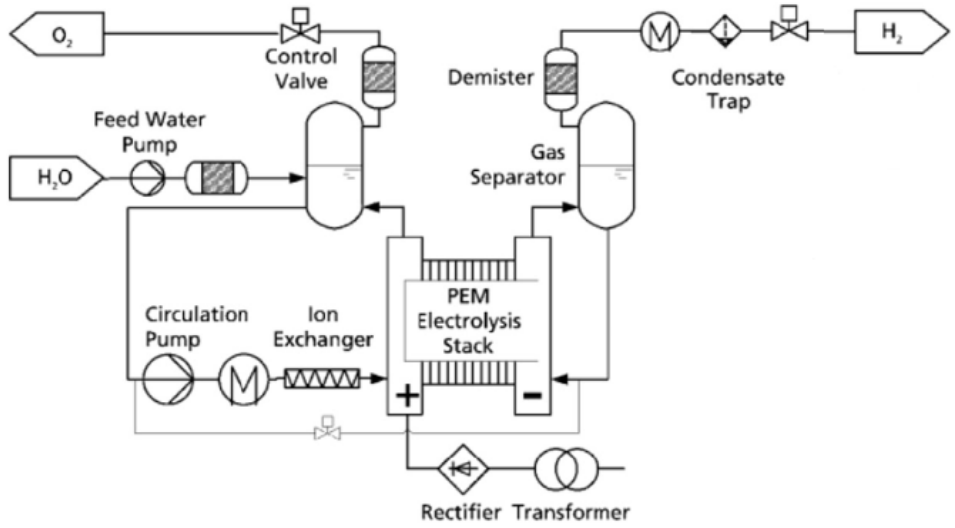

Figure 2.17: Scheme of the PEMWE system layout, from [46].

The PEMWE system is formed by [41], [46]:

- **Feed Water Pump** which is used to pump water to the cell stack at the anode side.

- **Water-gas separator tank** at the anode side de-ionized water is fed to the water-gas separation tank as well as the water that leaves the stack together with the produced oxygen, separating H_2O from O_2. At the cathode side hydrogen and water leave the stack, with liquid water being separated from hydrogen and drained back to the anodic water-gas separation tank [41].

- **Circulation water pump** is necessary on the anode side, but on the cathodic side is not necessary because there is a net transport of water from the anode to the cathode during operation due to the electro-osmotic drag [41].

- **Ion exchanger** is used for maintaining a low water conductivity which has to be lower than $0.1\,\mu S/cm$ according to [41] to avoid certain system degradation issues.

- **Heat exchanger** allows the system to maintain a certain working temperature typically in the range between 60 °C and 80 °C in the anodic cycle [41] and at the cathodic side the hydrogen-water mixture is cooled down close to ambient temperature (20 °C).

- **PEM Stack** is the core component of a PEMWE system. Is a connection of several single cells in series as shown in fig. 2.18.

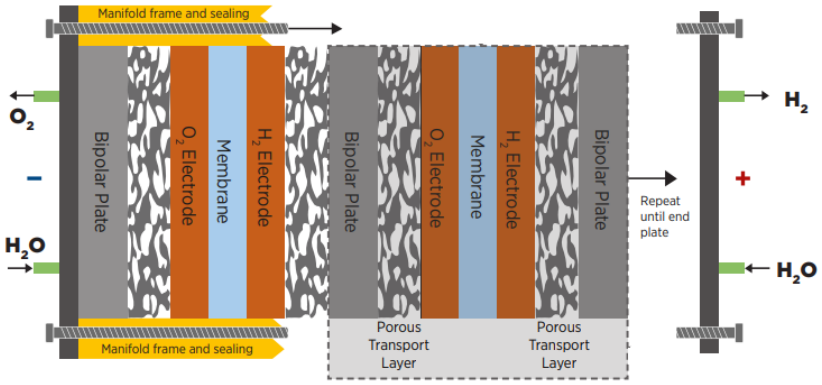

Figure 2.18: Scheme of the PEMWE stack, from [53].

Thick end plates made of aluminum or steel together with several bolts and sets of stacked flat springs are used to ensure an even compression of the cells. The stack lifetime of commercial systems is typically 40 000 to 60 000 h and is planned to reach 90 000 h in near future systems.

- **Demister** which catalytically cold burns the oxygen traces with hydrogen to water in order to remove impurities with the use of platinum group metals. After passing the cathodic water-gas separator unit, the produced hydrogen is saturated with a water vapor content of about 770 parts per million (ppm) [41] and some oxygen is also present in the cathodic product gas due to permeation processes across the membrane and is estimated to be about 800 ppm according to [41]. So the demister or catalytic de-oxo purification device, reduce the oxygen content to a level of $5\,ppm$ with the reaction 2.36:

$$2H_2 + O_2 \longrightarrow 2H_2O \tag{2.36}$$

While removing the $800\,ppm$ of oxygen, $15\,g\,H_2O/kg\,H_2$ is produced.

- **Condensate Trap or absorptive dryer** is a silica gel adsorbent that adsorbs water at its surface until it's completely covered, reducing the water content from $15\,g\,H_2O/kg\,H_2$ to values lower than $5\,ppm$. In order to maintain a continuous drying process, two silica tanks in a batch process are used. Energy and material requirements to produce silica gel range between 7100 and $8400\,kJ$ to evaporate $1\,kg\,H_2O$ from silica, resulting in an energy demand of $0.05\,kWh$ per kg dried H_2 at $30\,bar$ pressure according to the literature [41].

2.3.2.4 Overview of main PEM parameters

Table 2.5 shows an overview of the key parameters of the PEMWE system for 2020 and 2050 target, which are important for the LCA according to the literature.

Table 2.5: Current and estimated future PEMWE system parameters [41] and [53].

Parameter	**2020**	**2030**	**2050 target**
Cell voltage level (V)	1.5-2	1.5-2	1.5-1.7
Current density (A/cm^2)	1.5	3	4-6
Power density (W/cm^2)	2.25-3	4.5-6	6-10.2
Operating pressure (bar)	30	-	-
Operating temperature ($^\circ C$)	60-80	-	-
H_2 purity (%)	99.9-99.9999	99.9-99.9999	99.9-99.9999
$\eta_{cell,LHV}$ (%)	70	70	80
$\eta_{system,LHV}$ (%)	60	60	70
Anode Ir. loading (mg/cm^2)	2	0.2	0.2
Cathode Pt. loading (mg/cm^2)	0.2	0.05	0.05
Ti. bipolar plate thickness (mm)	3	0.3	-
Membrane thickness (μm)	200	50	-
Single cell format (cm^2)	500	1000	-
Stack unit size (MW)	1	10	10
Stack lifetime (kh)	50-80	80-100	100-120
BOP lifetime ($years$)	20	20	-

2.3.3 Water Purification for Electrolysis

Electrolyzers can not be operated directly with sea water, tap water or wastewater effluent since there is a maximum of 0.5 ppm of total dissolved solid units (TDS) allowed [54]. The water treatment includes desalination and/or purification.

For sea water, the desalination can be divided into electrical and thermal processes [54]:

- Reverse osmosis is the most used electrical technology.

- Multi-effect distillation and multi-stage flash distillation are the main thermal processes to produce better quality and require less post-treatment for demineralization (better for SOE technology since it requires steam).

After the desalination, a post-treatment process is necessary. It always includes chemical treatment in a resin polishing filter containing chemicals to bind remaining ions and other TDS in the desalinated water [54].

At energy park Mainz in Germany, hydrogen is produced with **tap water**. The electrolysis plant contains a water treatment plant to produce high purity water (<1 $\mu S/cm$) [52]. **The process of demineralization includes four stages: decalcification, reverse osmosis, membrane degasification and electro deionization [52].**

2.3.4 Oxygen as by Product

H_2 is the main product from the electrolysis process. However, splitting water generates $8\,kg$ of O_2 as a by-product per $kg\,H_2$. O_2 is a valuable product that can be used in several applications along industry, health or recreational sectors such as production of steel, polymers, welding, cutting of metals, rocket propellant, O_2 therapy and life support systems in aircraft, submarines, spaceflight and diving [55].

O_2 is typically produced by an air separation unit (ASU) through liquefaction of atmospheric air and separation of the O_2 by continuous cryogenic distillation. It can be transported either in liquid form or in gas cylinders.

O_2 is not the intended outcome of the electrolysis process, however could be tapped for many different uses.

2.3.5 Safety

Generally, hydrogen is not an explosive and reactive substance and a reactant agent is always required. Hydrogen has a very low density being fourteen times lighter than air and safer than other fuels in an open atmosphere followed by immediate dispersion in a ventilated area and releasing less energy during the explosion. Due to the buoyancy, hydrogen would immediately disperse in an open area to below its flammability limit, while in a given volume hydrogen explosion releases less energy compared to other fuels such as petrol and NG. Moreover, hydrogen severely interacts with various surfaces, shows high solubility and simply diffuses through almost all materials at ambient temperature. The biggest disaster involving hydrogen is probably the fire of the German Hindenburg airship in 1937. The Zeppelin airship was inflated with $200\,000\,m^3$ of H_2. Even though the origin of the ignition is unknown, the combined combustion of hydrogen and the coating of the shell (iron and aluminium oxide) is the probable cause [56]. As all the other fuels such as petrol, diesel and NG, hydrogen is certainly not without risk and should be handled in accordance with its specifications [42]. Between the main characteristics, some of them related to safety are underlined below [57]:

- Hydrogen can diffuse through materials due to the small size of its molecules, so only a few materials are suitable for use in combination with H_2 to decrease the probability of leakage.
- The number of connections shall be minimized such as welded and screwed connections.
- When released, hydrogen rises and disperses quickly at a speed of almost 20 m/s because it's fourteen time lighter than air. The risk of explosion or asphyxiation is therefore reduced. However, in closed rooms there is a risk of an accumulation at the top if there is no sensors and ventilation system. Furthermore, if the hydrogen leakage is from a small orifice, shock waves may cause overheating and ignition.
- Human senses can not detect hydrogen because it's odorless, colorless and tasteless. Unlike NG, adding odorants is not a solution since there is no odorant light enough to disperse with the same rate of hydrogen. Special thermal imaging cameras and/or ultraviolet (UV) measurement could be used to detect flame.

- The hydrogen delivery installations shall be chosen such that escaped hydrogen is blown in a safe direction.

- A mixture of hydrogen gas and air can be ignited along a very wide volume fraction interval: 4 to 75% (flammability range). A very little energy to ignite is required ($20\,\mu J$, compared to $290\,\mu J$ for NG). Constructions shall use materials that conduct electricity well, avoiding static charges accumulation.

- The self-ignition temperature is high (585 $^\circ$ C).

- Hydrogen is non-toxic and non-poisonous. It's a gas under normal conditions and does not contribute to atmospheric or water pollution.

If the guidelines of hydrogen safety are taken in consideration and users understand its behavior, hydrogen can be used as safely as other common fuels [57]. Therefore, companies that handle with hydrogen systems, such as NASA, have a set of guidelines for safety operation. One of the guidelines shall be the personnel training. Personnel handling hydrogen must become familiar with physical, chemical and specific hazardous proprieties. Also the personnel involved in equipment design and operation planning must be trained to carefully adhere the safety standards. Operator certifications, hazard communication programs and annual reviews of the operations should be applied.

The use of inherent safety features and controls are also very important. Adequate ventilation, prevention of leakage and elimination of potential ignition sources are some examples. To minimize risks and control failures, some barriers or safeguards should be provided. Safety systems should be installed to detect and control the possible hazards effects, such as vessel failures or ignitions. A safety interface must be maintained so at least some failures occur before hazardous events that could lead to personal injury or loss of life. Warning systems and flow controls should be installed to detect abnormal conditions [58].

2.3.6 Comparison Between Technologies

In table 2.6 is summarized the materials used for the component of the three technologies.

Table 2.6: Characterisation of the three types of water electrolyzers components materials [53].

Component	**AWE**	**PEMWE**	**SOE**
Anode	Nickel	Iridium	Perovskites
Cathode	Nickel	Platinum	Nickel/YSZ
Separator	Zirfon	Solid electrolyte	Solid electrolyte
Electrolyte	25% KOH	Nafion	Yttria-stabilized Zirconia (YSZ)
PTL anode	Nickel	Titanium	Nickel
PTL cathode	Nickel	Titanium	None
Bipolar plate	Nickel/Steel	Titanium	Steel

A general comparison of the different electrolysis technologies, covering the most relevant variables for the scope of this project are summed up in table 2.7:

Table 2.7: Comparison of the important parameters of the main water electrolysis technologies [46] and [43].

Specifications	**AWE**	**PEMWE**	**SOE**
Ions electrolyte	OH^-	H^+	O_2^-
Technology maturity	Fully mature	Scaling-up	Laboratory scale
Operation parameters			
Cell temperature ($^\circ C$)	60 - 80	50 - 80	500 1000
Typical pressure (bar)	10 - 30	2 - 50	1 - 15
Current density (A/cm^2)	0.2 - 0.4	1.0 - 2.0	0.3 1.0
Cell voltage (V)	1.8 - 2.4	1.8 - 2.2	1 - 1.5
Power density (W/cm^2)	1.0	2-5	—
Efficiency			
Stack efficiency (LHV %)	63-71	60-68	100
System Efficiency (LHV %)	51-60	46-60	76-81
Energy Consumption (kWh/Nm^3)	4.5 - 7.0	4.5 - 7.5	3.7-3.9
Durability			
Stack lifetime (kh)	55-120	60-100	8-20
System lifetime ($years$)	20 - 30	10 - 20	—
Degradation			
Degradation rate ($\mu V/h$)	$<$3	$<$14	—
Efficiency degradation (%/$year$)	0.25-1.5	0.5-2.5	3-50
Flexibility			
Cold start up time (min)	60-120	5-10	hours
Warm start up time (min)	1-5	$<$0.2	15
Load flexibility (% of NL)	20100	0100	0-100
Available capacity			
Cell area (m^2)	$>$4	$<$0.03	$<$0.06
Costs			
Investment costs (IC) (€/kW)	800-1500	1400 - 2100	$>$2000
Maintenance costs (% of IC)	2-3	3-5	—

As shown in table 2.7, **AWE** technology is the most mature and cheapest without noble catalysts and has the most durability. **PEM** are predicted to become the most prominent technology in the close future since they present better flexibility and good compactness (low cell area). **SOE** technology promises the better efficiencies since a source of heat is provided, however the technology is still in the R&D stage and poses uncertainties for investments and has the lowest durability of the three technologies.

2.4 Hydrogen Compression and Storage

Hydrogen has a low energy density by volume when compared to fossil fuels ($9.9\,MJ/Nm^3$ LHV) which could result in extremely large storage vessels. To avoid so large tanks, at least one of the three following features are required to store sufficient quantity of hydrogen: **high storage pressure, low storage temperature or using a material that attracts large amount of hydrogen molecules** [59]. Hydrogen storage technologies can be classified in two main types: **physical-based** being the compressed hydrogen (CH_2) storage, cold/cryo-compressed and liquid storage the most used methods and **material based** which can be divided in two main sub-groups of chemical sorption and physical sorption as shown in Figure 2.19.

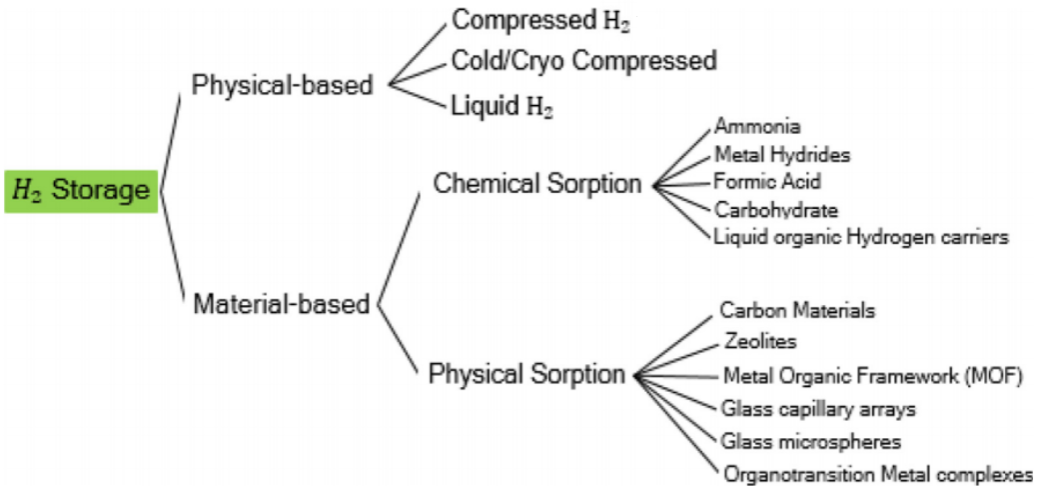

Figure 2.19: Hydrogen Storage methods, from [59].

2.4.1 Physical Based Storage

2.4.1.1 CH_2 Storage

Mechanical Compressors

The mechanical compressors are the most widespread type of compressors used nowadays and are based on the direct conversion of mechanical energy into gas energy. These work by reducing the confined volume in which hydrogen is contained by the use of a piston with gaseous hydrogen being squeezed into a smaller space, so that the number of collisions among particles and against the walls increases resulting in a higher gas pressure [60]. The different types of mechanical compression are presented in Figures 2.20 and 2.21 and briefly explained:

1. **Reciprocating piston compressor:** consists of a piston-cylinder system equipped with two automatic valves one for intake and one for delivery. The piston is linked to a crankshaft by a connecting rod converting the rotary motion of the moving units into the almost linear motion of the piston. This movement is known as reciprocating motion. The energy necessary for the compression is provided by either an electrical or a thermal machine. This is the most used system as ensures good

performances for high-pressure applications up to 850 bar with capacities of around 430 kg/h [60].

2. **Metal diaphragm compressor:** is a variant of the previous configuration where in this case are moving metal diaphragms that move in order to compress the gas. Diaphragm compressors reach very high efficiency levels. Even if piston compressors are still the most common worldwide, metal diaphragm ones are being deployed at a higher pace with output pressures up to $517\,bar$ and flow rates up to $280\,Nm^3/h$ [60]. However, one of the most important drawbacks of these compressors is their durability as they are weakened by mechanical stresses during operation, since too high flow rates can cause the early failure of the diaphragm, so a good design needs to include concavities and grooves ensuring proper flow distributions [60]. Diaphragm compressors are especially appropriate for applications requiring low flow rates also because of the limited volume of the compression chambers commonly used.

3. **Linear compressor:** These compressors are particularly used in cryogenic applications. They offer lower costs due to the simplicity of the system because a piston is directly connected to a linear motor coupled with a resonating spring system which has fewer rotating components than the cases mentioned above. Linear compressors work at the mechanical resonance frequency when their operating frequency is set at the natural value and this kind of frequency adjustment means very high levels of efficiency can be achieved [60]. The resonance frequency of the compressor can be obtained from the following equation 2.37:

$$\omega_{resonance} = \sqrt{\frac{k_{gas} + k_{mechanic}}{m}} \tag{2.37}$$

where k_{gas} is the stiffness of the gas spring, $k_{mechanic}$ is the axial stiffness of the mechanical springs and m is the moving mass. Although these compressors offer promising possibilities for H_2 compression, their use has still not been reported at an industrial scale.

4. **Liquid compressors:** are devices using liquids to directly compress the H_2 working in the absence of mechanical sliding seals. They are widely recognised as achieving inexpensive compression because they are able to ensure a quasi-isothermal process. In fact, the liquid and the gas are compressed together but since the liquid has a higher density and a higher heat capacity, the heat generated by compression is efficiently absorbed by the liquid and by the surrounding walls of the compression chamber. In addition, the resultant thermal management through the liquid itself means external heat exchangers do not need to be used thus reducing the cost of the overall system. This type of compression has a significant advantage over the other mechanical compressors in terms of efficiency with values higher than 83% [60].

   (a) **Liquid piston compressors:** H_2 confined in a closed space is directly compressed by a moving piston and in these devices, it's liquid that compresses the gas. This technology is already working in compressed air energy storage applications with outlet pressures of $200 - 300\,bar$ [60].

(b) **Liquid rotary compressor:** are particularly used to compress a gas with a high liquid content. An impeller is located eccentrically in a stator frame and made up of a series of blades extending radially from it. The impeller forces the liquid to move in an oscillatory manner, forming a ring compressing the gas introduced from a door placed in the rotor centre. However, they are not widely used because of their low overall efficiency of about 50% [60].

(c) **Ionic liquid pistons:** are compressors that have been specially developed for H_2 applications. The used compression elements are molten salts which are ionic liquids being very favorable at the time of compressing, since the H_2 solubility in them is negligible allowing for higher compression ratios [60]. Reported efficiencies are in the range of 83-93%, which is explained by the good lubricant and coolant properties of the ionic liquids while the capacities and outlet pressures are $90 - 340\, Nm^3/h$ and $450 - 900\, bar$ respectively [60]. Ionic liquids compressors for hydrogen applications have particularly been developed by the German international company Linde and is being used in the green hydrogen's project Park Mainz of $6\, MW$ for the compression necessities.

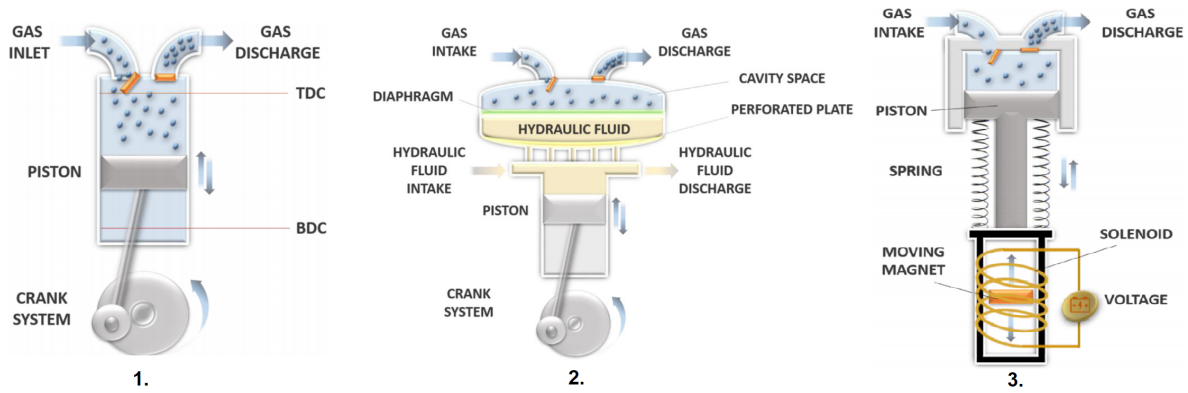

Figure 2.20: 1. Reciprocating piston compressor, 2. Metal diaphragm compressor, 3. Linear compressor, from [60].

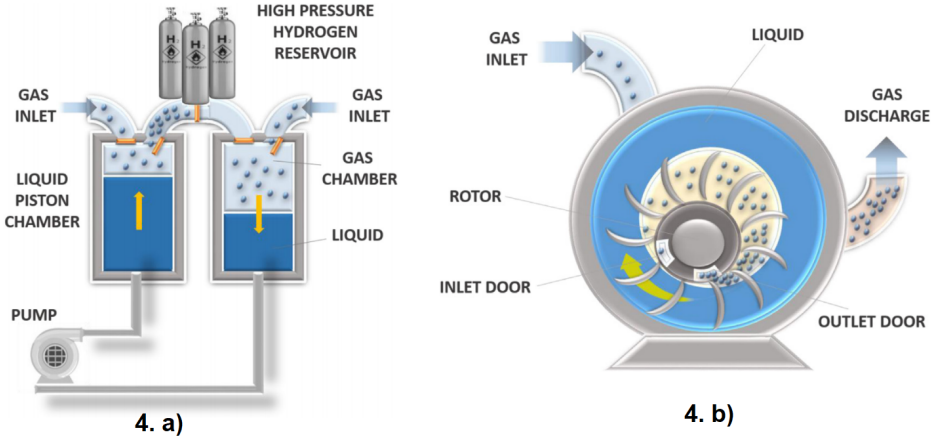

Figure 2.21: 4. a) Liquid piston compressors, 4. b) Liquid rotary compressor, from [60].

Compressed gaseous hydrogen is usually stored at pressures ranging from $200 - 1000\,bar$ according to [61] with between 5-15% energy loss depending on the final pressure as shown in Figure 2.22.

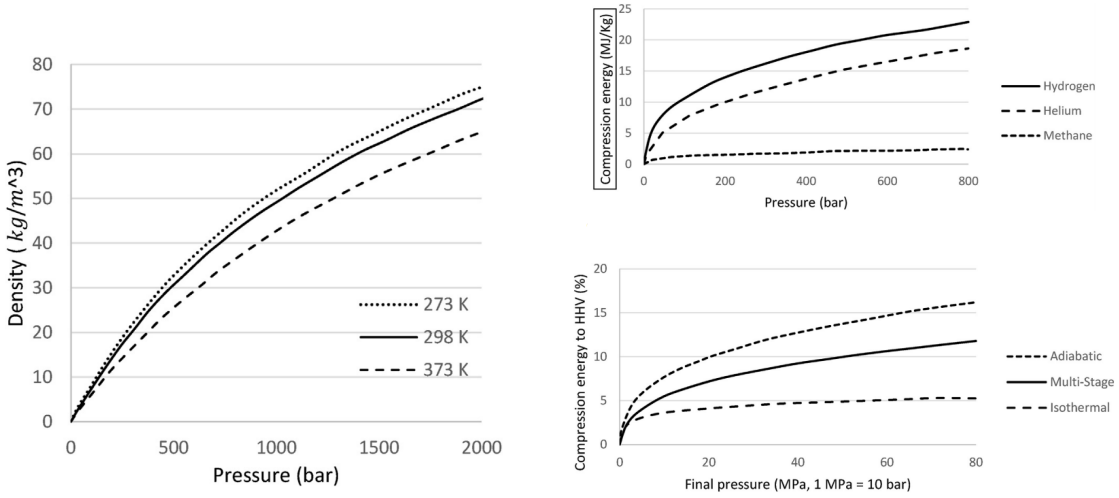

$a)$ $b)$

Figure 2.22: a) The change of the volumetric density of H_2 with respect to pressure change at three different temperatures, b) Energy required for hydrogen compression as a percentage of its energy content (HHV), from [62].

Hydrogen storage systems comprise different components like valves, sensors and storage containers. These components are made of different materials being the most used steel, aluminium, polyethylene and carbon fiber reinforced with epoxy resin. The material selection depends on the service, test pressures, external stresses, lifetime, the static and dynamic safety coefficients and dimensions. There are four types of pressure vessels that can be used for storing hydrogen [62] and [61]:

- **Type I: Fully metallic pressure vessels** are the most used and least expensive but heaviest with approximately $1.4\,kg$ per L. They are normally made from aluminum or steel and can contain pressures up to $500\,bar$.
- **Type II:** : **Steel pressure vessel with a glass fiber composite over wrap.** The steel and composite material share about the same amount of structural load. Manufacturing Type II vessels costs about 50% more than Type I but are 30 - 40% lighter.
- **Type III: Full composite wrap with metal liner.** The structural load is mainly carried by the composite structure (carbon fiber composite) and the liner (aluminum) is for sealing purposes sharing only about 5% of the mechanical load. This type of pressure vessel has proven to be reliable for $450\,bar$ working pressure but still has problems with passing the tests at $700\,bar$. Type III provides half of the type II weight with $0.45\,kg$ per liter of H_2 but with double of the cost of Type II.
- **Type IV: Fully composite.** Commonly a polymer like high density polyethylene (HDPE) is used as liner and carbon fiber or carbon glass composites are used for carrying the structural load. This

type of pressure vessel is the lightest but the price is still very high. Type IV pressure vessels can withstand pressures up to $1000\,bar$.

For vehicle applications, the service pressure of hydrogen storage vessels is normally 35 or 70 MPa. Utilizing 700 bar vessels will increase the volumetric storage density to about $38\,kg/m^3$ compared to $23\,kg/m^3$ at $350\,bar$.

2.4.1.2 Liquid/cryogenic Hydrogen Storage

Liquefying hydrogen is done at very low temperatures (-250 °C) and in order to maintain hydrogen at such a low temperature is both time and energy consuming and up to 40% of energy content can be lost in the process [59]. Thus, this storage method is most often used for medium to large scale storage and delivery such as truck delivery and intercontinental hydrogen shipping can carry up to 5000 kg of hydrogen which is about five times the capacity of CH_2 gas tube trailers.

2.4.1.3 Cryo-compressed Hydrogen Storage

Cryo-compressed storage combines properties of both compressed gaseous hydrogen and liquefied hydrogen storage systems with the objective of minimize the boil-off loss (dormancy) from liquefied hydrogen storage while retaining a higher system energy density [61]. Relies on the achievement of high pressures at very low temperatures at about -233 °C [59], having a high storage density when compared with liquid hydrogen and CH_2 as shown in Figure 2.23. High pressure hydrogen is obtained by using cryogenic pumps able to reach a discharge pressure as high as $850\,bar$, a hydrogen flow rate of $100\,kg/h$ and a hydrogen density up to $80\,g/L$ [61].

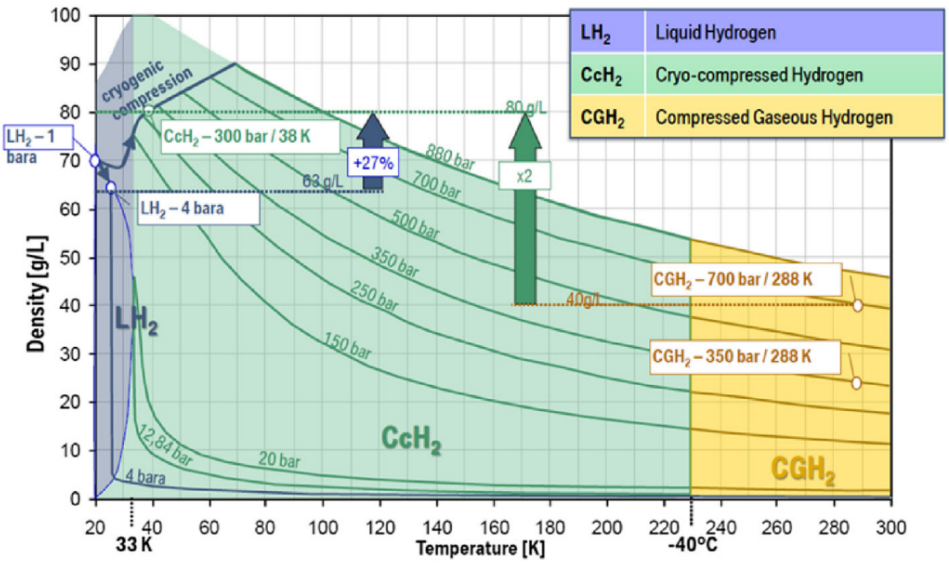

Figure 2.23: Hydrogen density versus pressure and temperature, from [61].

The tank consists of a type III composite pressure vessel with a metallic liner, whose role is to limit heat transfer between the hydrogen and the environment. Experiments have also been performed to

evaluate the effect of combined pressure and cryogenic temperature cycling on the composite material properties of tanks. Cryo-compressed storage tanks can be filled with hydrogen at any state between $20\,K$ liquid H_2 and ambient temperature gaseous H_2 [61]. Filling the tank with compressed gas instead of liquefied hydrogen is expected to be more economical. In terms of infrastructure, cryo-compressed tanks offer refuelling flexibility as they are compatible for gaseous and liquid [61].

2.4.2 Material Based Storage

Material-based storage are still in development stage and needs more time to prove itself as a viable long-term solution [59]. They can be divided in chemical and physical sorption.

2.4.2.1 Chemical sorption

Chemical sorption consists in to split molecules into atoms and to integrate them with the chemical structure of the material. Metal hydrides (MH) are the most famous group of materials that can be used for chemical sorption. MH is a process based on the reversible insertion (absorption) /de-insertion of hydrogen in a hydride-forming metal. More specifically, it uses reversible heat interactions driven by the combination of a hydride-forming metal with hydrogen into a metal hydride (MH) as shown in equation 2.38.

$$M(s) + \frac{x}{2}H_2 \longrightarrow MH_x(s) + Q \tag{2.38}$$

where M is a metal/alloy, the absorption reaction corresponds to the exothermic formation of MH and Q is the corresponding released of heat. MH compression offers simplicity in design and operation with compact systems that avoid moving parts reducing costs and noise. Also, their working principle allow to use waste heat, opening possibilities for their use in industrial applications [63]. It's not commercially available yet, with $350\,bar$ MH compressors being tested [63].

Liquid organic hydrogen carriers (LOHC) are among the most promising options as well. In LOHC storage systems, hydrogen is stored by chemically bonding with hydrogen-lean molecules and it's released by going through a catalytic dehydrogenation. These storage systems are attractive because they can be managed easily in ambient conditions, the store and release processes are carbon free and the carrier liquid is not consumed and can be used repeatedly. These carriers are not toxic or corrosive and the storage pressure is low [59].

2.4.2.2 Physical sorption

Physical sorption consists in the use of a porous storage systems as a mean to achieve high capacity and reliable storage units. Among all porous materials, Metal organic frameworks (MOF) and porous carbon materials are known to be most promising. Using this method will provide high surface area, low hydrogen binding energy, faster kinetics in charge and discharge processes and low cost of the materials. Plus, potentially physical absorption can mitigate thermal management issues during charge and discharge of the storage unit. On the other hand, the issues involved with this method are weight of the

carrier materials, requirement of low temperature, high pressure and still low gravimetric and volumetric hydrogen density. Physical sorption technologies are far from being widely used since all experiments have been conducted on small scales and the performance criteria like volumetric/gravimetric hydrogen density, pressure and temperature are not satisfactory [59].

2.4.3 Large Scale Storage

In the future hydrogen economy, large-scale storage can be used for storing the excess energy in the grid supplying a large number of customers with geological storage which is to inject hydrogen underground and storing it under pressure where it can be later withdrawn whenever needed. There are many types of geological storage such as depleted NG, oil reservoirs, aquifers, salt caverns, abandoned mines and rock caverns. The best option is salt caverns according to [59], because salt is inert and it would not react with hydrogen. Typical volume is about $700\,000\,m^3$ and pressure of $200\,bar$. Underground storage of hydrogen provides higher safety levels in comparison with above ground storage methods due to the thickness of the walls and low operating pressure. However, ecological and environmental concerns about the impacts of hydrogen leakage through the walls to the neighboring areas, plants and organisms needs to be addressed [59].

2.4.4 Hydrogen Delivery Technologies

Hydrogen delivery is a critical contributor to the cost, energy use and emissions associated with hydrogen pathways. It can occur by sea, road, rail and through a pipeline system. In the case of centralized hydrogen production, hydrogen delivery to end users includes two main phases: Transmission which consists on delivery of hydrogen from the production plants to the city gates and distribution (delivery from the city gates to the HRS or end users). There are three main pathways for delivery which depend largely on storage method [59]:

- Compressed gaseous hydrogen through pipelines or by road on trailer mounted vessel.
- Liquid hydrogen by road, sea or rail.
- Material based hydrogen carriers

The choice of the delivery method will depend on specific geographic, market characteristics like target population and consuming behaviors, size of HRS and market penetration of FCEV [59].

In this thesis, is considered a reciprocating piston compressor to compress the hydrogen to 350 bar to be stored in tanks type I and to be transported by road on a truck.

2.5 LCA

A life cycle assessment (LCA), which is explained in chapter 3, is going to be performed from cradle to grave in this thesis for the four stages of wind energy, hydrogen production, compression and storage described before in the state of the art. In the literature there are several studies for each of

these stages, but there are few studies considering a system composed by the four stages. Regarding the direct production of hydrogen at the HRS site, interesting results have been published in life cycle assessments carried out by Spath and Mann [64] and Patterson et al. [65]. Spath et al. [64] is a work with 20 years from 2001 which considered the life cycle of hydrogen production from wind energy with a system comprising a small electrolyzer ($30\,Nm^3/h$) being fed by three $50\,kW$ WTs and a HRS delivering hydrogen at $200\,bar$. They showed that the majority of emissions originated was from the systems construction, where WTs had the largest contribution (78%) to the systems specific GHG emissions of $0.97kg\,CO_2\,eq./kg\,H_2$. The system in [64] is in the kw range and in this thesis is in the MW range, so the results from[64] are expected to be lower from the ones in this thesis. Patterson et al. [65] concluded that the potential for a combination of renewable derived hydrogen fuelled vehicles with grid powered electric vehicles, contribute towards short and medium range transport requirements is a realistic means of achieving UK policy objectives in terms of energy security and climate change (CC). A more recent work from Burkhardt et al. [66] from 2016 makes a life cycle assessment on the fuel supply of hydrogen from wind energy to mobility only considering the construction, operation and decommissioning phases. [66] concluded that FCEV reduce emissions by 86-89% compared to ICE vehicles. The major (74%) primary energy input for providing hydrogen arises from the construction of WT, electrolyzer and the HRS. Due to the relatively low load factor of the electrolyzer (3000 full-load hours/year), the construction phase leaves a remarkable footprint in the GHG emissions ($1.919\,kg\,CO_2\,eq./kg\,H_2$).

Several studies for the life cycle of wind farms were found in the literature. Elginoz et al. [67] made a life cycle assessment of multi use offshore platforms combining wind and wave energy production, concluding that the material consumption in the semi-submersible floating concept is comparable to a spar platform. Wang et al. [68] made a life cycle gas emissions of offshore and onshore WTs, comparing the emissions from them concluding that an offshore WT has larger life cycle emissions than an onshore WT because of the floating platform which needs more material. Huang et al. [69] made a life cycle assessment and net energy analysis of offshore wind power systems, concluding that the factors with the most environmental impact were the steel used, electricity consumption in the production and construction phase and the concrete materials for an offshore substation. The environmental impact of offshore wind power systems can be further reduced by lowering the amount of material used for WTs, particularly steel and concrete. Weinzettel et al. [70] made a life cycle assessment of a floating offshore WT, founding that the end of life scenario of the wind farm is very important for the overall environmental impact of the electricity production. Yang et al. [71] made a life cycle energy and environmental impacts of a typical OWF in china, concluding that the emissions were dominated by WTs manufacturing and foundation materials production. Vestas made a LCA from an onshore V110-2MW WT [38].

For the life cycle of electrolyzers, some articles were found in the literature as well. Bareiss et al. [41] concluded that mainly the composition of the electricity mix determines the impacts like global warming potential (GWP) and that a reduction of the used materials causes only very little reduction in GWP. Further investigation, showed that hydrogen production with PEMWE in the future (2050) is definitely an alternative to conventional SMR production, concluding that PEMWE can contribute to a high reduction of greenhouse gas emitted by the transportation sector by up to 80%.

Chapter 3

Methodology

Life cycle assessment (LCA) is one of the most established methods for estimating the environmental performance associated to the life cycle of products and services from raw material through to production, use, end of life treatment, recycling and final disposal. The first LCA framework was published by the Society of Environmental Toxicology and Chemistry. After many modifications, the practice of LCA was regulated and nowadays its application follows the ISO 14040 and 14044 standards (ISOa, 2006 and ISOb, 2006) [72]. According to the International Organization for Standardization (ISO) 14040/44 standards, the LCA comprises four phases [73]:

- **Goal and scope definition** which identify the purpose of the LCA, the expected results of the study and defines the limits and assumptions based on the definition of the objective.

- **Life cycle Inventory (LCI)** which quantify the inputs and outputs of each unit operation including data collection.

- **Impact assessment** which allows to evaluate the possible environmental impacts associated with the system's inputs and outputs.

- **Interpretation of results** where the findings from the inventory analysis and the impact assessment phases are considered together to present consistent results based on the goal and scope definition phase of the study.

3.1 Goal and Scope of the Study

3.1.1 Goal of the Study

The goal of this project is to analyse the life cycle and to quantify the potential environmental impacts of hydrogen production in Portugal by PEMWE using electricity generated from offshore wind energy in a centralized way.

3.1.2 Functional Unit

The functional unit serves as a base for calculations and all inputs and outputs of the model are related to the functional unit. The chosen functional unit is defined as $1\,kg$ of dried hydrogen produced in Portugal in PEMWE plants with a standard quality of 5.0 and $350\,bar$ pressure at 60 °C operating temperature.

3.1.3 Limitations

The data collection relies on the data found in the literature and data gathered through contact with writers of earlier LCA reports. Due to this, this thesis is based on some key assumptions.

3.1.4 System Description and Boundaries

This study is a cradle-to-grave LCA, assessing the energy consumption and emissions associated with the hydrogen production using Siemens Silyzer 300 PEMWE with $17.5\,MW$ each (stage B) with the electricity generated from an OWF comprising of 70 Vestas $V164-8.0\,MW$ wind turbines with a total power of $560\,MW$ (stage A). The hydrogen is then compressed by a mechanical reciprocating piston compressor from $30\,bar$ to $350\,bar$ (stage C) and stored in tanks type I (stage D) to be transported by truck to the the refueling station. The OWF, includes as mention before in chapter 2, the WTs, $66\,kV$ inter array cables, an offshore substation, $150\,kV$ transmission cable and an onshore substation. **The lifetime of the system is considered to be 20 years [41].** The number of OWF and the number of PEMWE connected to each wind farm depends on the scenario. There are eight steps for each of the four stages of the system as shown in Figure 3.1:

1. **Raw material extraction.**
2. **Material processing**, activities needed to convert the raw material and energy inputs into the desired materials for the products of the system.
3. **Manufacturing of the components** with the materials that were produced in the material processing.
4. **Construction and set-up of each of the stages.**
5. **Operation and maintenance of the system.**
6. **Dismantling**
7. **Waste management**, after the product has served its intended function and is returned to the environment as waste.
8. **Landfill, incineration or recycling.**

In Figure 3.1 is presented the system boundaries of the LCA for this study. It includes all stages from wind energy until the distribution of the hydrogen to the HRS divided in four main stages: **OWF, PEMWE, compressor and storage**.

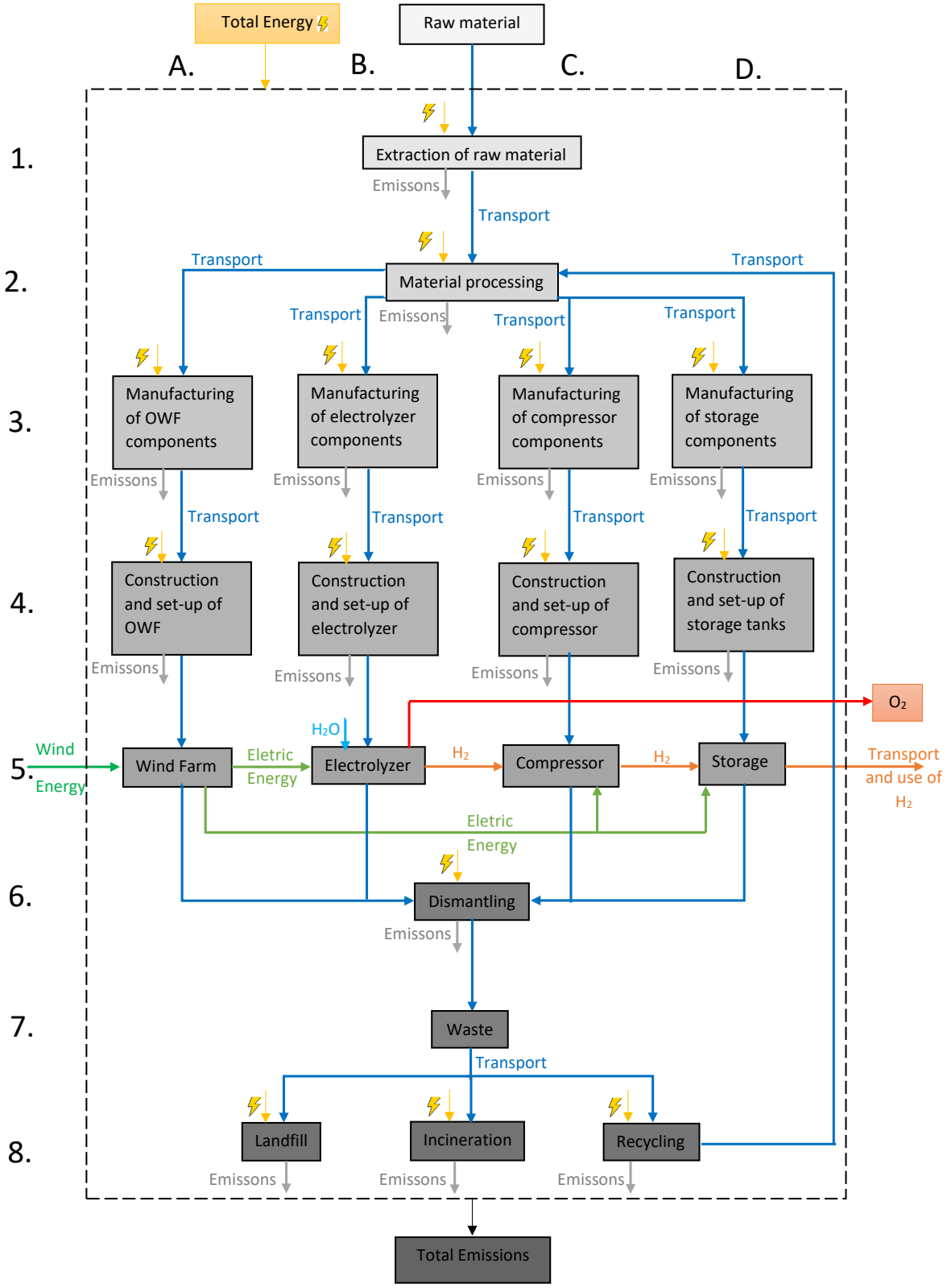

Figure 3.1: Diagram of system boundaries for LCA.

3.1.5 Definition of Scenarios

Two different scenarios are proposed in order to foresee the future of H_2 in the Portuguese fleet by offshore wind energy. Each scenario is divided in two different configurations, according to the plant power ratio (PPR) which is given by equation 3.1:

$$PPR = \frac{Rated\,PEMWE\,load\,capacity}{OWF\,load\,capacity} \times 100 \tag{3.1}$$

PPR is the ratio that will define the differences between configurations A and B.

3.1.5.1 Scenario 1 and 2

The difference between scenario 1 and 2 is the demand for hydrogen in the mobility sector. In scenario 1 only 5% of small vehicles and 16% of heavy vehicles of the Portuguese fleet would be moved by hydrogen in 2050. In scenario 2, the hydrogen needed for a 30% vehicle penetration by 2050 is considered as is going to be seen in the section 3.1.6. Each scenario is divided in configuration A and B, with different PPR.

Configuration A

Configuration A is only dedicated to produce hydrogen and almost all the energy generated by the OWF (96.4%) is going to be to produce hydrogen with a PPR of 62.5% because is the maximum PPR, considering the electricity used for H_2 compression and transmission losses as well. The system in this configuration is composed by an OWF which is connected to 20 PEMWE and to 8 compressors each one compressing hydrogen at a rate of $430\,kg/h$ from $30\,bar$ at the outlet of the PEMWE to $350\,bar$. After the compression stage, the hydrogen is stored in cylindrical type I tanks with capacity to $1000\,kg$ of hydrogen per tank, as already stated in the state of the art chapter, which are then transported by truck to the HRS. The hydrogen produced per day and per system is $77.52\,ton/day$, so 78 trucks are going to be needed per day and per system as shown in Figure 3.2.

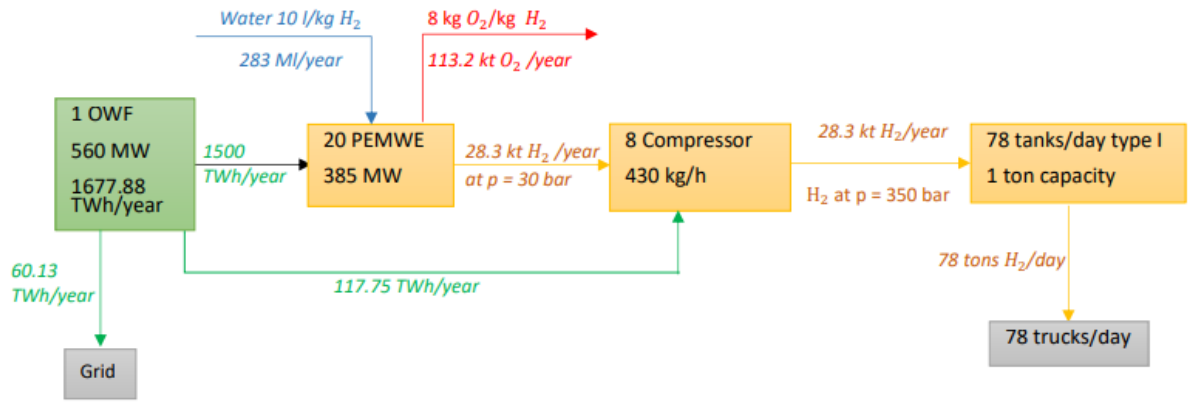

Figure 3.2: Diagram of the system main stages for configuration A.

Configuration B

Configuration B assumes that the PPR is 25% according to [74]. This configuration has the objective of representing the curtailment effect. Only 38% of the energy generated by the OWF is going to to produce hydrogen and 62% are going to be injected directed to the grid. The allocation of these 62% of energy is not considered in this thesis. The system in this configuration is composed by an OWF which is connected to 8 PEMWE and 3 compressors each one compressing hydrogen at a rate of $430\,kg/h$ from $30\,bar$ at the outlet of the PEMWE to $350\,bar$ and then the hydrogen is stored in a cylindrical type I tanks with capacity to $1000\,kg$ of hydrogen per tank which are then transported by truck to the HRS as in configuration A. The hydrogen produced per day and per system in this scenario is $35\,ton/day$, so 35 trucks are going to be needed per day and per system.

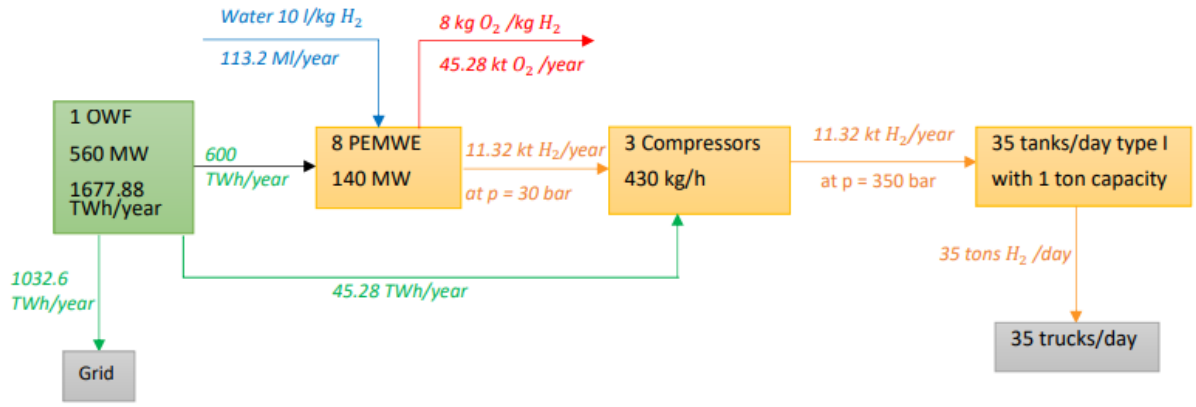

Figure 3.3: Diagram of the system main stages for configuration B.

According to the hydrogen demand in 2050, as shown next in the assumptions for each scenario:

- **Scenario 1A** 4 system's of Figure 3.2 are needed.
- **Scenario 2A** 16 system's of Figure 3.2 are needed.
- **Scenario 1B** 10 system's of Figure 3.3 are needed.
- **Scenario 2B** 39 system's of Figure 3.3 are needed.

3.1.6 Assumptions

This thesis will focus on green hydrogen production for the P2M value chain, so is going to be considered the application of hydrogen in the mobility sector because it's one of most dependent fossil fuel sectors and electrification is difficult. In order to calculate the quantity of hydrogen needed for the mobility sector, it's necessary to know about the number of vehicles in Portugal.

In table 3.1, an estimation of the number of small and heavy vehicles until 2050 assuming that small vehicles have the maximum weight of $3\,500\,kg$ is presented. The values between 2010 and 2020 were withdrawn from [75] and the values from 2020 until 2050 were calculated by doing a relation between

the Portuguese population and the average number from 2010-2020 of the number of vehicles per person. As shown in table 3.1, the Portuguese population is decreasing so the total number of vehicles is expected to reduce as well.

Table 3.1: Population of Portugal in thousands and number of vehicles by category 2010-2050.

		Small vehicles		Heavy vehicles	
Year	**Population (k)**	**Passenger car**	**Vehicle of goods**	**Trucks**	**Bus**
2010	10 573	4 692 000	1 337 373	65 236	15 425
2015	10 358	4 722 963	1 224 821	49 112	14 717
2020	10 206	4 632 324	1 232 764	50 443	14 676
2025	10 023	4 549 676	1 210 770	49 455	14 414
2030	9 841	4 467 028	1 188 775	48 560	14 152
2035	9 659	4 384 380	1 166 781	47 662	13 891
2040	9 477	4 301 732	1 144 786	46 763	13 629
2045	9 295	4 219 085	1 122 792	45865	13 367
2050	9 113	4 136 437	1 100 798	44 967	13 105

In table 3.2, the hydrogen consumption for a passenger car, small vehicle of goods and for buses and the annual distance cover per driver and per type of vehicle according to [76] are presented, being possible to calculate the annual consumption per vehicle. It was considered that trucks and buses had the same hydrogen consumption of $10\,kg/100km$. For the small vehicles of goods, it was considered that the fuel consumption was 1.5 times higher than a passenger car and the annual distance per driver to be double of a passenger car because no information about the vehicle of goods hydrogen consumption was found, so this assumption was made.

Table 3.2: H_2 consumption per driver by type of vehicle [76].

	Passenger car	**Small vehicle of goods**	**Bus & Truck**
H_2 **consumption** $kg/100km$	1	1.5	10
Annual distance per driver (km**)**	15 000	30 000	60 000
Annual H_2 **consumption per vehicle (**kg**)**	150	450	6 000

3.1.6.1 Scenario 1 H_2 consumption

Table 3.3 shows a conservative scenario for the number of small and heavy vehicles fueled by green hydrogen suggested by the Portuguese government in the script and plan for hydrogen in Portugal [14] and the annual hydrogen consumption was calculated by equation 3.2.

$$Hydrogen_{consumption} = 6000N_{heavy} + 150 \times 0.8N_{small} + 450 \times 0.2N_{small} \tag{3.2}$$

where N_{heavy} and N_{small} are the number of heavy and small vehicles. The small vehicles are divided in 80% passenger cars and 20% in small vehicle of goods.

This is a more conservative scenario because there is only a 5% incidence in the total of small vehicles and 16% in the heavy vehicles in Portugal by 2050 and if the goal of CO_2 neutrality is to be achieved, is necessary a greater effort.

Table 3.3: Scenario 1 (Conservative scenario) number of H_2 vehicles 2020-2050 according to [14] and the H_2 consumption.

Year	HRS	Small FCEV	Heavy FCEV	H_2 ($kton/year$)
2020	0	0	0	0
2025	10	2 000	500	3.42
2030	30	5 000	2 000	13.05
2035	50	50 000	3 000	28.5
2040	100	100 000	5 000	51
2045	150	175 000	7 000	78.75
2050	210	265 000	9 500	112.65

3.1.6.2 Scenario 2 H_2 consumption

A more optimistic scenario is presented in table 3.4 in which by the year 2050, 30% of the small vehicles and heavy vehicles were moved by H_2 with a progressive implementation of FCEV in the total Portuguese fleet between 2020 until 2050.

Table 3.4: Scenario 2 of number of H_2 vehicles 2020-2050 and H_2 consumption.

Year	Small FCEV	Heavy FCEV	H_2 ($kton/year$)
2020	0	0	0
2025	28 857	639	9.89
2030	56 665	1 881	23.19
2035	278 083	4 309	84.25
2040	545 681	7 247	158.08
2045	1 070 395	11 846	295.86
2050	1 574 140	17 422	435.1

3.2 Inventory Analysis

The LCI phase qualitatively and quantitatively analyses the materials and energy used (inputs), the products and by-products generated and the environmental releases in terms of non-retained emissions to specified environmental compartments and the wastes to be treated (outputs) in the entire life cycle of the system.

3.2.1 Offshore Wind Farm LCI

The WT considered for this study is the Vestas V164-$8\,MW$ wind turbine and the table 3.5 shows the specifications of the WT that are important for the study.

Table 3.5: Vestas V164-$8\,MW$ specifications from [77] and [78].

Parameters	**Value**
Power regulation	Pitch regulated with variable speed
Operating data	
Rated power (kW)	8 000
Cut-in wind speed (m/s)	4
Rated wind speed (m/s)	13
Cut-out wind speed (m/s)	25
Survival wind speed (m/s)	50
Tip speed (m/s)	104
Rotor speed range (rpm)	4.8-12.1
Nominal rotor speed(rpm)	10.5
Rotor orientation	upwind
Gearbox	Planetary gearbox
Electrical	
Generator	Permanent magnet generator
Converter	Full scale
Nominal voltage (kV)	33-35 or 66
Dimensions	
Rotor diameter (m)	164
Swept area (m^2)	21 124
Number of blades	3
Tower height (m)	106
Blade length (m)	80
Hub height (m)	Site specific (105-140)
Lifetime ($years$)	20
Weights	
Nacelle and hub (ton)	390 $\pm$ 10%
Blade (ton)	35
Tower (ton)	558

Tables 3.6 and 3.7 show the quantity and the bill of materials needed for the WT and the respective floating foundation (FF) with the information gathered by many articles [79], [71], [68], [80], [38], [67], [27] and [81]. The values in parentheses are the ones taken from the catalog of the turbine, which as shown in table 3.6 are very similar to the ones from the formulas found on the literature.

Table 3.6: Material inventory for the WT components [79], [71], [68], [80], [38], [67].

Components	**Formula**	**Mass (ton)**	**Material**
Rotor	—	222	—
Blades	$12.58P$	101 (105)	65% Fiber Glass, 35% Epoxy resin
Hub	$11.522P$	92.2 (90)	Cast iron
Pitch system	$2.98P$	23.8	Steel
Nose Cone	$0.65P$	5.2	Steel
Nacelle	—	283.5 (285)	—
Generator [80]	$10.51P^{0.9223}$	41.8	75% Cast iron, 5% Copper, 20% Aluminium
Low speed shaft	$3.13P$	25	Steel
Gearbox	$8P$	64	50% Steel, 50% Cast iron
Main bearings [80]	$2 \times (\frac{8D}{600} - 0.033) \times 0.0092D^{2.5}$	13.6	Cast iron
Brake and high-speed shaft [80]	$1.9894P - 0.1141$	15.9	Steel
Mainframe	$5.25P$	42	Steel
Cover [80]	$\frac{11.537P+3849.7}{10}$	9.6	60% Fiber glass, 40% Epoxy resin
Yaw system	$4P$	32	Steel
Hydraulics and cooling [80]	$0.08P$	0.64	95% Steel, 5% Lubricating oil
Transformer and converter [79]	$4.85P$	38.8	60% Cast Iron, 20% Copper, 20% Aluminium
Tower and cables	—	(558)	90% Steel, 2% Copper,1% PP, 2% Aluminium, 1% PE, 2% Electronics, 1% Epoxy resin, 1% Lubricating Oil
Total wind turbine	—	1 063.5	64% Steel, 18% Cast iron, 7% Fiber glass, 2% Copper, 1% Electronics, 4% Epoxy resin, 0.5% Lubricating Oil, 0.5% PP, 3% Aluminium,0.5% PE

In table 3.6, P is the power of the WT in MW and D is the diameter of the rotor in meters.

Table 3.7: Material inventory for the wind turbine floating foundation [27], [81].

Components	**Mass (ton)**	**Material**
Hull steel mass	3 914	Steel
Tower interface mass	100	Steel
Fixed ballast mass	2 540	Concrete
Fluid ballast mass	11 300	Sea water
Mooring system [81]	344	Steel
Total FF [27]	6898	63% Steel, 37% Concrete

The floating foundation is mainly composed by steel, with some concrete used as ballast for the stability of the foundation [27]. The mooring system configuration consists of two $850\,m$ and one with

$450\,m$ long chain catenary lines [27] which connects the structure of the foundation to the sea ground. The weight density of the mooring system is constant and assumed to be $160\,kg/m$ according to [81] and [67].

In table 3.8, the inventory of an OWF is shown with all the components. N is the number of wind turbines, m_{WT} and m_{FF} are the mass of each WT and FF respectively. These parameters are presented and calculated in tables 3.6 and 3.7, P is the power of the wind farm in MW, h is the depth at which the offshore substation is located in meters and l is the length of the export cable also in meters. The inter array cables mass density is going to be assumed to be $30\,kg/m$ and the weight density of $75\,kg/m$ was considered for the export cables as already stated in the state of the art. **The onshore substation was assumed to have the same mass as the topside of the offshore substation.** The greatest material contribution is from steel with 63% of all the mass of the OWF, followed by concrete with 31%. Steel and concrete together make 94% of all the mass of the OWF.

Table 3.8: Inventory OWF components [79], [71], [68], [80], [38], [67], [69].

Component	**Formula**	**Mass ($kton$)**	**Material**
Wind Turbines	$N.m_{WT}$	74.43	————
Floating Foundation	$N.m_{FF}$	482.86	60% Steel 40% Concrete
Inter array cable	$0.03 \times (0.0007P^2 + 0.02P + 6.07)$	7.11	30% Copper, 40% Aluminium, 10% PE, 10% PP, 10% Steel
Offshore Substation [67]	$0.016(h)^{0.19}(\frac{P}{0.133})^{0.48}$+ $\frac{P}{0.133}$	5.99	95% Steel, 2% Copper, 0.5% PE, 1.5% Aluminium, 1% Lubricating oil
Export Cable [30]	$0.075L$	0.75	40% PE, 25% PP , 15% Steel, 10% Copper, 10% Aluminium
Onshore Substation [67]	$16.042(h)^{0.19}(\frac{P}{0.133})^{0.48}$	4.21	95% Steel, 2% Copper, 0.5% PE, 1.5% Aluminium, 1% Lubricating oil
Total Offshore WF	————	575.35	63% Steel, 31% Concrete 0.7% Copper, 0.2% PE, 0.2 % PP, 0.9% Aluminium, 2% Cast Iron, 0.1% Lubricating oil, 0.1 % Electronics, 0.9 % Fiber Glass, 0.5 % Epoxy Resin

In table 3.9, the OWF data is presented.

Table 3.9: General data about the OWF.

Wind Farm	**Value**
Number of turbines, N	70
Depth, $h\,(m)$ [82]	40
Distance from shore (km)	20
Offshore substation distance to shore, l (km)	10
Wind Farm Power, P (MW)	560
Capacity Factor, CF (%)	41
AEP_{WT} ($TWh/year$)	28.73
AEP_{OWF} ($TWh/year$)	1677.88
Energy 20 years (PWh)	33.56

3.2.1.1 Wind farm operation and maintenance

Lubricating oil replacement, transport by barge and by helicopter is considered in the operation and maintenance phase while part or platform replacement during the lifetime of the OWF is not considered [67].

Lubricating oil used in the operation phase is considered to be 10 times of beginning lubricating oil [67], so $4720\,ton$ of extra lubricating oil is needed during the lifetime of the wind farm.

Maintenance by barge is assumed to be 10 times a year [68] with a distance of approximately $100\,km$ cover per day and per barge which is about $10\,h$ of work. Each maintenance is considered to be done in 5 days ($50\,h$) which means 50 days ($500\,h$) per year [69] and the fuel consumption of the barge is considered to be $100\,kg/h$ of diesel according to [69] which means a $5000\,kg$ diesel consumption for each time a maintenance is needed, $50\,ton$ annual diesel consumption and a $1000\,ton$ consumption of diesel for the lifetime is considered.

For transport by helicopter is considered 4 hours per wind turbine and per year [67] and the OWF considered has 70 turbines which means 280 hours per year of operation and for the lifetime of the OWF means 5600 hours. The helicopter fuel consumption considered is $100\,kg/hour$ taken from [83], which means $560\,ton$ of gasoline consumption by the helicopter for the lifetime of the system. In table 3.10 is summarized all the data about the O&M of the OWF.

Table 3.10: O&M of the OWF

O&M	**Value (year)**	**Value (lifetime)**
Lubricating oil (ton)	236	4720
Transport by barge, diesel (ton)	50	1000
Transport by helicopter, gasoline (ton)	28	560
Total (ton)	314	6.28

3.2.1.2 Construction and set-up

All the WTs and FFs are installed in the harbour. First the foundation is implemented, followed by the tower which is connected to the foundation. Then the nacelle is elevated by a crane and putted on the top of the tower and finally the rotor is connected to the nacelle. After the WT and FF are all set, they are transported to the OWF by barge. For cables, excavation of the trenches are estimated as $0.6\,m^3$ and $0.8\,m^3$ for medium voltage and high voltage cables respectively [67] and for the installation of the substation, excavation with hydraulic digger is considered [67].

Energy payback time (EPT) represents the time required when the energy output equals the energy input at it 's production, installation, O&M, and EoL stages [69]. The net EPT is considered to be around 1 year, so 20 times less than the energy produced for the lifetime of 20 years of the OWF [38], [69].

3.2.1.3 Complete LCI of OWF

In table 3.11 all the inventory for the OWF including O&M and the energy used for the construction and installation of the OWF is presented.

Table 3.11: Inventory of one OWF with 70 turbines and 560 MW power.

Material	**Total mass ($kton$)**	**Mass (g/kWh)**	**Mass (g/kgH_2) Configuration A**	**Mass (g/kgH_2) Configuration B**
Steel	362.64	10.79	372.76	934.53
Concrete	178.7	5.32	183.85	460.94
Cast iron	13.47	0.38	13.87	34.77
Aluminium	5.01	0.14	5.15	12.92
Fiber Glass	4.99	0.14	5.13	12.87
Copper	3.9	0.11	4.01	10.06
Epoxy resin	3.13	0.089	3.22	8.06
PE	1.43	0.041	1.47	3.69
PP	1.27	0.036	1.31	3.28
Electronics	0.74	0.02	0.76	1.9
Lubricating Oil (with O&M)	5.19	0.15	5.34	13.4
Diesel (O&M)	1	0.03	1.03	2.58
Gasoline (O&M)	0.56	0.017	0.58	1.44
	Total energy (TWh)		**($kWh/kg\,H2$)**	**($kWh/kg\,H2$)**
Energy	1677.88		3.07	7.7

3.2.2 PEMWE LCI

This section presents the LCI data applied for the production of hydrogen including the electrolyzer plant, facility, electricity and water input.

Table 3.12 and table 3.13 show the main materials from the state-of-the-art and future PEM stack per MW and for the balance of plant (BOP) respectively. In this thesis is going to be considered the 2017 values for the stack. **As the lifetime of the stack is half the lifetime of the system, it's going to be considered that the stack is replaced after 10 years, so 2 stacks are considered [41].**

Table 3.12: Materials for a PEMWE stack state-of-the-art and near future [41].

.

Material (kg/MW)	**2017**	**Near future**
Titanium	528	37
Aluminum	27	54
Steel	100	40
Copper	4.5	9
Nafion	16	2
Activated carbon	9	4.5
Iridium	0.75	0.037
Platinum	0.075	0.010
Total	685.33	146.55

Table 3.13: Materials for a PEMWE BOP [41], [84], [85], [86].

Materials	**Components**	**Mass (kg/MW)**	**BoP (%)**
Steel	Container, pumps, Air blast chiller	10 000	50
Concrete	infrastructure	7 000	35
Electronics	Power, control	1 400	
Copper	Transformer, rectifier	1 000	5
PE	Vessel, pipping, tank	300	1.5
Aluminum	Transformer, rectifier	200	1
Lubricating oil	adsorbent, lubricant	200	1
Ion exchange resins	Resin filter	100	0.5
Total		20 000	100

A Siemens Silyzer-300 PEM electrolyzer was chosen because they have been used in different projects of green hydrogen production and is one of the biggest PEM system in the world. Currently, most of the projects with Siemens electrolyzers utilize the Silyzer 200 of $2\,MW$, but with the improvement of these technology the tendency is to increase the size of PEMWE plant.

According to Siemens [87], the efficiency of the PEM stack is 77% HHV which corresponds to 65% LHV. For all the system including the PEM module, the rectifier, transformer, transformer cooling, gas cooling and others auxiliaries the efficiency is 76% HHV or 64.2% LHV. With compression to $30\,bar$, the efficiency of the plant drops to 74% HHV or 62.6% LHV. The number of Siemens Silyzer-300 PEMWE connected to each OWF depends on the scenario which will be shown further in this thesis. In table 3.14 the specifications of the Siemens Silyzer 300 PEM electrolyzer are presented.

Table 3.14: Specifications of $17.5\,MW$ Siemens Silyzer 300 PEM electrolyzer [87].

Parameter	**Value**
Dimension full module array (l, w, h) (m)	$13.0 \times 6.0 \times 3.0$
Current density (A/cm^2)	1.5
Number of stacks	24
Power of Stack (MW)	0.73
Power of electrolyzer (MW)	17.5
System efficiency LHV (%)	63%
Specific system consumption $(kWh/Kg\,H_2)$	53
H_2 flow rate (kg/h)	340
O_2 flow rate (kg/h)	2 720
Plant availability (%)	95
Capacity factor (%)	50
Annual H_2 production $(ton/year)$	1414.74
Annual O_2 flow rate $(kton/year)$	5.66
Annual energy consumption (TWh)	75
Water consumption $(l/kg\,H_2)$	10
Annual Water consumption $(kl/year)$	14 147.4
Plant lifetime $(year)$	20
Stack lifetime $(year)$	10

3.2.2.1 PEMWE Operation and Maintenance

For the electrolyzer, lubricating oil replacement is considered for every $2500/3000\,h$ of operation, so 3 times per year. For the lifetime of 20 years, results in 60 replacements which means that for the lifetime of the electrolyzer the lubricating oil is going to be 60 times of the initial one [66].

3.2.2.2 Complete LCI PEMWE

Table 3.15 shows all the inventory for each of the Siemens Silyzer 300 PEMWE including the operation and maintenance lubricating oil replacement and the energy for construction of the PEMWE.

Table 3.15: Siemens Silyzer 300 PEM electrolyzer inventory.

Material	**Mass (ton)**	**Mass ($g/kg\,H_2$)**
Steel	178.5	6.3
Concrete	122.5	4.32
Electronics	24.5	0.86
Copper	17.66	0.62
Titanium	18.48	0.66
PE	5.25	0.186
Aluminum	4.45	0.16
Lubricating oil (including O&M)	210	7.42
Ion exchange resins	1.75	0.06
Nafion	0.56	0.02
Activated carbon	0.315	0.012
Iridium	0.026	0.001
Platinum	0.0026	0.0001
Total	584	20.62
Energy ($kWh/kg\,H_2$) [86]	-	1.67

3.2.3 Compressor and Storage LCI

3.2.3.1 Compression Operation and Maintenance

The compressor was designed to run simultaneously to the electrolyzer, so the hydraulic aggregate driving the pistons of the compressor is going to be changed the same times as the electrolyzer [66] which is 60 times during the lifetime of the system.

3.2.3.2 Complete LCI Compressor

The energy consumption during the compression of hydrogen is calculated based on the exit pressure of the compressor which is considered to be $350\,bar$ and is presented in table 3.16. The energy to compress the hydrogen is from the electricity generated by the OWF.

The material and energy consumption during manufacturing of components and construction of the compressor is presented in table 3.17. The compressor has an efficiency of 70% and lifetime of 20 years.

Table 3.16: Compressor and storage energy consumption of the power plant.

Component	**Electric energy ($kWh/kg\,H_2$)**
Compression and storage	4

Table 3.17: Compressor material [66], [73].

Material	**%**	**Mass ($g/kg\,H_2$)**
Steel	34	5.90
Concrete	40	7.00
Cast Iron	5	0.87
Copper	2	0.35
Lubricating Oil (including O&M)	17	2.95
Aluminium	1.5	0.26
PP	0.3	0.05
Electronics	0.2	0.03
Total	100	17.4
Energy ($kWh/kg\,H_2$)	—-	1.4

3.2.3.3 Storage LCI

In the storage stage, a $350\,bar$ pressure and type I tanks with capacity to $1000\,kg$ of hydrogen will be considered.

Type I storage tanks have a weight density of $1400\,kg/m^3$ of hydrogen according to [59] and at $350\,bar$ the density of hydrogen is $23\,kg/m^3$ which means a volume of $43.5\,m^3$ for a $1000\,kg\,H_2$ tank capacity with the tank weighting $60.9\,ton$. A lifetime of 20 years was considered for the tanks according to [88], which means 7300 cycles if each tank is used once a day, so the mass of steel is $8.3\,g/kg\,H_2$.

Type III tanks have a lower mass density but the materials are more expensive and have a greater environmental impact than type I tanks. Type III storage tanks have a weight density of $450\,kg/m^3$ of hydrogen according to [59] and at $350\,bar$ with a density of hydrogen of $23\,kg/m^3$, the tank weights approximately $20\,ton$. For the same 7300 cycles if each tank is used once a day, the mass of carbon fiber and aluminium are 2.4 and $0.3\,g/kg\,H_2$ respectively.

Type I tanks are going to be considered in this thesis. In table 3.18 the material in order of the functional unit for type I and type III tanks are presented.

Table 3.18: Storage tanks material.

Material	**Type I ($g/kg\,H_2$)**	**Type III ($g/kg\,H_2$)**
Carbon fiber	0	2.4
Aluminium	0	0.3
Steel	8.3	0
Total	8.3	2.7

3.2.4 Material Processing and Manufacturing of System Components

The material processing of the materials used for all the system were the ones assumed by the simaPro software.

All the components of the system are assumed to be produced in their own factory. It's considered that the production is within Europe, therefore Europe grid mix was assumed to be the electricity used for the manufacturing process.

3.2.5 Transportation

Transport steps that have been included in this study are described below [38]:

- **Transport associated with raw materials to material processing** is assumed to be $600\,km$ by truck.
- **Transport of the material to the manufacturing factories of the components** is assumed to be $600\,km$ by truck.
- **Transport from the factories to the sites** are assumed to be $1000\,km$ by truck plus by barge for the OWF site.
- **Transport associated with EoF, recycling or disposal** assumed to be $200\,km$.
- **Transport to deliver hydrogen at the HRS** is out of the boundary of this study, so is not going to be considered.

The truck total average transport distance is $2400\,km$ with capacity to $60\,ton$ and the consumption intensity of the diesel is estimated as $50\,L/100\,km$ [89] with a diesel density of $0.83\,kg/L$ which means $41.5\,kg/100\,km$.

The calculation done to put the truck transportation relative to the functional unit was done by assuming that each truck transports $60\,ton$ of material which means is at full load and one system needs approximately $590\,kton$ of material, so 9819 trucks are needed to transport all the material. Each of the trucks makes $2400\,km$ in average, so in total the distance cover is 23.57 million km per system. Together with the diesel consumption and the hydrogen produced during the lifetime of the system which is $566\,kton$ and $226.4\,kton$ for configuration A and B respectively, is possible to reach the value of $17.28\,g/kg\,H_2$ for configuration A and $43.19\,g/kg\,H_2$ for configuration B.

For the transportation by barge, it was assumed that for each WT the distance cover is $40\,km$. The OWF has 70 turbines, so $2800\,km$ are needed for the WTs transportation. For the offshore substation and cables, is going to be considered $200\,km$. So the total distance of $3000\,km$ for barge transportation is considered. With a fuel consumption of $100\,kg/h$ of diesel and a velocity of $10\,km/h$ the barge diesel consumption is $30\,ton$. For configuration A the value is $0.05\,g/kg\,H_2$ and for configuration B is $0.13\,g/kg\,H_2$. So, the major diesel consumption comes from the truck transportation, with the total values for configuration A and B being 17.33 and $43.32\,g/kg\,H_2$ respectively.

3.2.6 End of Life

The end of life corresponds to the phase of landfill, recycle and incineration. In table 3.19 the type of disposal and ratios considered in this thesis for the different materials are summed up.

Table 3.19: Considered EoL methods for materials in the main analysis [69], [38], [67].

Material	Type of disposal and ratios
Polymers	50% incinerated + 50% landfilled
Lubricating oil	Incineration
Concrete	100% Landfill
Electronics	Dismantling, 50 % recycling, 50 % incineration
Steel	Recycle 90%, Landfill 10%
Cast Iron	Recycle 90%, Landfill 10%
Aluminium	Recycle 90%, Landfill 10%
Copper	Recycle 90%, Landfill 10%
Other materials	100% Landfill

In the overall of the system materials, 59% is recycled, 3% incinerated and 38% land filled. The percentage of recycled materials is high because 90% of the steel is recycled which is the material most used in the system with 60%, so the environmental impacts is expected to decrease when the EoL is considered.

3.2.7 Final LCI of the System

In table 3.20, the final LCI for all the system for configuration A and B are presented. These values will be used to evaluate the environmental impacts on the SimaPro software for configuration A and B.

Table 3.20: LCI of configuration A and B.

Materials ($g/kg\,H_2$)	OWF A (PPR = 62%)	OWF B (PPR = 25%)	PEMWE ($g/kg\,H_2$)	Compression	Storage	Transportation A	Transportation B	Total A	Total B
Steel	372.76	934.53	6.3	5.9	10	0	0	394.96	956.73
Cast iron	13.87	34.77	0	0.87	0	0	0	14.74	35.64
Aluminium	5.15	12.92	0.16	0.26	0	0	0	5.57	13.34
Copper	4.01	10.06	0.62	0.35	0	0	0	4.98	11.03
Fiber Glass	5.13	12.87	0	0	0	0	0	5.13	12.87
Epoxy resin	3.22	8.06	0	0	0	0	0	3.22	8.06
PE	1.47	3.69	0.186	0	0	0	0	1.656	3.876
PP	1.31	3.28	0	0.05	0	0	0	1.36	3.33
Electronics	0.76	1.9	0.86	0.03	0	0	0	1.65	2.79
Concrete	183.86	460.94	4.32	7	0	0	0	195.18	472.26
Lubricating oil	4.87	12.22	7.42	2.95	0	0	0	15.24	22.59
Ion exchange resins	0	0	0.06	0	0	0	0	0.06	0.06
Nafion	0	0	0.02	0	0	0	0	0.02	0.02
Activated carbon	0	0	0.012	0	0	0	0	0.012	0.012
Iridium	0	0	0.001	0	0	0	0	0.001	0.001
Titanium	0	0	0.66	0	0	0	0	0.66	0.66
Platinum	0	0	0.0001	0	0	0	0	0.0001	0.0001
Diesel	1.03	2.57	0	0	0	17.33	43.32	18.36	45.89
Gasoline	0.58	1.46	0	0	0	0	0	0.58	1.46
Total	598.02	1499.27	20.62	17.41	10	17.33	43.32	663.38	1590.62
Energy ($kWh/kg\,H_2$)	3.07	7.7	1.67	1.4	0.8	0	0	6.94	11.57

3.3 Impact Assessment Methodology

SimaPro software is a professional tool to evaluate the environmental impacts of products, processes and services through their life cycle. It allows to model and analyse the life cycle of a product or service

in a systematic and transparent way, following the recommendations of the ISO 14040 series (ISO14040, 2006). The midpoints impacts are considered a point in the chain of cause and effect, focusing on unique environmental problems such as climate change and the endpoint method analyses the environmental impact at the end of this chain of cause and effect. In the ReCiPe methodology, eighteen midpoint indicators and three more uncertain endpoint indicators are calculated. The conversion of midpoints into endpoints simplifies the interpretation of the LCA results, partly because there are too many impact categories and have a very abstract meaning. In this way, the endpoint approach provides results with a higher degree of interpretation but greater uncertainty. On the other hand, the midpoint approach is more reliable but does not provide damage information.

Due to the advantages and disadvantages of the midpoint and endpoint indicators, both methodologies have been combined in this study. In this way, on one hand, decisions can be made using midpoint indicators, which are more certain but, in some cases, may have less relevance for decision support. On the other hand, endpoint indicators are used, which have been shown to be more relevant and decisions can be made more easily but have less certainty [84].

Eighteen midpoint impacts were screened for all scenarios: **climate change (CC), ozone depletion (OD), terrestrial acidification (TA), freshwater eutrophication (FE), marine eutrophication (ME), human toxicity (HT), photochemical oxidant formation (POF), particulate matter formation (PMF), terrestrial ecotoxicity (TE), freshwater ecotoxicity (FEco), marine ecotoxicity (MEco), ionising radiation (IR), agricultural land occupation (ALO), urban land occupation (ULO), natural land transformation (NLT), water depletion (WD), metal depletion (MD) and fossil depletion(FD)** [84].

In addition, for a better understanding, the final point indicators were addressed. The following endpoint impacts were examined: **damage to human health (HH), damage to ecosystem diversity (ED) and damage to resource availability (RA).**

In the LCIA phase, three steps are considered: characterisation, normalisation, and weighting. In the characterisation process, the inventories results are transformed into impact categories and the results are presented as impact indicators. In the normalisation process, the normalised results are divided by a reference (typically the total contribution to the impact category per citizen per year). In the weighting process, the magnitude of the environmental impact can better be assessed. The unit of the normalised results is person equivalents. All the results were considered in the characterisation process, which facilitates the comparison between impact scores of different impact categories.

Chapter 4

Results and Discussion

In this chapter, the results obtained after applying the methodologies described in chapter 3 are presented and discussed.

4.1 Impact Assessment Analysis and Interpretation

LCA results for each evaluated impact category associated with the scenario considered are reported in this section. A positive impact potential indicates a burden to the environment (negative environmental effect), while a negative potential indicates environmental emissions savings (positive environmental effect).

In this section the values are all in order of the functional unit of $1\,kg$ of H_2.

Midpoint analysis

In Figures 4.1 and 4.2 the midpoint analysis with eighteen different categories are presented. The units in the graphics vary between categories and are in order of scale of units. CC, MD and HT are in kg, FD in hg, TE, FEco, MEco and ME in dg, TA, FE, PDF and PMF in g and OD in $0.1\,mg$. It's possible to see that for configuration A the OWF has the biggest impact in almost all categories except on the OD category where the PEMWE has a slightly higher influence with 48.24% compared to the 37.65% from the OWF. In the land occupation, ALO has the higher values when compared to ULO and NLT. These values were the expected because in the LCI phase, it's possible to see that the OWF has the major mass contribution by far and is the part of the system that needs more energy. In the WD category, the values are very similar between the OWF and the PEMWE which can be explained by the $10\,kg$ of water needed to produce $1\,kg$ of H_2. The storage of H_2 and transport of material have the lowest impact in every category, because the hydrogen storage tanks are going to be used 7300 times in their lifetime and in the transportation stage is only considered the diesel consumption of the trucks transporting the material necessary and each truck transports $60\,ton$ of material which means that the fuel consumption per kg of material and in order of the functional unit's very low.

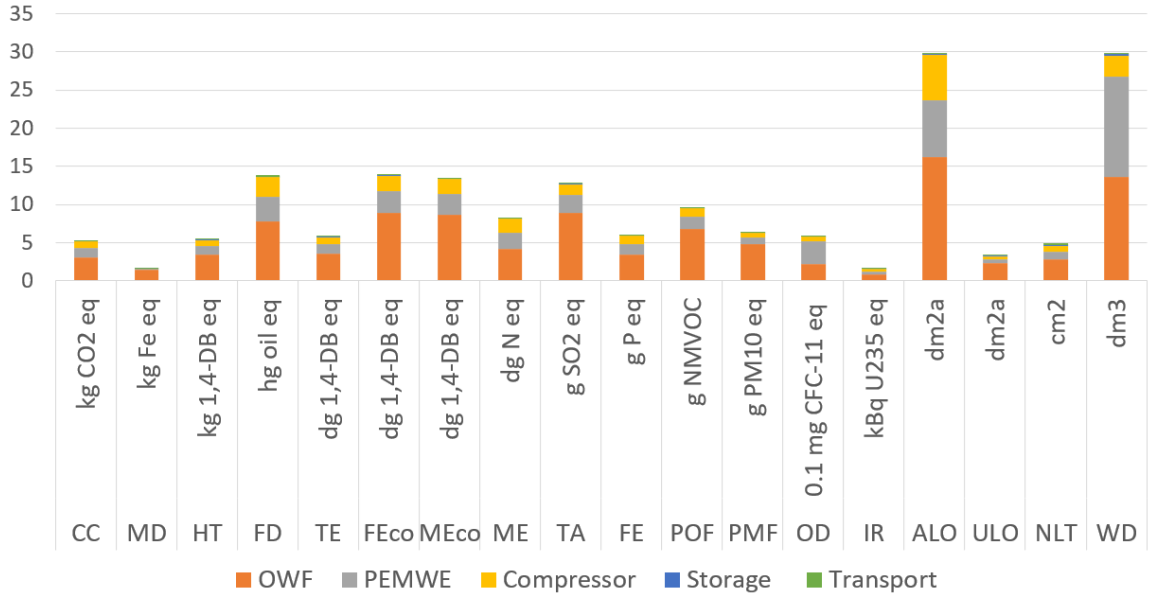

Figure 4.1: Midpoint analysis of the configuration A.

In configuration B, OWF has the highest influence in all categories because the PPR is going to be 25% for configuration B compared to 62.5% from configuration A, which means that the OWF will have even more impact in all the system because for each OWF there is less hydrogen being produced. Storage of H_2 and transport of material has the lowest impact as in configuration A and as shown in Figure 4.2.

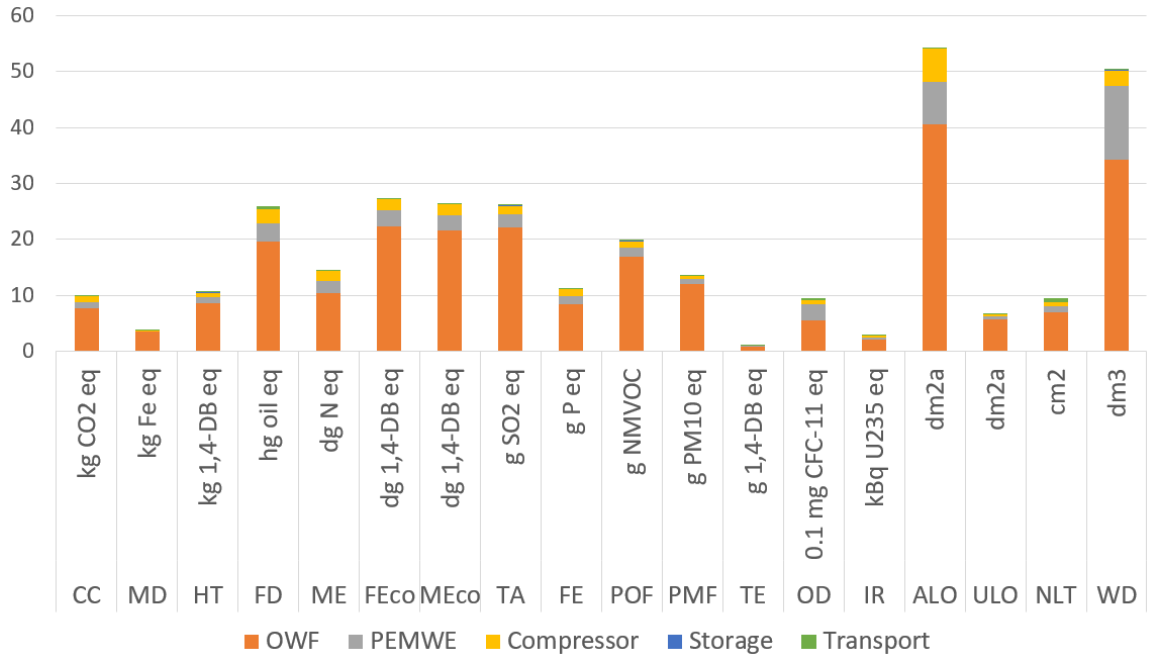

Figure 4.2: Midpoint analysis of the configuration B.

Endpoint analysis

Figures 4.3 and 4.4 show the endpoint analysis of configuration A and B.

For configuration A presented in Figure 4.3, resources is the category with the biggest environmental impacts with 58.3% of the contribution, followed by human health and ecosystems which account for 38.9% and 2.8% respectively.

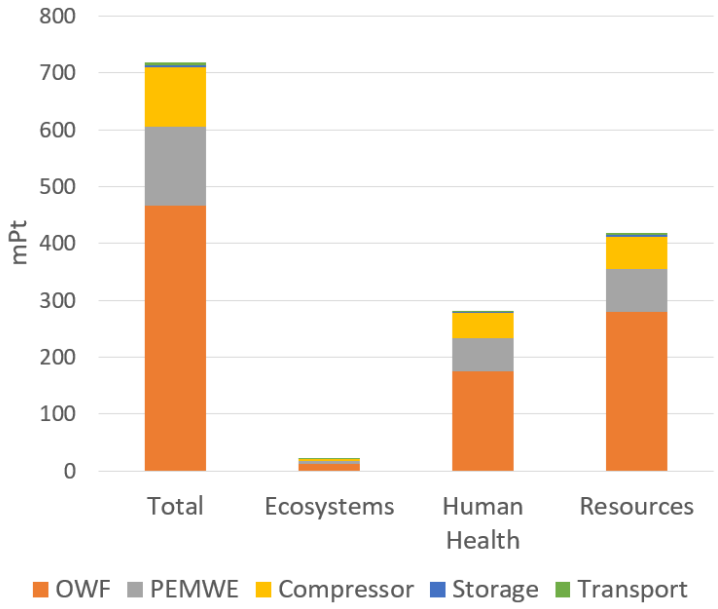

Figure 4.3: Endpoint analysis of the scenario A.

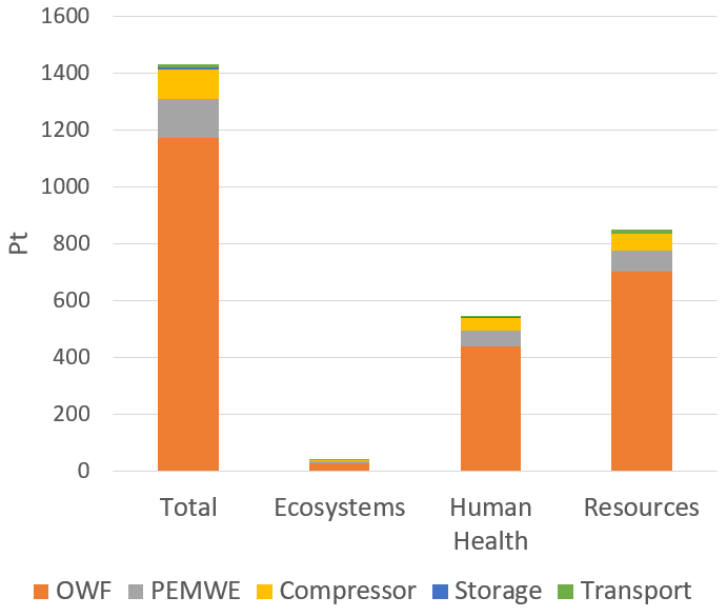

Figure 4.4: Endpoint analysis of the scenario B.

For configuration B presented in Figure 4.4, resources shows also the biggest environmental impact with 59.3%. The contribution from human health and ecosystems is 38% and 2.7% respectively. From the analysis of the Figure is possible to understand that the main contribution comes from the OWF with a contribution of 64.9% for configuration A and 81.8% for configuration B. In configuration B the contribution of the OWF is higher than in configuration A because in configuration B, there is part of the

energy that is not used to produce hydrogen, while in configuration A almost all the energy from the OWF is used to produce H_2. The contribution from the other stages for configuration A and B are 19.3% and 9.7 % from PEMWE, 14.5% and 7.3% from the compressor, 0.6% and 0.3 % from storage and 0.7% and 0.9% from transport respectively.

4.2 Comparison of Scenarios

4.2.1 Configuration A and B

Figure 4.5 shows the difference between the scenarios A and B for the midpoint parameters in order to the functional unit. There is only necessity to do this comparison for configuration A and B because scenario 1 and 2 have the same values in order to the functional unit, being only different in the demand for hydrogen. Configuration B has higher impacts in every parameter compared to configuration A which is the expected because of the PPR as already explained before and because the allocation of the energy that is injected into the grid in configuration B is not considered. If the functional unit was kWh and all the energy was considered in both configurations, there would be no difference between configurations.

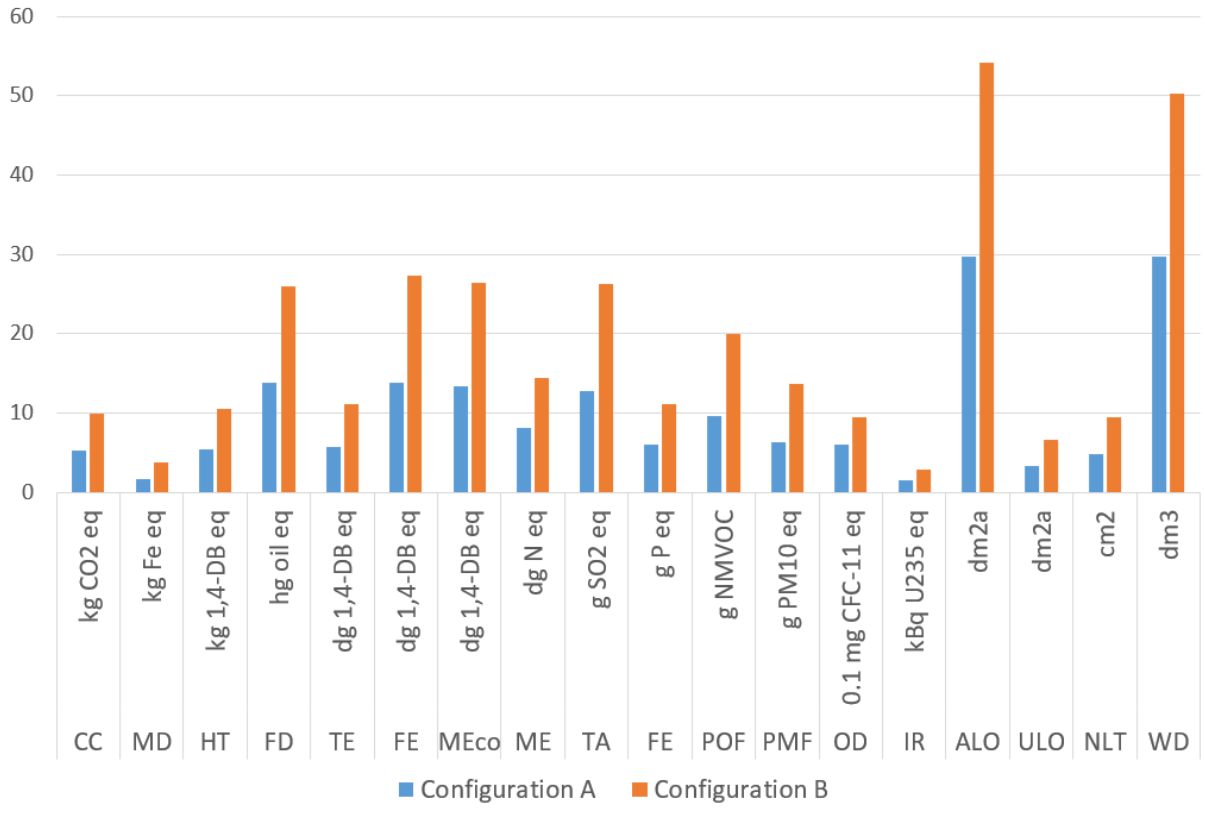

Figure 4.5: Comparison between configuration A and B using a midpoint analysis.

Figure 4.6 shows the difference between the scenarios A and B for the endpoint parameters. Configuration B has again higher impacts in every parameter compared to configuration A.

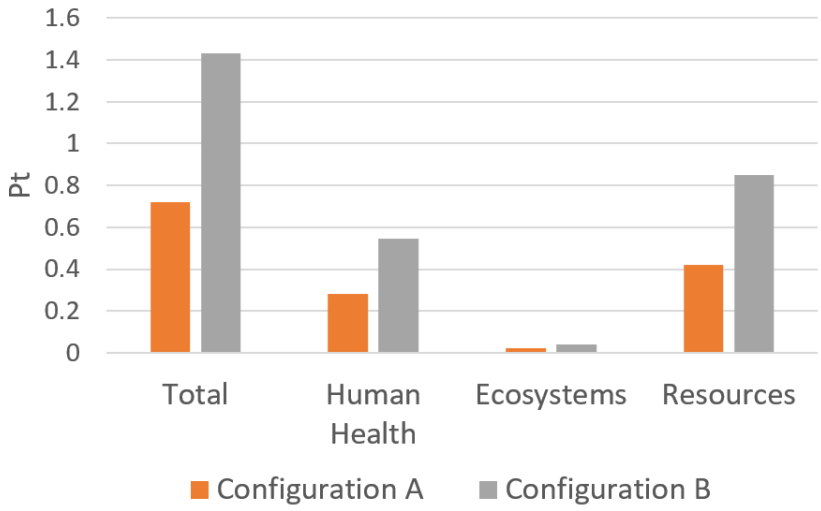

Figure 4.6: Comparison between configuration A and B using a endpoint analysis.

4.2.2 All Scenarios

The difference between scenario 1 and 2 is the quantity of hydrogen demand as already explained in chapter 3 of this thesis.

Scenario 1 has a demand of $112.65\,kton$ by the year of 2050 with a 5% and 16% incidence of small and heavy vehicles respectively.

Scenario 2 has a demand of $435.1\,kton$ by 2050 with a 30% of the small and heavy vehicles moved by hydrogen.

In Figure 4.7 is presented **the total values** for scenario 1A, 1B, 2A and 2B with the midpoint analysis and in Figure 4.8 for the endpoint analysis.

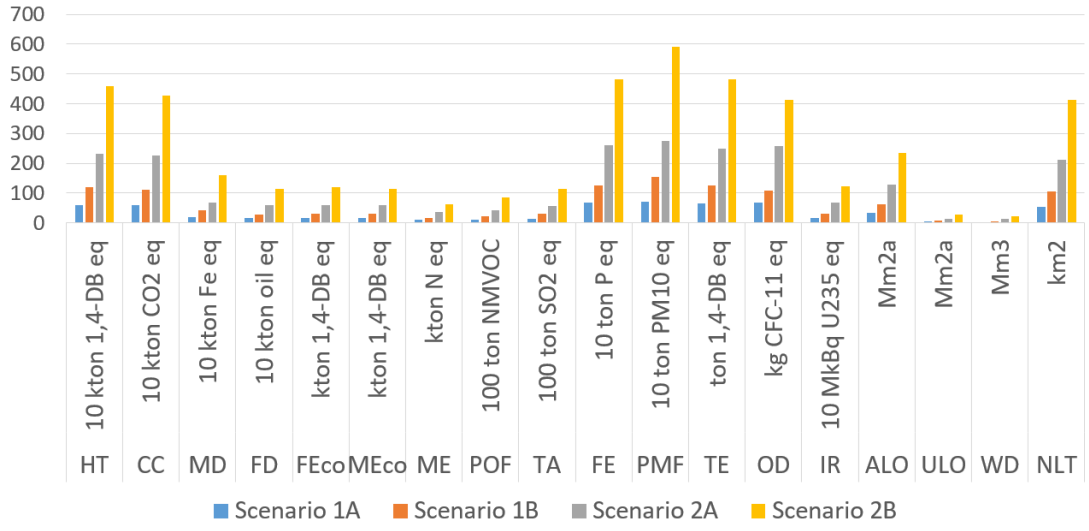

Figure 4.7: Comparison between scenario 1A, 1B, 2A and 2B using midpoint analysis.

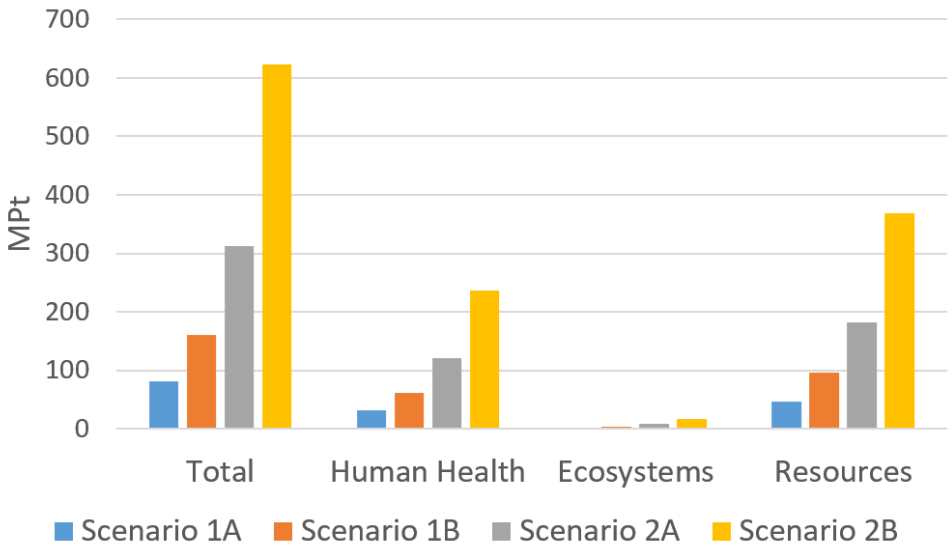

Figure 4.8: Comparison between scenario 1A, 1B, 2A and 2B using endpoint analysis.

4.3 Discussion of Results

4.3.1 Comparison with Different Energy Sources

The production of hydrogen in a SMR process is out of the scope of this study, but it's going to be considered as a reference value to compare with the values obtained. SMR process has average emissions of $11.5\,kg\,CO_2\,eq./kg\,H_2$ according to [41]. The $CO_2\,eq./kg\,H_2$ for configuration A and B are presented in table 4.1.

For configuration A the value of $5.21\,kg\,CO_2\,eq./kg\,H_2$ was found with the major contribution from the OWF with 58.77%, followed by the PEMWE, Compressor, storage and transport with a 22.58%, 18.13%, 0.34% and 0.19% contribution respectively.

For configuration B the value increases to $9.84\,kg\,CO_2\,eq./kg\,H_2$ with a even bigger contribution of the OWF with 78.02%.

This values does not include the EoF and most of the materials can be recycled, reducing the environmental impact by 25-35% according to [69] and [73]. It's going to be considered a reduction of 30% in the CC value of CO_2 emissions considering the EoL process. So, the total emissions are 3.65 and $6.89\,CO_2\,eq./kg\,H_2$ with the EoL for configuration A and B respectively. Comparing with SMR process, the emissions reductions from configuration A are 55% and almost 70% without and with EoL respectively and for configuration B are 15% and 40% without and with EoL respectively. In configuration B the emissions reduction is not the ideal result with low CO_2 emissions reduction compared to the SMR process, but can not be forgotten that this values are in function of kg of H_2 and in configuration B great part of the electricity is going to be injected on the grid which is not take into consideration.

Table 4.1: GHG emissions ($CO_2\ eq.$), whole system with and without EoL.

Configuration A	**CC ($kg\,CO_2\,eq./kg\,H_2$)**	**%**	**Configuration B**	**CC ($kg\,CO_2\,eq./kg\,H_2$)**	**%**
Total without EoL	5.21	100	**Total without EoL**	9.84	100
OWF	3.06	58.77	**OWF**	7.68	78.02
PEMWE	1.18	22.58	**PEMWE**	1.18	11.95
Compressor	0.94	18.13	**Compressor**	0.94	9.6
Storage	0.018	0.34	**Storage**	0.018	0.18
Transport	0.01	0.19	**Transport**	0.025	0.25
EoL	-1.56	-30%	**EoL**	-2.95	-30%
Total with EoL	3.65	-	**Total with EoL**	6.89	-

The values found on the literature for a similar process of this thesis are around $2\,kg\,CO_2\,eq./kg\,H_2$ including EoL and only producing hydrogen. When comparing the results of this thesis with the literature, the value of the configuration A with EoL should be the one to be used. The value is $3.65\,kg\,CO_2\,eq./kg\,H_2$ which is 80% higher when compared to the value of $2\,kg\,CO_2\,eq./kg\,H_2$. This can be explained by the fact that in that study from [66], is only considered a WT and the cable connection to the electrolyzer for the wind farm part and is not even considered the foundation of the WT. In this thesis is considered all the components of the OWF with the FF having the biggest material impact in the inventory of the OWF with 84% of the mass of all the OWF as already stated in the chapter 3 of this thesis.

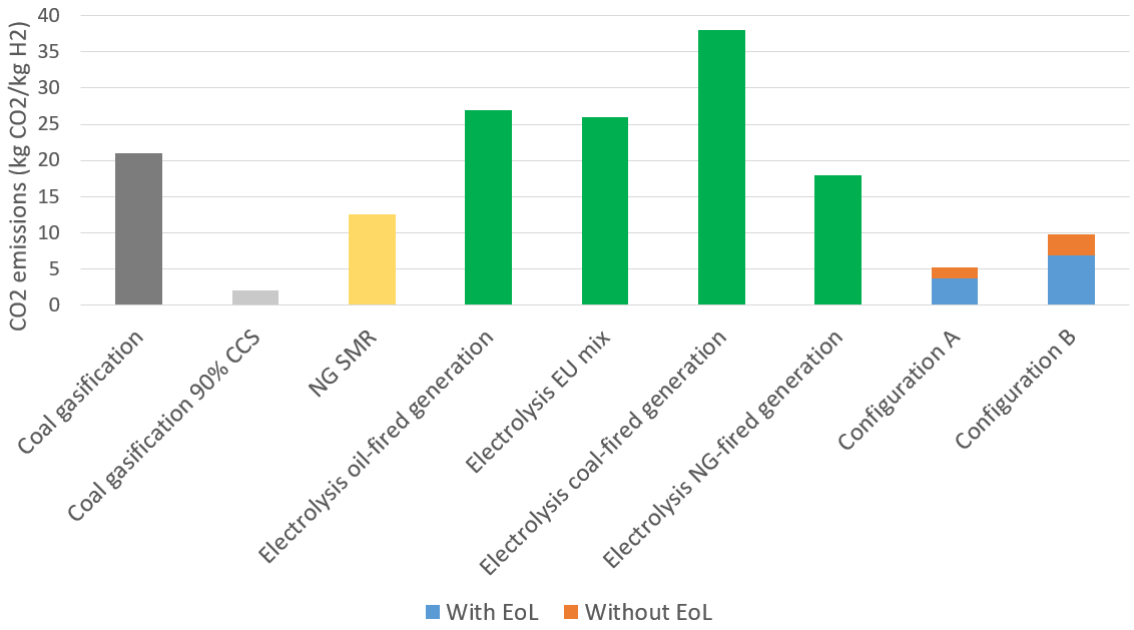

Figure 4.9: CO_2 emissions during hydrogen production from different energy sources [16].

In Figure 4.9 is possible to see the $kg\,CO_2/kg\,H_2$ emissions by different energy sources. Electrolysis from coal-fired generation causes $38\,kg\,CO_2/kg\,H_2$, followed by oil fired generation with $27\,kg\,CO_2/kg\,H_2$ and $18\,kg\,CO_2/kg\,H_2$ for natural gas (NG) according to [16]. When compared to the process of electrolysis by coal-fired generation, hydrogen production by the offshore wind energy according to the results

of this thesis has 90.4%, 86.3%, 82% and 74.2% less $CO_2/kg\,H_2$ emissions produced for configuration A and B with and without EoL respectively. Compared with electrolysis from oil-fired generation, configuration A has 86.5% and 80.7% with and without EoL $CO_2/kg\,H_2$ emissions reduction and configuration B has 75% and 64% less $CO_2/kg\,H_2$ emissions with and without EoL respectively. Compared with electrolysis from NG, configuration A has 80% and 71% and configuration B has 62% and 45.4% $CO_2/kg\,H_2$ emissions reduction with and without EoL respectively. Electrolysis from EU electricity mix causes $26\,kg\,CO_2/kg\,H_2$ which means a 86.5%, 80%, 73.5% and 62.2% reduction for configuration A and B with and without EoL. Coal gasification has $21\,kg\,CO_2/kg\,H_2$ emissions and SMR from NG has $11.5\,kg\,CO_2/kg\,H_2$. The $CO_2/kg\,H_2$ emissions reduction for configuration A and B with and without EoL respectively are 82.6%, 75.2%, 67.2% and 53.2% compared with coal gasification. For the SMR process from NG the comparison has already been made. Coal gasification with 90% CCS has emissions of only $2.1\,kg\,CO_2/kg\,H_2$ which is 42.5% less than configuration A with EoL. This can be explained by the fact that the emissions in that process are only from the combustion and from the CCS process, without counting with the infrastructure necessary.

In Figure 4.10 it's possible to see the emissions in $g\,CO_2/MJ$ of the respective fuel. It's considered the emissions regarding the production and combustion of the fuel. There are only emissions regarding the combustion in the petrol, diesel and CNG cases which have the major contributions when compared to the production for the same cases. Configuration A with and without EoL has lower emissions per MJ of fuel when compared with all the others fuels. Configuration B counting with the EoL stage has only greater emissions when compared to hydrogen from coal gasification with CCS. If the EoL is not considered, configuration B has almost the same value of the diesel and petrol cases.

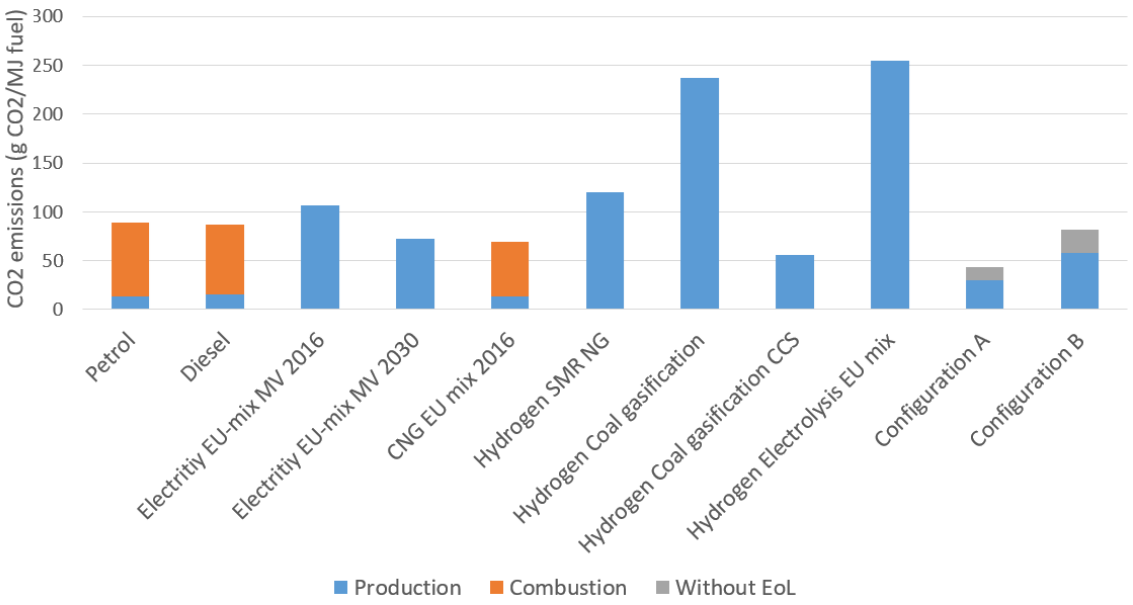

Figure 4.10: CO_2 emissions per MJ of final fuel.

In Figure 4.11 is presented the energy consumption of the selected pathways. It shows the net energy expended per MJ energy content of the final fuel, which means the energy necessary per MJ

of the fuel. For configuration A the energy expendure is $24.984\,MJ/kg\,H_2$ and in configuration B is $41.652\,MJ/kg\,H_2$. The LHV of H_2 is $120\,MJ/kg\,H_2$, so the MJ/MJ of final fuel is 0.21 and 0.34 for configuration A and B respectively. The values found in the literature for petrol and diesel are 0.24 and 0.26 respectively, which are not very different when compared to configuration A and B. CNG has a value of $0.17\,MJ/MJ$ final fuel which is 20% and 50% lower than configuration A and B. This Figure has the objective to show the energy benefit compared to the energy input. Configuration A needs 38.2% less energy to produce one MJ of hydrogen compared to configuration B.

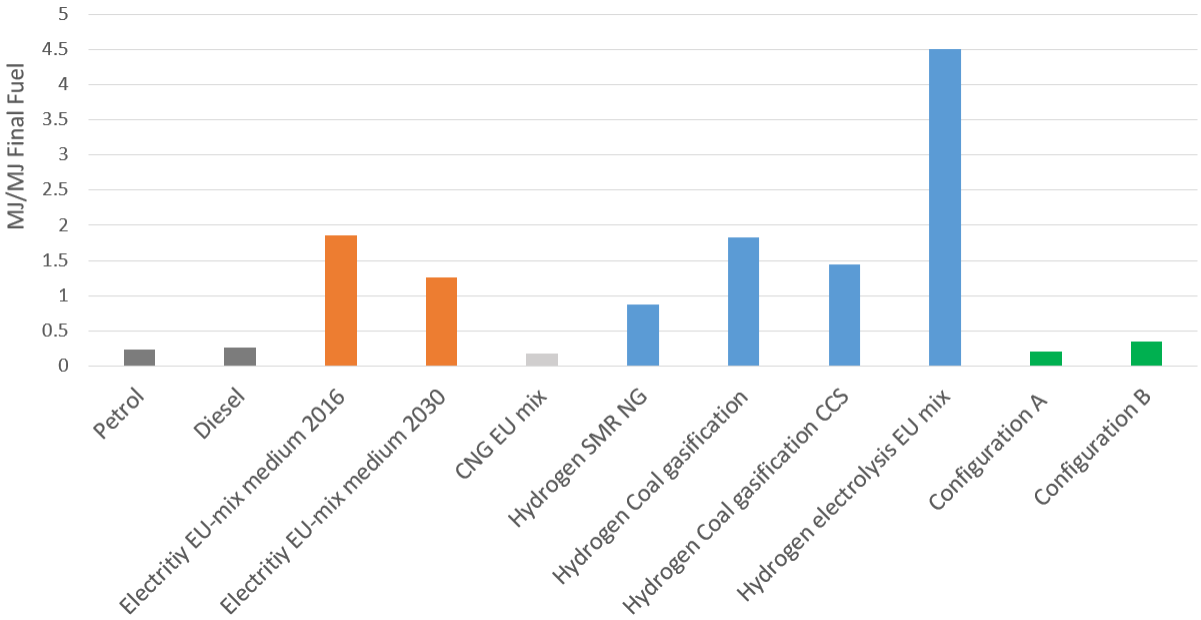

Figure 4.11: MJ per MJ of Final Fuel.

4.3.2 Comparison to the Mobility Sector from Conventional Fuels

To obtain a comparison in the mobility sector from conventional fuels, results are compared based on specific GHG emissions ($kg\,CO_2\,eq./km$). Data for conventional fuels are taken from [66] and [89] including upstream processes such as exploration of mineral oil and refinery processes. The GWP of petrol is around $84\,g\,CO_2\,eq./MJ$ [41] and the energy density of petrol is $35\,MJ/L$, which leads to a $2940\,g\,CO_2\,eq./L$ of petrol. Considering a fuel consumption of $6.2\,L/100\,km$ for small vehicles from [66], means a $182.28\,g\,CO_2\,eq./km$ for petrol vehicles.

For diesel vehicles it's around $88\,g\,CO_2\,eq./MJ$ [41] and the energy density of diesel is $45.5\,MJ/L$, which leads to a $4004\,g\,CO_2\,eq./L$ of diesel. Considering a fuel consumption of $4.6\,L/100km$ for small vehicles according to [66] and $40\,L/100km$ for heavy vehicles, this means a $184.18\,g\,CO_2\,eq./km$ and $1601.6\,g\,CO_2\,eq./km$ for small and heavy vehicles respectively.

The values for the small vehicles found for configuration A and B are 52.1 and $98.4\,g\,CO_2\,eq./km$ respectively without the EoL. Considering the EoL stage, the emissions will reduce to $36.5\,g\,CO_2\,eq./km$ for configuration A and $68.6\,g\,CO_2eq./km$ for configuration B.

For the heavy vehicles, the values for the CO_2 emissions are 521 and $984\,g\,CO_2\,eq./km$ for configuration A and B respectively without the EoL and counting the EoL the values reduce to 365 and $689\,g\,CO_2\,eq./km$ repectively for configuration A and B.

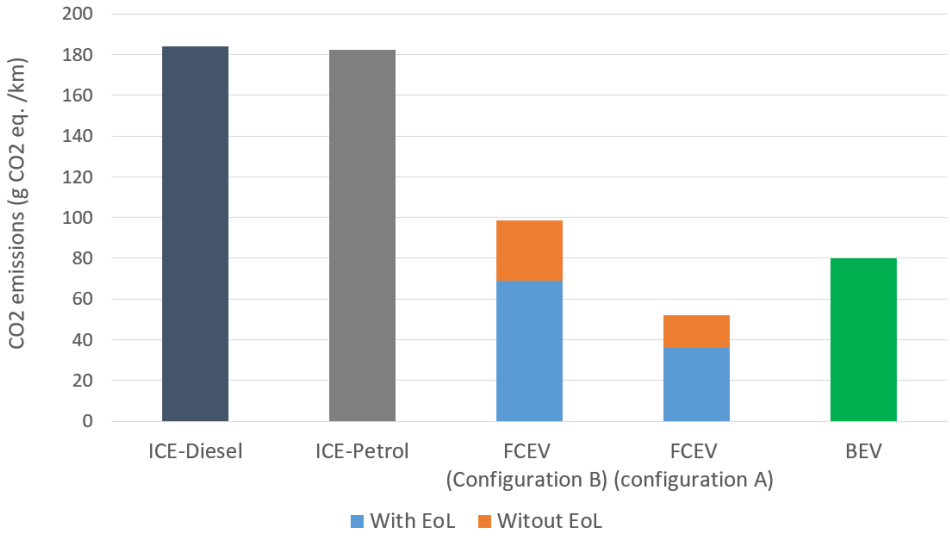

Figure 4.12: Specific $g\,CO_2\,eq./km$ emissions of different power trains for small vehicles.

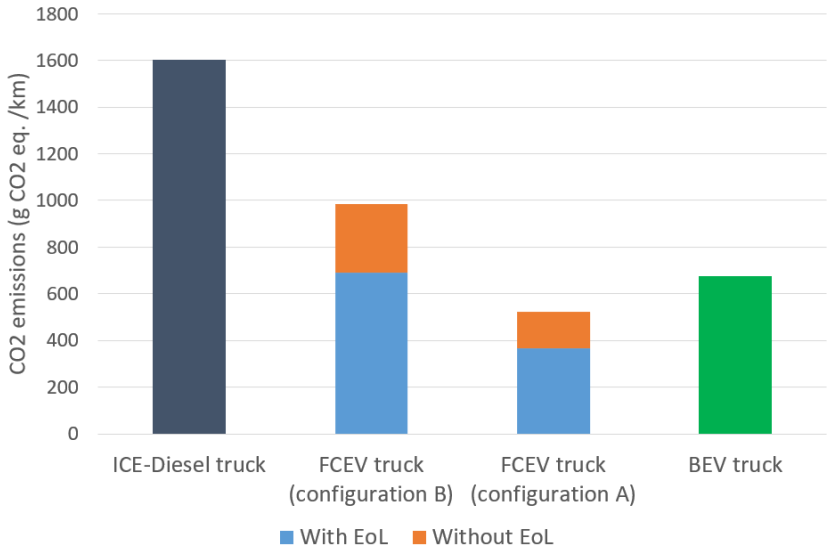

Figure 4.13: Specific $g\,CO_2\,eq./km$ emissions of different power trains for heavy vehicles.

In Figures 4.12 and 4.13 it's possible to see that the FCEV has always lower $g\,CO_2\,eq./km$ emissions when compared to the diesel and petrol vehicles in small and heavy vehicles.

For small vehicles shown in Figure 4.12, there is a reduction of almost 80% and 60% for configuration A and B with EoL and 70% and 50% for configuration A and B respectively without EoL in the $g\,CO_2\,eq./km$ emissions comparing with ICE vehicles. When compared to a small battery electric vehicle (BEV), only the configuration B without EoL has higher emissions, with around 20% more $g\,CO_2\,eq./km$ emissions than a BEV vehicle. Configuration A with and without EoL have 55% and 35% respectively

lower $g\,CO_2\,eq./km$ emissions and configuration B with EoL has 14% $g\,CO_2\,eq./km$ emissions reduction when compared to BEV.

For heavy vehicles presented in Figure 4.13 there is a reduction of 77.2% and 67.5% in the $g\,CO_2\,eq./km$ emissions for configuration A with and without EoL respectively and of 57% and 38.5 for configuration B with and without EoL, comparing with an ICE diesel truck. Comparing with an heavy BEV which has $674\,g\,CO_2\,eq./km$ emissions, only configuration A has lower emissions with a 46% and 23% $g\,CO_2\,eq./km$ emissions reduction with and without EoL. Configuration B has 2.2% and 46% higher emissions with and without EoL comparing with an heavy BEV.

Chapter 5

Conclusion

5.1 Achievements

Throughout the course of this study, taking into account the initial objectives, several achievements were attained:

- Currently, there are three main technologies of electrolyzers: AWE, PEM and SOE. A PEMWE Siemens Silyzer 300 was chosen for the calculations due to its better operational flexibility to the intermittent wind production.
- There are many ways to store hydrogen, with either the necessity to compress the hydrogen or to lower the temperature to very low levels because of the high volume density. In this thesis the hydrogen is compressed and stored in tanks type I, because although these tanks are the heaviest, they are the best economical option without expensive materials.
- In configuration A the system is only dedicated to producing hydrogen (96% of the energy) with a PPR of 62.5%. For configuration B a PPR of 25% is considered with only 38% of the energy generated by the OWF to produce hydrogen with the objective to take advantage of the **the curtailment effect**. This means that more systems for the same demand of hydrogen are needed, so configuration B is going to have higher impact in all categories compared to configuration A in terms of the functional unit.
- In the LCI phase, it was concluded that the major material contribution came from the OWF with around 90% of the weight of the system. In the OWF, the major contribution is from the FF with 84% of the total weight of the OWF. Reducing the FF quantity of material would decrease significantly the environmental impacts, although would not be simple because the FF needs to have a proper mass distribution in order to maintain stability on the WT.
- For the PEMWE system, if it was considered the values of the stack mass values for the future (2050) the contribution of the electrolyzer would decrease. But as the major contribution is from the OWF, the overall environmental impact of the system wouldn't decrease significantly.

- The storage stage has a very low contribution for the $CO_2\,eq./kg\,H_2$ emissions with only 0.34% and 0.18% contribution from configuration A and B respectively, because the storage tanks are used every day for 20 years. This means that during their lifetime they complete a total of 7300 cycles of filling up the tanks with hydrogen and empty the hydrogen in the HRS, resulting in a high utilization of these tanks.
- For the impact assessment, midpoint and endpoint analysis were considered for a better evaluation of the environmental impacts. In the midpoint, OWF had the greatest environmental impact in every category, except on the ozone depletion (OD) category in configuration A where PEMWE has greater impact. In the end point analysis, it became clear that resources are the category with the most impact for both configurations.
- In the CC category the values obtained were 3.65 and $5.21\,kg\,CO_2\,eq./kg\,H_2$ for configuration A with and without EoL and 6.89 and $9.84\,kg\,CO_2$ eq./kg of H_2 for configuration B with and without EoL respectively. Compared to the SMR process, there is between 55-70% reduction in emissions for configuration A and 15-40% for configuration B respectively.
- Comparing the CO_2 emissions with coal gasification and electrolysis from non renewable energy sources, it was possible to conclude that the reduction on $kg\,CO_2/kg\,H_2$ emissions were between 40-90%. Comparing with coal gasification with 90% CCS, the $kg\,CO_2/kg\,H_2$ emissions are between 40-80% higher.
- According to the values obtained in this thesis, hydrogen is a better option than fossil fuels in a LCA perspective for the mobility sector, with a range of approximately 40-80% reduction of the $CO_2\,eq./km$ emissions compared to ICE vehicles. Compared to BEV, configuration A has between 20-55% less $CO_2\,eq./km$ emissions, so green hydrogen is an alternative which should be exploited according to this study and from a LCA perspective.

5.2 Future Work

A few ideas for future work are presented below:

- Integrate also solar power plants as a complement to the wind energy for the case that there is no wind and the solar resource is available.
- Instead of onshore H_2 production, study the environmental impacts of its production integrated in offshore wind platforms installed in places far from the coast.
- Make a more profound techno-economic assessment of hydrogen production from the energy produced by the OWFs, in order to better understand the economic impacts.
- Study more accurately other storage options such as pipelines and liquid hydrogen transportation.
- Study the hydrogen transportation and dispenser options and all associated costs to understand what is the H_2 cost for the end-user in the mobility frame work.

Bibliography

[1] E. Taibi, T. W. J.-C. L. Raul Miranda (IRENA) Wouter Vanhoudt, and F. B. (Hinicio). Hydrogen from renewable power: Technology outlook for the energy transition. *International Renewable Energy Agency*, 2018.

[2] D. Gielen and R. Gorini. Future of wind: Deployment, investment, technology, grid integration and socio-economic aspects (A Global Energy Transformation paper). *International Renewable Energy Agency*, 2019.

[3] D. ao-Geral de Energia e Geologia. Road map for carbon neutrality 2050: Long term strategy for carbon neutrality of the portuguese economy by 2050. 2019.

[4] R. Roesch, F. B. E. Ocenic, A. S. J. Hecke, and G. Castellanos. Fostering a blue economy: Offshore renewable energy. *International Renewable Energy Agency*, 2020.

[5] C. F. Kate Freeman and F. Barth. Our energy, our future How offshore wind will help Europe go carbon-neutral. *WindEurope*, 2019.

[6] D. Gielen, E. Taibi, and R. Miranda. Hydrogen: A renewable energy perspective. *International Renewable Energy Agency*, 2019.

[7] L.-C. Ma, B. Castro-Dominguez, N. K. Kazantzis, and Y. H. Ma. Integration of membrane technology into hydrogen production plants with CO2 capture: An economic performance assessment study. *International Journal of Greenhouse Gas Control*, 42:424–438, 2015. ISSN 1750-5836.

[8] M. Voldsund, K. Jordal, and R. Anantharaman. Hydrogen production with CO2 capture. *International Journal of Hydrogen Energy*, 41(9):4969–4992, 2016. ISSN 0360-3199.

[9] E. Bianco and H. Blanco. Green Hydrogen: A guide to policy making", journal = "International Renewable Energy Agency. 2020.

[10] Between Green and Blue: a debate on Turquoise Hydrogen. `https://fsr.eui.eu/between-green-and-blue-a-debate-on-turquoise-hydrogen/`. Accessed: 2021-06-30.

[11] F. Z. Joyce Lee. Global offshore wind: Annual market report 2020. *Global Wind Energy Council*, 2020.

[12] M. Aneke and M. Wang. Energy storage technologies and real life applications A state of the art review. *Applied Energy*, 179:350–377, 2016. ISSN 0306-2619.

[13] M. F. Ruth, P. Jadun, N. Gilroy, E. Connelly, R. Boardman, A. J. Simon, A. Elgowainy, and J. Zuboy. The Technical and Economic Potential of the H2@Scale Hydrogen Concept within the United States. 10 2020.

[14] D.-G. de Energia e Geologia. Roteiro e Plano de Ação para o Hidrogénio em Portugal. 2019.

[15] P. Partidário, R. Aguiar, P. Martins, C. Rangel, and I. Cabrita. The hydrogen roadmap in the Portuguese energy system - Developing the P2G case. *International Journal of Hydrogen Energy*, 45, 11 2019. doi: 10.1016/j.ijhydene.2019.10.132.

[16] IEA. The Future of Hydrogen. 2019. URL `https://www.iea.org/reports/the-future-of-hydrogen`.

[17] Flagship project for green hydrogen. `https://www.aquaventus.org/presse/flagship-project-for-green-hydrogen/`. Accessed: 2021-05-15.

[18] European consortium to deliver 95GW of solar and 67GW of hydrogen by 2030. `https://reneweconomy.com.au/30-european-companies-form-hydeal-ambition-project-to-deliver\-95gw-of-solar-67gw-of-hydrogen/`. Accessed: 2021-06-15.

[19] P. de Laat. Overview of Hydrogen Projects in the Netherlands.

[20] Gigastack renewable hydrogen from offshore wind project advances to next phase; 100MW electrolyzer system. `https://www.greencarcongress.com/2020/02/20200219-gigastack.html`. Accessed: 2021-05-10.

[21] Conheça os 37 projetos já aprovados pelo Governo no âmbito do hidrogénio verde.

[22] J. F. Manwell, J. G. McGowan, and A. L. Rogers. *Wind energy explained: theory, design and application*. John Wiley & Sons, 2010.

[23] S. Boersma, B. Doekemeijer, P. Gebraad, P. Fleming, J. Annoni, A. Scholbrock, J. Frederik, and J. W. Wingerden. A tutorial on control-oriented modeling and control of wind farms. pages 1–18, 05 2017. doi: 10.23919/ACC.2017.7962923.

[24] Z. Jiang. Installation of offshore wind turbines: A technical review. *Renewable and Sustainable Energy Reviews*, 139:110576, 2021. ISSN 1364-0321.

[25] M. Vieira, E. Henriques, M. Amaral, N. Arantes-Oliveira, and L. Reis. Path discussion for offshore wind in portugal up to 2030. *Marine Policy*, 100:122–131, 2019. ISSN 0308-597X.

[26] F. Huera-Huarte. *Deep Water: The next step for offshore wind energy. A report by the European Wind Energy Association*. 10 2013.

[27] Allen, Christopher, A. Viselli, H. Dagher, A. Goupee, E. Gaertner, N. Abbas, M. Hall, and G. Barter. Definition of the UMaine VolturnUS-S Reference Platform Developed for the IEA Wind 15-Megawatt Offshore Reference Wind Turbine. July 2020.

[28] Windfloat atlantic project: The first maritime wind farm in portugal. https://noctula.pt/projeto-windfloat-atlantic-primeiro-parque-eolico-maritimo-em-portugal/.

[29] G. H. Kate Freeman, C. Nordstrom, A. Roberts, B. Valpy, C. W. B. Associates), P. T. (Totaro, Associates), M. Ayuso, and F. B. (IRENA). Floating foundations: A game changer for offshore wind. *International Renewable Energy Agency*, 2016.

[30] M. Kaiser and B. Snyder. Offshore Wind Energy Installation and Decommissioning Cost Estimation in the U.S. Outer Continental Shelf. U.S. Dept. of the Interior. 2011.

[31] M. Zaaijer. *Great expectations for offshore wind turbines: Emulation of wind farm design to anticipate their value for customers*. PhD thesis, TU Delft, 2013.

[32] Two hvac transformer platforms for greater changhua offshore wind farms. https://ramboll.com/projects/taiwan/two-hvac-transformer-platforms. Accessed: 2021-07-10.

[33] J. Limpo. Assessment of offshore wind energy in portuguese shallow waters. 2011.

[34] A. Fernández-Guillamón, K. Das, N. A. Cutululis, and A. Molina-García. Offshore wind power integration into future power systems: Overview and trends. *Journal of Marine Science and Engineering*, 7(11), 2019. ISSN 2077-1312.

[35] Global wind atlas. https://globalwindatlas.info/. Accessed: 2021-07-01.

[36] E. Cheynet, J. B. Jakobsen, and C. Obhrai. Spectral characteristics of surface-layer turbulence in the north sea. *Energy Procedia*, 137:414–427, 2017. ISSN 1876-6102. 14th Deep Sea Offshore Wind R&D Conference, EERA DeepWind'2017.

[37] B. F. P. FERREIRA. Estudo da previsão de produção de energia eólica offshore, 2017.

[38] P. Razdan and P. Garrett. Life Cycle Assessment of Electricity Production from an onshore V110-2.0 MW Wind Plant . *Vestas Wind Systems A/S*, 12 2015.

[39] R. Barthelmie, S. Frandsen, N. Nielsen, S. Pryor, P. Rethore, and H. Ejsing Jørgensen. Modelling and measurements of power losses and turbulence intensity in wind turbine wakes at middelgrunden offshore wind farm. *Wind Energy*, 10(6):517–528, 2007. ISSN 1095-4244.

[40] R. Bhandari, C. A. Trudewind, and P. Zapp. Life cycle assessment of hydrogen production via electrolysis a review. *Journal of Cleaner Production*, 85:151 – 163, 2014. ISSN 0959-6526. Special Volume: Making Progress Towards More Sustainable Societies through Lean and Green Initiatives.

[41] K. Barei, C. de la Rua, M. Mckl, and T. Hamacher. Life cycle assessment of hydrogen from proton exchange membrane water electrolysis in future energy systems. *Applied Energy*, 237:862 – 872, 2019. ISSN 0306-2619.

[42] S. S. Kumar and V. Himabindu. Hydrogen production by PEM water electrolysis A review. *Materials Science for Energy Technologies*, 2019. doi: https://doi.org/10.1016/j.mset.2019.03.002.

[43] M. Carmo, D. L. Fritz, J. Mergel, and D. Stolten. A comprehensive review on pem water electrolysis. *International Journal of Hydrogen Energy*, 38(12):4901 – 4934, 2013. ISSN 0360-3199.

[44] C. Sundin. Environmental assessment of electrolyzers for hydrogen gas production, 2019.

[45] J. Chi and H. Yu. Water electrolysis based on renewable energy for hydrogen production. *Chinese Journal of Catalysis*, 39(3):390 – 394, 2018. ISSN 1872-2067.

[46] A. Buttler and H. Spliethoff. Current status of water electrolysis for energy storage, grid balancing and sector coupling via power-to-gas and power-to-liquids: A review. *Renewable and Sustainable Energy Reviews*, 82:2440 – 2454, 2018. ISSN 1364-0321.

[47] A. Ursua, L. M. Ganda, and P. Sanchis. Hydrogen Production From Water Electrolysis: Current Status and Future Trends. *Proceedings of the IEEE*, 100:410–426, 02 2012.

[48] M. Ni, M. K. Leung, and D. Y. Leung. Technological development of hydrogen production by solid oxide electrolyzer cell (SOEC). *International Journal of Hydrogen Energy*, 33(9):2337–2354, 2008. ISSN 0360-3199.

[49] O. Schmidt, A. Gambhir, I. Staffell, A. Hawkes, J. Nelson, and S. Few. Future cost and performance of water electrolysis: An expert elicitation study. *International Journal of Hydrogen Energy*, 42(52): 30470 – 30492, 2017. ISSN 0360-3199.

[50] Ángel Hernández-Gómez, V. Ramirez, and D. Guilbert. Investigation of pem electrolyzer modeling: Electrical domain, efficiency, and specific energy consumption. *International Journal of Hydrogen Energy*, 45(29):14625 – 14639, 2020. ISSN 0360-3199.

[51] A. Abdol Rahim, A. S. Tijani, S. Kamarudin, and S. Hanapi. An overview of polymer electrolyte membrane electrolyzer for hydrogen production: Modeling and mass transport. *Journal of Power Sources*, 309:56 – 65, 2016. ISSN 0378-7753.

[52] M. Kopp, D. Coleman, C. Stiller, K. Scheffer, J. Aichinger, and B. Scheppat. Energiepark mainz: Technical and economic analysis of the worldwide largest power-to-gas plant with pem electrolysis. *International Journal of Hydrogen Energy*, 42(19):13311 – 13320, 2017.

[53] H. B. Emanuele Taibi and R. Miranda. Green Hydrogen Cost Reduction: Scaling up Electrolysers to Meet the 1.5 $^\circ$C Climate Goal. *International Renewable Energy Agency*, 2020.

[54] K. Meier. Hydrogen production with sea water electrolysis using norwegian offshore wind energy potentials. *International Journal of Energy and Environmental Engineering*, 2014. URL https://doi.org/10.1007/s40095-014-0104-6.

[55] What are the most important applications of oxygen? https://www.oxygen-plants.com/blog/what-are-the-most-important-applications-of-oxygen/. Accessed: 2021-05-30.

[56] Accidentology involving hydrogen. https://www.aria.developpement-durable.gouv.fr/wp-content/files_mf/SY_hydrogen_GB_2009.pdf.

[57] F. C. E. Buses. General Hydrogen Safety Facts. https://www.fuelcellbuses.eu/wiki/safety-framework/general-hydrogen-safety-facts. Accessed: 2021-05-29.

[58] NASA. Safety standard for hydrogen and hydrogen systems: Guidelines for hydrogen system design, materials selection, operations, storage and transportation. 01 1997.

[59] R. Moradi and K. M. Groth. Hydrogen storage and delivery: Review of the state of the art technologies and risk and reliability analysis. *International Journal of Hydrogen Energy*, 44(23):12254–12269, 2019. ISSN 0360-3199.

[60] G. Sdanghi, G. Maranzana, A. Celzard, and V. Fierro. Review of the current technologies and performances of hydrogen compression for stationary and automotive applications. *Renewable and Sustainable Energy Reviews*, 102:150–170, 2019. ISSN 1364-0321.

[61] H. Barthelemy, M. Weber, and F. Barbier. Hydrogen storage: Recent improvements and industrial perspectives. *International Journal of Hydrogen Energy*, 42(11):7254–7262, 2017. ISSN 0360-3199. Special issue on The 6th International Conference on Hydrogen Safety (ICHS 2015), 19-21 October 2015, Yokohama, Japan.

[62] A. M. Elberry, J. Thakur, A. Santasalo-Aarnio, and M. Larmi. Large-scale compressed hydrogen storage as part of renewable electricity storage systems. *International Journal of Hydrogen Energy*, 46(29):15671–15690, 2021. ISSN 0360-3199.

[63] E. Stamatakis, E. Zoulias, G. Tzamalis, Z. Massina, V. Analytis, C. Christodoulou, and A. Stubos. Metal hydride hydrogen compressors: Current developments & early markets. *Renewable Energy*, 127:850–862, 2018. ISSN 0960-1481.

[64] P. L. Spath and M. K. Mann. Life cycle assessment of renewable hydrogen production via wind/electrolysis. *National Renewable Energy Laboratory*, 2001.

[65] T. Patterson, S. Esteves, S. Carr, F. Zhang, J. Reed, J. Maddy, and A. Guwy. Life cycle assessment of the electrolytic production and utilization of low carbon hydrogen vehicle fuel. *International Journal of Hydrogen Energy*, 39(14):7190–7201, 2014. ISSN 0360-3199.

[66] J. Burkhardt, A. Patyk, P. Tanguy, and C. Retzke. Hydrogen mobility from wind energy - a life cycle assessment focusing on the fuel supply. *Applied Energy*, 181:54–64, 2016. ISSN 0306-2619.

[67] N. Elginoz and B. Bas. Life cycle assessment of a multi-use offshore platform: Combining wind and wave energy production. *Ocean Engineering*, 145:430–443, 2017. ISSN 0029-8018.

[68] S. Wang, S. Wang, and J. Liu. Life-cycle green-house gas emissions of onshore and offshore wind turbines. *Journal of Cleaner Production*, 210:804–810, 2019. ISSN 0959-6526.

[69] Y.-F. Huang, X.-J. Gan, and P.-T. Chiueh. Life cycle assessment and net energy analysis of offshore wind power systems. *Renewable Energy*, 102:98–106, 2017. ISSN 0960-1481.

[70] J. Weinzettel, M. Reenaas, C. Solli, and E. G. Hertwich. Life cycle assessment of a floating offshore wind turbine. *Renewable Energy*, 34(3):742–747, 2009. ISSN 0960-1481.

[71] J. Yang, Y. Chang, L. Zhang, Y. Hao, Q. Yan, and C. Wang. The life-cycle energy and environmental emissions of a typical offshore wind farm in china. *Journal of Cleaner Production*, 180:316–324, 2018. ISSN 0959-6526.

[72] J. Pryshlakivsky and C. Searcy. Fifteen years of ISO 14040: a review. *Journal of Cleaner Production*, 57:115 – 123, 2013. ISSN 0959-6526.

[73] S. Ghandehariun and A. Kumar. Life cycle assessment of wind-based hydrogen production in western canada. *International Journal of Hydrogen Energy*, 41(22):9696–9704, 2016. ISSN 0360-3199.

[74] T. J. R. Lucas. Feasibility of wind energy for hydrogen production: the windfloat atlantic case-study, 2020.

[75] Veículos rodoviários motorizados em circulação: total e por tipo de veículos. `https://www.pordata.pt/Portugal/Ve+c3+adculos+rodovi+c3+a1rios+motorizados+em+circula+c3+a7+c3+a3o+total+e+por+tipo+de+ve+c3+adculos-3100`.

[76] T. D., M. D. (Colruyt), M. (Sustesco), V. der Laak W., and F. I. Power-to-Gas Roadmap for Flanders. *WaterstofNet vzw*, 2016.

[77] Vestas wind systems a/s. `https://pdf.archiexpo.com/pdf/vestas/vestas-v164-80-mw/88087-134417.html`. Accessed: 2021-04-01.

[78] C. Desmond, J. Murphy, L. Blonk, and W. Haans. Description of an 8 MW reference wind turbine. *Journal of Physics: Conference Series*, 753:092013, sep 2016.

[79] B. B. Roelofs. *Material Recovery from Dutch Wind Energy*. PhD thesis, TU Delft, 2020.

[80] L. Fingersh, M. Hand, and A. Laxson. Wind Turbine Design Cost and Scaling Model. 2006.

[81] J. George. WindFloat design for different turbine sizes, 2014.

[82] Fish track. `http://www.fishtrack.com/fishing-charts/portugal_100168`.

[83] How Much Fuel Does a Helicopter Burn? `https://pilotteacher.com/how-much-fuel-does-a-helicopter-burn-get-your-visa-card-out/`. Accessed: 2021-06-01.

[84] G. Zhao and E. Ravn Nielsen. *Environmental Impact Study of BIG HIT*. Department of Energy Conversion and Storage, Technical University of Denmark, 2018.

[85] A. Lotri, M. Sekavnik, I. Kutrin, and M. Mori. Life-cycle assessment of hydrogen technologies with the focus on EU critical raw materials and end-of-life strategies. *International Journal of Hydrogen Energy*, 46(16):10143–10160, 2021. ISSN 0360-3199. Hydrogen and Fuel Cells.

[86] M. Delpierre, J. Quist, J. Mertens, A. Prieur-Vernat, and S. Cucurachi. Assessing the environmental impacts of wind-based hydrogen production in the Netherlands using ex-ante LCA and scenarios analysis. *Journal of Cleaner Production*, 299:126866, 2021. ISSN 0959-6526.

[87] Large Scale PEM Electrolysis for Industrial Applications. `https://www.co2neutraalin2050.nl/wp-content/uploads/Van-der-Laag.pdf`.

[88] O. Comond, D. Perreux, F. Thiebaud, and M. Weber. Methodology to improve the lifetime of type III HP tank with a steel liner. *International Journal of Hydrogen Energy*, 34(7):3077–3090, 2009. ISSN 0360-3199.

[89] E. Helmers, J. L. ao, U. Tietge, and T. Butler. CO2-equivalent emissions from European passenger vehicles in the years 19952015 based on real-world use: Assessing the climate benefit of the European diesel boom. *Atmospheric Environment*, 198:122–132, 2019. ISSN 1352-2310.

Appendix A

Material breakdown

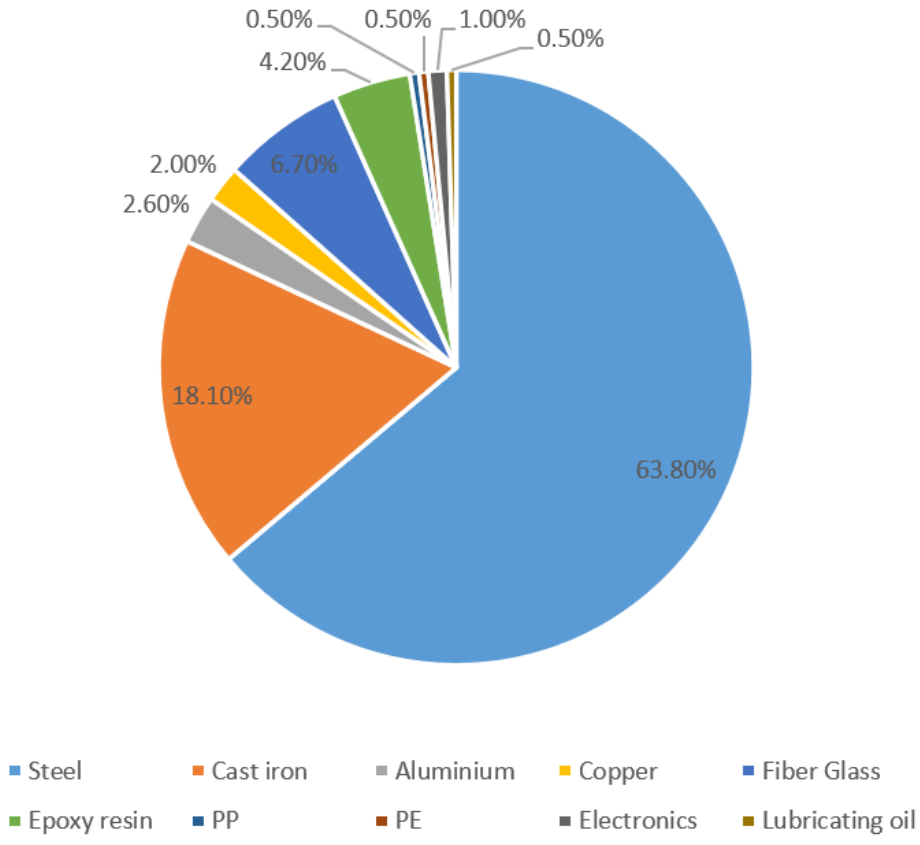

Figure A.1: Material breakdown of Vestas-164 8MW WT.

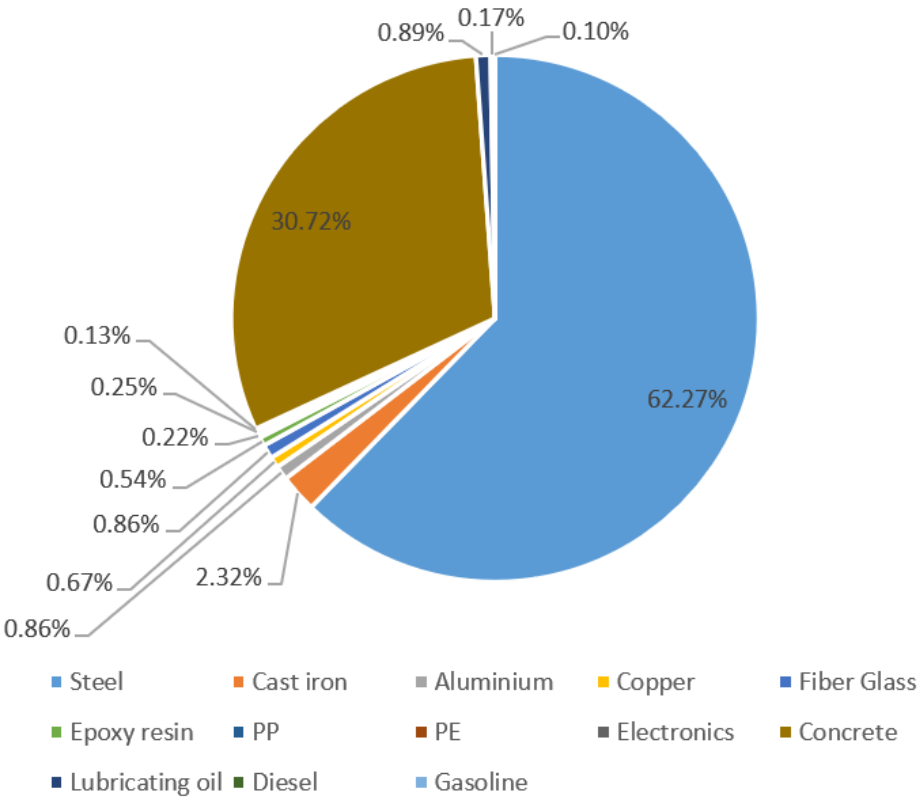

Figure A.2: Material breakdown of 560 MW OWF.

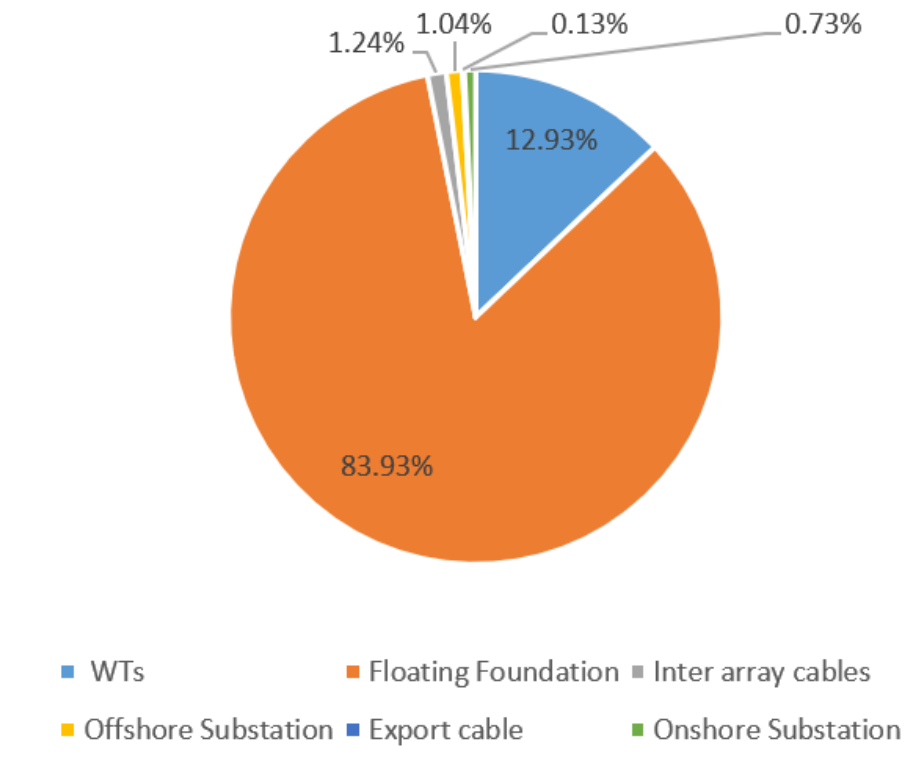

Figure A.3: Mass share of OWF components.

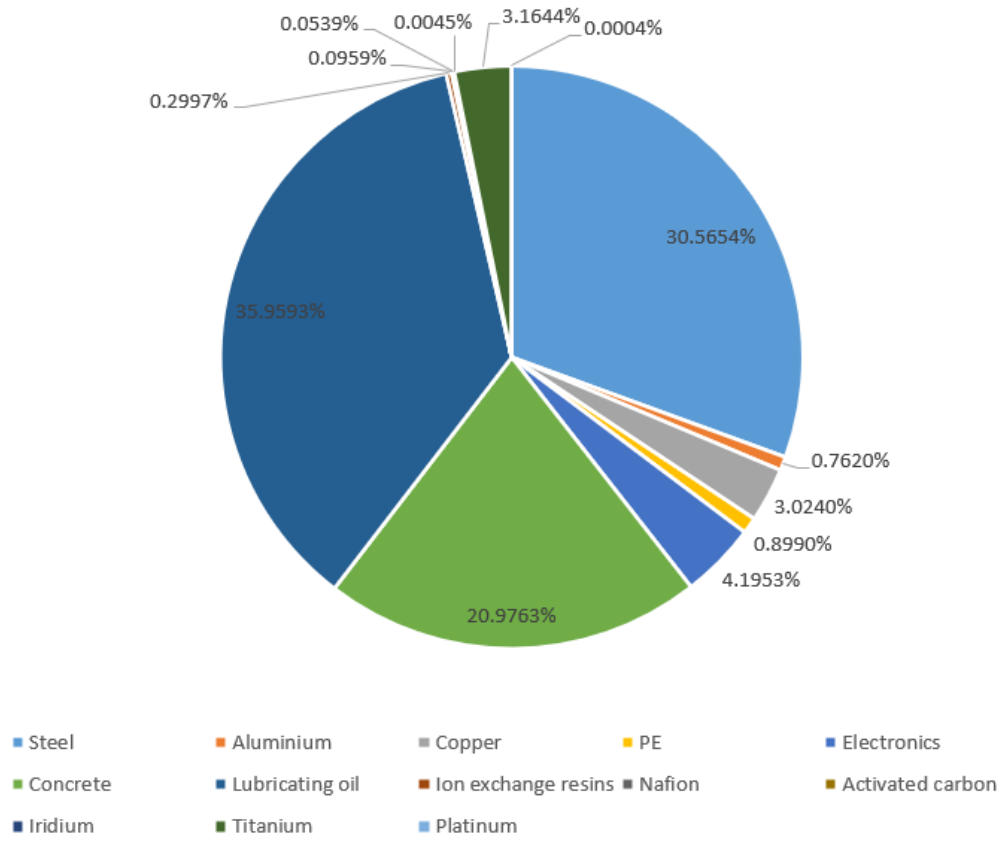

Figure A.4: Material breakdown of PEMWE.